# A BIO-MIMETIC APPROACH TO DESIGN A TARGETED DRUG DELIVERY SYSTEM

A Dissertation

by

AKSHI SINGLA

Submitted to the Office of Graduate and Professional Studies of
Texas A&M University
in partial fulfillment of the requirements for the degree of

DOCTOR OF PHILOSOPHY

Chair of Committee, Hung-Jen Wu
Committee Members, Arul Jayaraman
Joseph Sang-II Kwon
Vladislav Panin
Head of Department, Arul Jayaraman

May 2020

Major Subject: Chemical Engineering

# ABSTRACT

Bacterial resistance is rapidly emerging worldwide, endangering the efficacy of existing antibiotics. As a result, extensive research is being done on the development of new antimicrobials; however, these new drugs could be toxic. An effective targeted drug delivery technique, which could increase the local drug concentrations at the site of infection, is an ideal tool to reduce drug toxicity and enhance drug efficacy. Here, we aim to develop a novel hetero-multivalent targeted liposome system to deliver antibiotics by mimicking the process of bacterial adherence to epithelia. Here, we particularly focus on *Pseudomonas aeruginosa*, because *P. aeruginosa* is among the top three pathogens that are in a critical need of new antibiotics.

Inspired by the nature of bacterial adhesion to the host cells, we have discovered previously unknown molecules from host cells that mediate the bacterial adhesion. *P. aeruginosa* interaction with host cells is primarily mediated by the adhesion of bacterial lectins (carbohydrate binding proteins) to glycans (carbohydrates) on host cell surfaces. We have investigated the role of multiple glycolipids and the fluidity of cell membrane in two different multivalent binding systems, including pentavalent cholera toxin subunit B (CTB) and tetravalent *P. aeruginosa* lectin PA-IL (LecA). Based on the experimental observations, we have proposed a hetero-multivalent binding mechanism based on Reduction in Dimensionality (RD), which might be playing a major role in the bacterial adhesion. Kinetic Monte Carlo (kMC) simulations were then used to further validate these experimental observations and the hetero-multivalent binding.

We then used these new ligands as targeting ligands on the surface of liposomal carriers to mimic the host cell membrane environment. Because the liposomal drug carriers are made of

host cell molecules, the whole assembly poses minimal toxicity and immunogenicity. A two times higher targeting efficiency was achieved. Furthermore, the antimicrobial activity of a common antibiotic, ciprofloxacin, was evaluated using this targeted drug delivery system and showed higher drug efficacy *in vitro* and *in vivo* compared to non-targeted liposomes and free drug. We envisage that this research will lead to development of similar drug delivery systems for treatment against other pathogens too.

# ACKNOWLEDGEMENTS

I would, first, like to thank my advisor, Dr. Hung-Jen Wu, for his support and encouragement through-out my PhD. From brainstorming ideas to designing experiments with limited resources, from writing simply but clearly to honing verbal presentation skills, Dr. Wu has been a great mentor and I have learnt a lot under his guidance. I would also like to thank my committee members, Dr. Joseph Sang-II Kwon, Dr. Arul Jayaraman, Dr. Victor Ugaz, and Dr. Vladislav Panin, for their guidance. I am also very grateful to Dr. Carolyn Cannon for her direction and patience during the last (but never ending) project of my PhD research. I really appreciate all the discussion sessions and the joint lab work with wonderful graduate students from my research group, Pratik Krishnan, Nolan Worstell, Joshua Weatherston, Chin-An Lee, Anirudh Gairola and Qiang Hu and feel thankful to have worked with all of them. Also, working with some of the undergraduate students in the group, especially Rachel Tindall, Alberta Lin and Lina Karkoub, had been a refreshing break from regular experimental work on many occasions. It has been my absolute pleasure to get to know and work with Sabona Simbassa and Bhagath Chirra from Dr. Cannon's group and Dongheon Lee and Hyun-Kyu Choi from Dr. Kwon's group that has resulted in successful collaborations and a few published manuscripts. My thanks also go to the Chemical Engineering department faculty and staff, especially Ashley Henley and Bridgette Gray for making my time at Texas A&M University a great experience.

My stay in Bryan/College Station wouldn't have been bearable and cherishable (you know what I mean) if it wasn't for these two wonderful women, Nandini Kundu and Joshiba Venkatachalapathy. With them (separately), I have shared the saddest and the happiest moments/months/years of my PhD life and I hope to continue bothering them in future as we all

live in different places. I can't thank these two and others -- Pratik, Puneet Kawatra, Purvali Chaudhari, Anuvab Das, Deepthi Sen, Cort Wernz, and Pooja Tilak -- enough for obliging me with their amazing company on many many lunch/dinner/movie dates, board game nights and impromptu trips to Houston, San Antonio etc. I really appreciate Nairita Mitra, Sayan Banerjee, Ratnamala Mandal and Isita Jhulki for always being super-friendly, inviting me to their awesome parties and providing me with food and car rides. I wish you could read this, Baltu and especially Cricket have given me immense love and taught me about love I didn't know I was capable of. The credit for me surviving 5 years in BCS also goes to these lovely people in Austin, Indu Venu Sabaraya, Rohit Satija, Shaivya Vashishtha, Sarah Seraj, Mark Campmier, Nilabh Roy, Shifra Fernandes, Rashmi Mohanty, Marie Nunez, Minh Pham and Sahil Bhandari. I feel so happy to have spent such beautiful moments and make amazing memories with y'all.

And, then there are people who make long distance seem nothing. I don't think I can justify in words what Charu Mehta, my soul sister, means to me (can't believe it took us to do PhD to realize this). I get anxiety if I go 15 days without talking to this woman, who understands me so well and always has my back. I am also grateful to Afreen Faridi for always being there, I have learnt so much from you. My heart feels so full because of the love and support that Rajat Jain, Urvi Agrawal, Surabhi Yadav, Arshad Nasser, Surbhi Garg, Pawan Rawal, Shruti Singla, Nidhi Gupta, Simar Marwah, Sneha Lakhotia, Rahul Goel and Riccha Tripathi have given me over these past 5 years and I appreciate them always being just a phone call (or sometimes a missed call) away. I would also like to apologize to WB sisterhood, Divya Ahlawat, Sonakshi Goel, Pankhuri Goel, Paridhi Khandelwal, Nikita Navral, Kanika Khanna and Sarneet Broca for not attending any weddings/reunions, I will try to make up for it once this is all done. A special

mention to Prof. Vijayaraghavan Chariar whom I knew of as an amazing teacher in IIT but became my counselor and a friend during my PhD.

Last but not the least, I could not have done any of it without the strongest pillars of my strength. I feel grateful to have the most amazing sister, Yashu, who is my all-time confidante, sometimes my counselor, the best partner in crime and my commander in chief at home. I feel so proud of the woman she has become and I have learnt a lot from her. My biggest thanks goes to my best friend, Zishi (Shahzad), who has borne with me the most during this PhD (and even before) and been patient with me in my journey of self-exploration. You have inspired me to push my comfort envelope, listened to my rants (including all the non-sense) and almost always managed to make me laugh at your "jokes", please continue doing the same. Finally, I am immensely grateful to my mummy-papa who have always believed in me and supported me unconditionally even when everyone around tried their best to convince them otherwise and at times when they, themselves, could not understand my decisions. I am who I am today because of them, they taught me to fly and then let me be free to explore my own skies.

Writing this section has overwhelmed me with love and happiness and made me realize that so many people have touched my life in so many ways. Now, I can say, it wasn't bad after all.

# CONTRIBUTORS AND FUNDING SOURCES

This work was supported by a dissertation committee consisting of Professor Hung-Jen Wu and Professors Arul Jayaraman and Joseph Sang-II Kwon of the Department of Chemical Engineering and Professor Vladislav Panin of the Department of Biochemistry and Biophysics.

Chapter II experiments were: conceived and designed by myself, Pratik Krishnan, and Hung-Jen Wu of the Department of Chemical Engineering; performed by myself and Pratik Krishnan of the Department of Chemical Engineering; and analyzed by myself, Pratik Krishnan, and Hung-Jen Wu of the Department of Chemical Engineering. Experimental results were analyzed by myself, Pratik Krishnan and Hung-Jen Wu of the Department of Chemical Engineering. The contributed reagents/materials/analysis tools for Chapter II were from myself, Pratik Krishnan, Joshua D. Weatherston, Chin-An Lee, Nolan C. Worstell and Hung-Jen Wu of the Department of Chemical Engineering. Chapter II was written by myself, Pratik Krishnan, and Hung-Jen Wu of the Department of Chemical Engineering.

Chapter III experiments were: conceived and designed by myself, Nolan C. Worstell, and Hung-Jen Wu of the Department of Chemical Engineering; performed by myself and Nolan C. Worstell of the Department of Chemical Engineering and by Panatda Saenkham, Thushara Galbadage of the Department of Microbial Pathogenesis and Immunology; and analyzed by myself, Nolan C. Worstell and Hung-Jen Wu of the Department of Chemical Engineering. The contributed reagents/materials/analysis tools were from myself, Nolan C. Worstell and Hung-Jen Wu of the Department of Chemical Engineering, and by Preeti Sule and Jeffrey D. Cirillo of the Department of Microbial Pathogenesis and Immunology. Chapter III was written by myself, Nolan C. Worstell, and Hung-Jen Wu of the Department of Chemical Engineering.

Chapter IV experiments were: conceived and designed by myself, Nolan C. Worstell, and Hung-Jen Wu of the Department of Chemical Engineering; performed by myself and Nolan C. Worstell of the Department of Chemical Engineering; and analyzed by myself, Nolan C. Worstell and Hung-Jen Wu of the Department of Chemical Engineering. The contributed reagents/materials/analysis tools were from myself, Nolan C. Worstell and Hung-Jen Wu of the Department of Chemical Engineering. Chapter IV was written by myself, Nolan C. Worstell, and Hung-Jen Wu of the Department of Chemical Engineering.

Chapter V experiments were: conceived and designed by myself and Hung-Jen Wu of the Department of Chemical Engineering, and Sabona Simbassa and Carolyn L. Cannon of the Department of Microbial Pathogenesis and Immunology; performed by myself of the Department of Chemical Engineering and Sabona Simbassa of the Department of Microbial Pathogenesis and Immunology; and analyzed by myself and Hung-Jen Wu of the Department of Chemical Engineering, and Sabona Simbassa and Carolyn L. Cannon of the Department of Microbial Pathogenesis and Immunology. The contributed reagents/materials/analysis tools were from myself and Hung-Jen Wu of the Department of Chemical Engineering, and Sabona Simbassa and Carolyn L. Cannon of the Department of Microbial Pathogenesis and Immunology. Chapter V was written by myself and Hung-Jen Wu of the Department of Chemical Engineering, and Sabona Simbassa and Carolyn L. Cannon of the Department of Microbial Pathogenesis and Immunology.

Graduate study was supported by a fellowship from Texas A&M and funds from the National Institutes of Health under award number R03AI113585, R03AI139650.

# TABLE OF CONTENTS

Page

# LIST OF FIGURES

Page

Page

# LIST OF TABLES

Page

# CHAPTER I

# INTRODUCTION

Infectious diseases were the leading cause of deaths in the world in the 20th century. In 1900, pneumonia, tuberculosis and gastrointestinal infections led to one third of all the deaths in the United States[1]. During the First World War, infected wounds caused by shrapnel and shells contaminated with soil led to numerous deaths[2]. With the discovery and development of penicillin, bacterial infections were successfully controlled during Second World War[3]. Antibiotics have been crucial in increasing the life expectancy in the United States from 47 years in 1900 to 78.6 years in 2017[4]. However, the evolution of bacterial strains to resist antibiotic treatment is one of the biggest health threats today[5-8]. Approximately 2.8 million antibiotic-resistant infections occur in the United States every year, leading to more than 35,000 deaths[9]. Antibiotic resistance typically develops through genetic changes over time (chromosomal DNA mutation or extra chromosomally during plasmid or transposons exchange) [10,11]. Enzymatic degradation of antibiotics, prevention of antibiotic permeation through bacterial membrane, and alteration of the antibiotic targets are fundamental mechanisms behind antibacterial resistance[12]. However, the inappropriate use of antibiotics such as overuse and misuse of medicines is accelerating this phenomenon[13-15]. For example, antibiotics are used as growth promoters and to prevent diseases in healthy animals. As a result of this increased antibiotic resistance, extensive research effort is focused on development of new antibiotics. However, these new antibiotics could be toxic both to the bacterial target and to the healthy host cells. Additionally, continuous and frequent drug dosing for long periods may be required to treat certain multi drug resistant (MDR) pathogen which may further lead to adaptive resistance to antibiotics [16]. The long

duration of the therapy often leads to incomplete adherence to the treatment, also resulting in the development of drug resistance. A potential solution to these challenges is targeted drug delivery. An effective targeted drug delivery system can increase the local drug concentrations at the site of infection resulting in enhancement of drug efficacy but reduction of drug toxicity. Consequently, the drug dosage can also be controlled.

## Targeted drug delivery

Most often, drugs are administered either orally or intravenously, leading to a uniform distribution of drug in the body. As a result, only a proportion of the total dose reaches the actual infection site. Targeted drug delivery system increases the concentration of drug at the infection site, whilst minimizing the accumulation in healthy organs. The increased drug concentrations at the site of infection enhances the drug efficacy but reduces the drug toxicity. Consequently, the treatment duration can also be controlled. Targeted drug delivery can be of two types: a) passive and b) active. Passive drug delivery systems change the circulation time of the drug because of the body's natural response to physicochemical characteristics of the drug or drug carrier system while active targeting enhances the effect of passive targeting by functionalizing the drug carrier surface specifically enabling it to reach the infection site. The passive targeted drug delivery systems that have been used as anti-bacterial treatments are stimuli-responsive systems which are either exogenous i.e. subjected to specific physical stimulation (light, temperature, magnetic, ultrasound) or endogenous i.e. react dynamically after recognizing the bacterial microenvironments (pH, enzymes, variation in redox gradient)[17]. On the other hand, active targeting further enhances the effect of passive targeting by functionalizing the drug carrier surface and specifically binding to the receptors present on the surface of bacteria. The active

targeting approaches that have been used against bacteria are primarily targeting specific sites on bacterial cell wall, cell membrane or essential bacterial enzymes[11].

The aim of this dissertation is to design a bio-mimetic drug delivery system that actively targets the bacteria. Typically, antibodies are used as targeting ligands, however, the classic antibody-based drug delivery is expensive and often immunogenic. Another alternative is to use glycans as targeting ligands because they are already present in host cells and hence are biocompatible. Glycans are sugar molecules which play a major role in physical and structural integrity of the cell, cell-cell communication, and most importantly, mediate the bacterial adhesion on host cells before the onset of infection. The focus of this dissertation is to identify the potential glycan ligands to target the bacteria and use these ligands to design a drug carrier which will mimic the bacterial adhesion mechanism. The challenges in the identification of potential glycans are: a) the lack of understanding of the bacterial adhesion mechanism, and b) lack of appropriate analytical and computational tools to investigate such binding mechanisms. Thus, it is imperative to first explore the bacterial adhesion mechanism.

**Bacterial adhesion with host cells**

Most of the bacterial interactions with their hosts are influenced by the binding between glycan and glycan binding proteins[18]. Therefore, a lot of research is focused on targeting lectins for drug delivery[19-22]. A large fraction of bacterial adhesins is lectins (glycan binding proteins) that bind to cell surface glycolipids (glycans attached to lipids) or glycoproteins (glycans attached to membrane proteins). Therefore, to decipher the bacterial adhesion mechanism, lectin-glycan binding mechanism needs to be understood first. Often, these lectins are multivalent i.e. contain multiple binding sites. For example, the binding subunit of Cholera Toxin i.e. subunit B (CTB) from *Vibrio cholerae* has a pentameric ring containing five equivalent binding pockets

and PA-IL (LecA) from *Pseudomonas aeruginosa* is tetravalent[23,24]. Research in molecular docking predominantly considers the classic lock and key binding model for protein binding[25]. However, these multivalent lectins often do not specifically bind with a single glycan but rather bind to different glycan ligands with different affinities[26-30]. For example, the binding affinity between CTB and different glycans have the following reported trend: GM1 > fucosyl-GM1 > GD1b > GM2 > GM3[26,31,32]. A monovalent lectin–glycan interaction is typically weak (equilibrium dissociation constants range from nanomolar to millimolar)[28,32]. Thus, most lectins multivalently bind to glycans i.e. a single lectin simultaneously interacts with multiple glycan molecules, giving rise to a strong overall binding avidity (up to picomolar dissociation constants)[30,33]. Additionally, the fluidic nature of the cell membrane influences the lectin-glycan binding. These characteristics distinguish the lectin–glycan binding from the other established ligand–receptor binding models such as antibody–antigen and nucleic interactions[28]. Therefore, the lock-and-key binding model is rather too simplistic to capture these complexities. Besides, lectins are also used for blood typing[34]. Lectins are used as stains for detection and quantification of glycolipids on cell membranes[35,36]. Despite the prominence of lectin-glycan interactions, the mechanism governing this is still not well understood.

To illustrate this, cholera toxin (CT) is a good example[28]. Although GM1 ganglioside has long been considered as the major ligand for CT, many studies have questioned the importance of GM1 ligand in CT intoxication. First, GM1 is of low abundance on the human small intestinal epithelial cell surfaces (GM1 = 0.0015–0.003 mol% of total glycosphingolipids)[37], raising a question, "is GM1 density sufficient to induce CT intoxication?"[38]. Second, many in vitro studies have indicated that the number of CT binding to the cells does not correlate with the density of GM1 on the cell membranes[36,39,40]. Third, the epidemiology studies have found that cholera

infection is associated with the blood group antigens[41-45]. The recent molecular structure studies have suggested that the blood-group dependence is caused by the interactions between CT and blood groups[46,47]. Fourth, Kohler and her coworkers recently showed that the CT intoxication is GM1-independent and, surprisingly, fucosylated molecules (e.g. trisaccharide Lewis X, $Le^x$ and fucosylated proteins) could influence the CT internalization process[38,48,49]. This observation is unintuitive, because most of the ligand–receptor binding assays have shown that the binding between CT and fucosyl glycans, including blood groups, is weak and only detectable at millimolar concentrations[38,48-53]. However, if the ligands are present on the cell surfaces, the nanomolar concentration of CT was sufficient to interact with fucosyl glycans, leading to CT intoxication[48].

Interestingly, CT is not an exception. Similar binding phenomenon has been observed in other bacterial and viral infections[47,54]. For example, globotriaosylceramide (Gb3) is generally considered as the major ligand of shiga toxin. However, the concentration of Gb3 is almost undetectable in intestinal epithelia[55]. Thus, the same question arises, why shiga toxin internalization is not correlated with its major ligand[56-59]. Following these studies, the other glycan ligands seem more important than the major ligands, even though these other ligands may have extremely weak affinities with lectins. This observation is completely different from the classic conviction in biochemistry that the receptor binding should be determined by its major ligands.

**Hetero-multivalent lectin-glycan binding**

Since, the cell membrane contains multiple glycolipids and glycoproteins, multivalent lectins can also hetero-multivalently bind with glycans i.e. a single lectin binds with different kinds of glycans at the same time. Prior research has reported that bispecific antibodies which

hetero-multivalently bind with two different antigens have higher selectivity[60]. This has further been validated through Monte Carlo simulations and estimated that effective affinity of the bivalently bound bispecific antibody is about 4 orders of magnitude higher than the monovalently bound species influenced by surface diffusion[61]. Hetero-multivalency has also been observed in other systems such as CTB binding to mixtures of glycolipids[27,62,63]. In fact, it has also been demonstrated that the binding between CTB and 2 mol% fucosyl-GM1 is comparable to the binding between CTB and a mixture of 1 mol% fucosyl-GM1 and 1 mol% GM2. This is surprising because CTB binding with even 2 mol% GM2 (in the absence of fucosyl-GM1) is negligible. This indicates some cooperative actions between fucosyl-GM1 and GM2 and fucosyl-GM1 seems to have activated GM2, leading to enhanced CTB binding. However, the characteristic mechanism behind this observation hasn't been explored yet. Current standpoint in glycobiology is that lectins recognize glycan epitopes based on their number, density and spatial distribution along with molecular structures[28,64-67]. Although the concept of pattern recognition seemingly explains the prior observations, the underlying mechanism is not clear. Additionally, while it is a common agreement in glycobiology community that the membrane diffusion influences the host-pathogen interactions[68], the inherent process behind this is still uncertain.

## Analytical tools to study lectin-glycan binding

To appropriately capture the essence of lectin-glycan binding, the cell membrane-like conditions need to be mimicked. Detailed studies that have explored lectin-glycan interactions have constructed glycan microarrays to screen potential lectin binding ligands from large libraries of natural and synthetic glycans. However, most often, these ligands are immobilized on a substrate and hence, miss the essence of cell membrane fluidity[69,70]. Fluidic glycan microarrays

have also been employed such as supported lipid bilayer[71-74], tethered liposome[75] and cell-based glycan array[76], but these are very specialized technologies and not yet available for wide range of scientific communities. In addition, glycan microarrays, often, screen one specific glycan at a time. The published combinatorial glycoarray that imprints two different glycans in 1:1 ratio on a polyvinylidene difluoride (PVDF) membrane is a potential tool to resolve this issue[77,78]. However, this labor-intensive technique is not appropriate for the large-scale screening. For example, the glycan microarray, developed by the Consortium for Functional Glycomics (CFG), currently contains over 600 unique glycan molecules; therefore, at least 179,700 combinatory conditions have to be evaluated. Furthermore, commonly used detection tools are either fluorescent based or equilibrium binding assays such as immunostaining[79]. However, incubation conditions, photobleaching and instrumental variations can cause large intra- and inter-day variations[80]. Thus, tedious calibrations have to be performed every time to measure the absolute number of lectins bound, but a full quantitative analysis is rarely conducted[28]. A label-free detection tool such as nanocube sensors and turbidity based agglutination assay (TEA) developed by Wu's group[81,82] could be used. These sensors employ fluidic supported lipid bilayers and the lipid bilayer composition can be tuned as required, and hence mimics the cell membrane environment. It is, therefore, an ideal tool to study lectin-glycan binding.

**Overview of following chapters**

In the subsequent chapters, I will delve into details of my PhD research: exploration of the lectin-glycan binding process and development of a new targeted drug delivery technique. Chapter II will focus on investigating the hetero-multivalent lectin binding of CTB with heterogeneous mixtures of glycolipids using the nanocube sensor. Chapter III will demonstrate the same heteromultivalency in case of another lectin, *Pseudomonas aeruginosa* lectin PA-IL

(LecA) and the whole bacterium. Chapter IV will introduce a new semi-quantitative assay, the turbidity based agglutination assay (TEA), which can help screen potential lectin binding partners from a library of glycans. This new assay needs only common laboratory tools and, hence, can be used by scientists across the world. Lastly, Chapter V will discuss the design and development of the new targeted drug delivery system and will demonstrate a higher efficacy of a common antibiotic, ciprofloxacin, against the bacteria *P. aeruginosa*.

# CHAPTER II

# HETERO-MULTIVALENT BINDING OF CHOLERA TOXIN SUBUNIT B WITH GLYCOLIPID MIXTURES[†]

## Chapter Summary

GM1 has generally been considered as the major receptor that binds to cholera toxin subunit B (CTB) due to its low dissociation constant. However, using a unique nanocube sensor technology, we have shown that CTB can also bind to other glycolipid receptors, fucosyl-GM1 and GD1b. Additionally, we have demonstrated that GM2 can contribute to CTB binding if present in a glycolipid mixture with a strongly binding receptor (GM1/fucosyl-GM1/GD1b). This hetero-multivalent binding result was unintuitive because the interaction between CTB and pure GM2 is negligible. We hypothesized that the reduced dimensionality of CTB-GM2 binding events is a major cause of the observed CTB binding enhancement. Once CTB has attached to a strong receptor, subsequent binding events are confined to a 2D membrane surface. Therefore, even a weak GM2 receptor could now participate in second or higher binding events because its surface reaction rate can be up to 104 times higher than the bulk reaction rate. To test this hypothesis, we altered the surface reaction rate by modulating the fluidity and heterogeneity of the model membrane. Decreasing membrane fluidity reduced the binding cooperativity between GM2 and a strong receptor. Our findings indicated a new protein-receptor binding assay, that can mimic complex cell membrane environment more accurately, is required to explore the inherent hetero-multivalency of the cell membrane. We have thus developed a new membrane

[†] Reproduced from Ref. 26 with permission from Colloids and Surfaces B: Biointerfaces

perturbation protocol to efficiently screen receptor candidates involved in hetero-multivalent protein binding.

## Introduction

Many proteins recognize glycolipid receptors in cell membranes via multivalent binding mechanisms[83]. Such dynamic binding, driven by a series of binding domains, brings a protein to a membrane surface and initiates biological processes. Interactions between a single glycolipid receptor and a protein binding subunit are often weak, and therefore multivalency enhances the protein binding avidity and specificity to cell surfaces. Cholera toxin (CT), the virulence factor of *Vibrio cholerae*, is a type of multivalent glycolipid binding protein. This $AB_5$ toxin consists of a single A subunit associated with five identical B subunits. The B pentamer binds to cell membranes and delivers the catalytic A subunit into the cytoplasm. A potential stepwise reaction of pentavalent cholera toxin subunit B (CTB) binding to the cell membrane[84,85] is shown in Figure. 1. (1) CTB moves from the solution phase to the membrane surface, followed by one of its binding sites attaching to a glycolipid receptor; (2) Free glycolipids diffuse two dimensionally, encounter the bound CTB, and then enable subsequent binding. The synergistic effort amongst various binding pockets, membrane receptors, and membrane dynamics dramatically influences the overall association.[86]

We recently developed a unique nanocube sensor by integrating supported lipid bilayer and plasmonic sensing technologies[81]. This new tool has enabled label-free detection of protein binding to model membrane surfaces by using a standard laboratory spectrophotometer to observe the extinction spectrum shift of the quadrupolar localized surface plasmon resonance (LSPR) peak[27]. The nanocube sensor was used to investigate the multivalent binding principle of CTB interacting with various glycolipids[27]. We observed that the amount of CTB binding onto

the surface containing fucosyl-GM1 was higher than GM1 although the dissociation constant of GM1 was an order of magnitude lower than that of fucosyl-GM1. This unintuitive result might be attributed to a reduced binding cooperativity between fucosyl-GM1 receptors leading to an increased binding capacity[27]. Our previous findings indicated that dissociation constants cannot exclusively represent multivalent CTB bindings and that binding cooperativity also plays an essential role in determining CTB-cell membrane recognition.

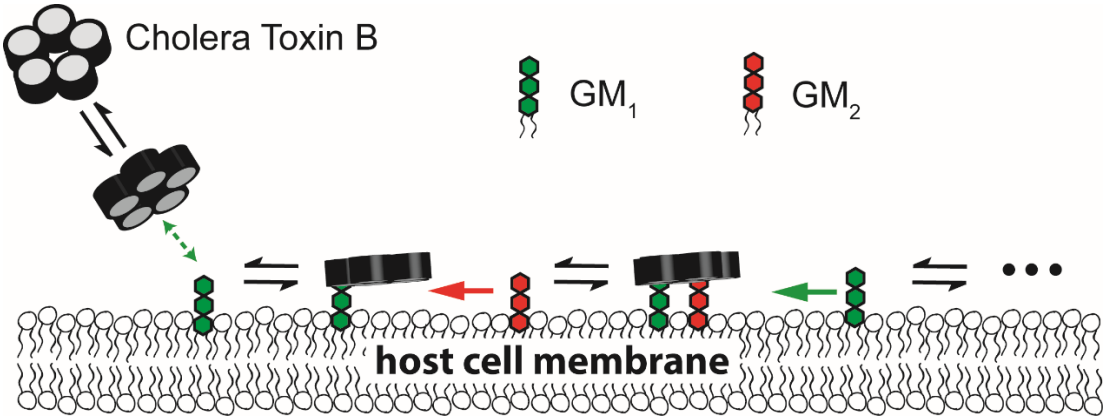


Figure 1: A schematic of the proposed CTB binding mechanism. CTB first diffuses from the solution phase to a membrane surface. One of its binding subunit finds a strongly binding receptor and then forms a relatively stable membrane bound state. Free glycolipid receptors diffuse two dimensionally, encounter the bound CTB, and then enable subsequent binding. The reaction rate on the 2D membrane surface is significantly higher than the rate in 3D bulk solutions. Thus, a weakly binding receptor, such as GM2, can participate in subsequent binding, leading to an enhanced binding capacity. Reprinted from reference 26.

Multivalent binding can be either homo-multivalent (i.e. a protein binds to multiple copies of the same type of receptor) or hetero-multivalent (i.e. a protein simultaneously binds to two or more different types of receptors)[27]. Due to the complexity of hetero-multivalency, most studies have focused on homo-multivalency. However, homo-multivalent models neglect the inherent heterogeneity of cell membranes. We recently reported that adding a weak glycolipid

receptor (GM2) to a model membrane containing fucosyl-GM1 significantly increased the total amount of bound CTB[27]. This was unexpected, as GM2 receptors have negligible binding avidity in bilayers with GM2 as the only glycolipid receptor. A few other studies have also reported that lectin binding to glycan mixtures is stronger than the binding to a single glycan.[77,87-89] However, the mechanism of such hetero-multivalency is not clear.

The goal of this study was to gain insight into the mechanism of hetero-multivalent CTB binding. We first investigated the binding cooperativity of CTB to various glycolipid mixtures. Positive cooperativity was observed when GM2 was mixed with any of the other three strongly binding receptors (GM1, fucosyl-GM1, and GD1b). We hypothesized that the increase of CTB binding is caused by a reaction rate enhancement mechanism, "reduction of dimensionality" (Figure. 1). Once CTB has attached to a strong receptor, subsequent binding events are confined on the 2D membrane surface. Therefore, even a weak GM2 receptor could now participate in second or higher binding events because its surface reaction rate is around $10^4$ times higher than the rate in bulk solution. To test this hypothesis, we modulated the fluidity and heterogeneity of the model membrane by adding cholesterol or altering fatty acid composition of phospholipids and observed significant changes in the heterogeneous binding cooperativity. This complies with the surface reaction's strong dependence on the membrane environment. Our results indicated that the traditional protein binding assay, which detects protein interactions with a specific receptor one by one (e.g. microarray technology), is not appropriate to explore multivalent binding interactions. To discover all possible receptors which could participate in a binding process, we designed a new membrane perturbation protocol that can efficiently screen possible glycolipid receptors involved in multivalent protein binding.

## Materials and methods

### Materials

Monosialoganglioside GM1 ($NH_4^+$salt) (Galβ1-3GalNAcβ1-4(Neu5Acα2-3)Galβ1-4Glc-Ceramide, GM1), monosialoganglioside GM2 ($NH_4^+$salt) (GalNAcβ1-4(Neu5Acα2-3)Galβ1-4Glc-Ceramide, GM2), monosialoganglioside GM3 ($NH_4^+$salt) (Neu5Acα2-3Galβ1-4Glc-Ceramide,GM3), fucosylated monosialoganglioside GM1 ($NH_4^+$salt) (Fucα1-2Galβ1-3GalNAcβ1-4(Neu5Acα2-3)Galβ1-4Glc-Ceramide, fucosyl-GM1) and disialoganglioside GD1b($NH_4^+$salt) (Galβ1-3GalNAcβ1-4(Neu5Acα2-8)(Neu5Acα2-3)Galβ1-4Glc-Ceramide,GD1b) were purchased from Matreya LLC (State College, PA). 1,2-dioleoyl-sn-glycero-3-phosphocholine (DOPC), 1,2-dioleoyl-sn-glycero-3-phospho-L-serine - sodium salt (DOPS), 1,2-dimyristoyl-sn-glycero-3-phosphocholine (DMPC) and 1,2-dimyristoyl-sn-glycero-3-phospho-L-serine – sodium salt (DMPS) were obtained from Avanti Polar Lipids (Alabaster, AL). Cholera Toxin B subunit (CTB, lyophilized powder) from *Vibrio cholerae*, cholesterol and casein from bovine milk were purchased from Sigma-Aldrich. GM1 oligosaccharide (GM1os) (Galβ1-3GalNAcβ1-4(Neu5Acα2-3)Galβ1-4Glc) sugar was purchased from Elicityl (Crolles, France). All the CTB binding experiments were performed in Tris-buffered saline-TBS (Sigma Aldrich).

### Synthesis & calibration of the nanocube sensor

Silica coated silver nanocubes were prepared as reported in our previous publication.[27] The silver nanocube synthesis was based on the polyol method. The silica shell synthesis over nanocubes was performed in a scaled-up synthesis batch using 2-propanol as solvent. The quality of the nanocube sensor, including silica shell thickness, nanocube size and uniformity, was confirmed by transmission electron microscopy (FEI Technai G2 F20 FE-TEM). (Figure. 2) The

refractive index sensitivity of silica coated silver nanocubes was reported as peak shift (reported in nm) per refractive index unit (RIU). (Figure. 3) Since the change in refractive index is directly proportional to the amount of bound proteins, LSPR peak shift allows an estimation of the amount of protein bound[81].

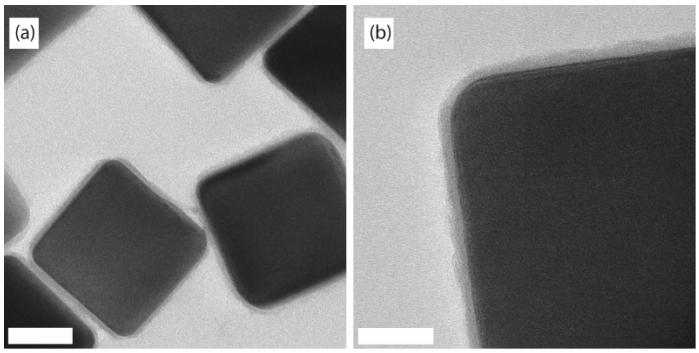


Figure 2: TEM images of silica shell coated onto the Ag nanocubes. Scale bar = (a) 40nm and (b) 20nm. Reprinted from reference 26.

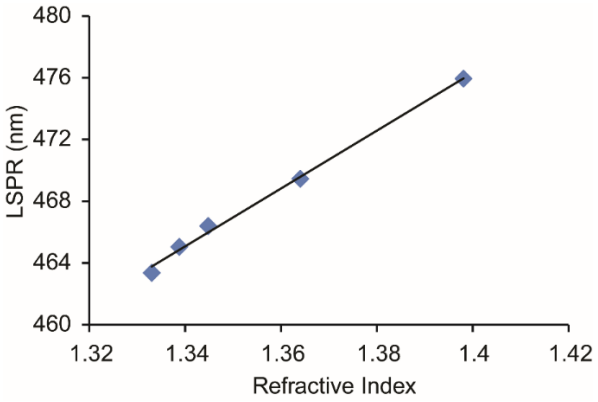


Figure 3: Sensor sensitivity characterization. Change in quadrupole LSPR peak location vs. Refractive Index (RI) using silica coated silver nanocubes in various glycerol-water mixtures measured with a spectrophotometer. The slope is 187.44 nm/RIU. Reprinted from reference 26.

**Supported lipid bilayer preparation**

Lipids stored in organic solvents (chloroform for DOPC, DOPS, DMPC, and DMPS or chloroform/methanol/water mixture for glycolipids) were mixed to obtain the desired final composition. They were then dried using a rotary evaporator (Heidolph Hei-VAP Value®), followed by rehydration with Milli-Q® water. Small unilamellar vesicles (SUVs) were prepared by the standard extrusion protocol described in our prior publication.[27] A previously established modified vesicle fusion technique[27] was used to form supported lipid bilayers. The lipid bilayer coated nanocubes were incubated with 0.5 mg/ml casein in 1X TBS solution for 1 hour to prevent nonspecific binding of CTB.

**CTB binding measurement**

The lipid bilayer coated nanocubes were incubated with the required CTB concentration for 1.5 hours. Blank solutions were also prepared for each CTB concentration by mixing buffer and CTB corresponding to that composition. The extinction spectra of the solutions were measured in a 384 well plate with a UV/Vis microplate spectrophotometer equipped with a CCD (FLUOstar Omega®, BMG-Labtech). All measurements were carried out at room temperature, except the membrane fluidity experiment involving DMPC. The location of the quadrupolar LSPR peak was calculated by fitting the measured absorption spectra to a seventh order polynomial. Each protein binding measurement was repeated in eleven wells. Each data point is represented as the mean ± standard deviation (S.D.) where n = 11. The experimental conditions for each binding measurement are described below.

*Combinatorial glycolipid array*: To acquire binding curves for pure glycolipid systems (1 mol% glycolipid along with 89 mol% DOPC and 10 mol% DOPS), the CTB concentration was varied

from 0 to 1726 nM. For the binary mixture of glycolipids (1 mol% of each glycolipid along with 88 mol% DOPC and 10 mol% DOPS), the CTB concentrations used were 706 nM and 1726 nM.

*GM1os pre-bound CTB binding experiment*: 345 nM CTB was incubated at various sugar (GM1os) concentrations (0 ~ 38.1 μM) prior to the binding measurement. The resulting GM1os-CTB complex was incubated with the bilayer containing 2 mol% glycolipid along with 88 mol% DOPC and 10 mol% DOPS.

*Membrane Perturbation protocol*: The reference bilayer comprised of 0.25 mol% of each glycolipid (GM1, GM2, GM3, fucosyl-GM1 and GD1b), 10 mol% DOPS and 88.75 mol% of DOPC. For the perturbed membranes, one of the glycolipids was increased to 2 mol% while other glycolipids were maintained at 0.25 mol% along with 10 mol% DOPS and 87 mol% DOPC. Each experiment was treated with 0.5 mg/ml Casein in 1X TBS buffer to block non-specific binding and then incubated with 1726 nM CTB for 2 hours.

## Results

### CTB binding to glycolipid pairs

Our previous study demonstrated that mixing GM2, a weak binding receptor, with fucosyl-GM1 could enhance the overall CTB binding.[27] In order to understand the mechanism of the hetero-multivalency, we constructed a combinatorial array of glycolipids to evaluate cooperativity of CTB binding. The array was composed of glycolipids like GM1, GM2, GM3, fucosyl-GM1, and GD1b (Figure. 4a). We first examined CTB binding to model membranes containing 1 mol% of a glycolipid (Figure. 4b). The shift in the location of the LSPR peak with respect to the control is directly proportional to the amount of CTB bound. CTB exhibited significant binding to the bilayers containing GM1, fucosyl-GM1, or GD1b. (Figure. 4b) GM2 and GM3 showed negligible binding with CTB even at the highest CTB concentrations (1726

nM); this result is consistent with prior studies.[84,90] Thus, we categorized GM1/fucosyl-GM1/GD1b as strongly binding receptors and GM2/GM3 as weakly binding receptors.

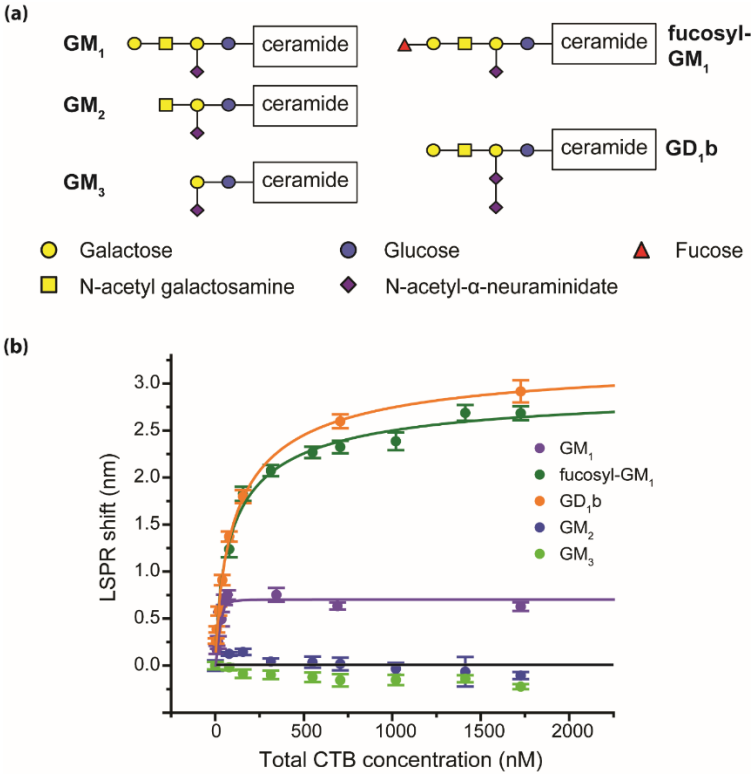


Figure 4: Homo-multivalent CTB binding. (a) Structures of glycolipids used in the study. (b) Equilibrium binding of CTB to pure glycolipids. The glycolipid composition in each case was 1 mol%. Data points are reported as mean ± S.D (n = 11). Reprinted from reference 26.

The combinatorial array was prepared by mixing two glycolipids in a 1:1 ratio (1 mol% of each glycolipid). The amount of CTB bound to the glycolipid mixtures was measured at two different CTB concentrations (706 nM and 1726 nM). From the CTB-glycolipid binding curves (Figure. 4b), we can see that CTB binding to the model membrane is approximately saturated at 1726 nM. Thus, we used this value to estimate the maximum binding capacity of the model

membrane. We also measured the CTB binding at a lower CTB concentration (706 nM) to observe the influence of CTB concentration on binding cooperativity.

To quantify the binding cooperativity of hetero-multivalency, we have defined heterogeneous binding cooperativity (θ) as:

$$\theta = \frac{\text{LSPR shift when CTB binds to a bilayer containing paired glycolipids}}{\text{Sum of LSPR shift when CTB binds to a bilayer containing each individual glycolipid}} \quad \text{Equation 1}$$

Table 1: Calculated heterogeneous binding cooperativity between two glycolipids. Column and row headings represent the mixture of two glycolipids. Each cell contains two values that represent the calculated cooperativity at the two CTB concentrations, 706 nM (top)/1726 nM (bottom). Cooperativity values are reported as mean ± S.D (n = 11). The raw data of CTB binding was reported in Figure. 5. Reprinted from reference 26.

| GM1 | fucosyl-GM1 | GD1b | GM2 | GM3 | |
|---|---|---|---|---|---|
| | 1.08 ± 0.03<br>1.12 ± 0.03 | 0.92 ± 0.02<br>1.05 ± 0.04 | 1.46 ± 0.17<br>1.99 ± 0.28 | 1.16 ± 0.26<br>0.92 ± 0.20 | GM1 |
| | | 0.94 ± 0.02<br>1.10 ± 0.03 | 1.57 ± 0.07<br>1.54 ± 0.09 | 1.19 ± 0.06<br>1.11 ± 0.04 | fucosyl-GM1 |
| | | | 2.06 ± 0.08<br>1.96 ± 0.10 | 1.05 ± 0.05<br>0.98 ± 0.05 | GD1b |
| | | | | 1.00 ± 0.77<br>1.00 ± 0.12 | GM2 |
| | | | | | GM3 |

If there is no cooperativity between two glycolipids, θ should equal 1. When θ is larger or smaller than 1, it represents positive or negative cooperativity, respectively. The calculated heterogeneous cooperativity was reported in Table 1. We observed positive cooperativity when GM2 was mixed with any of the strongly binding receptors (GM1, fucosyl-GM1, and GD1b) at both CTB concentrations. Since negligible CTB binding was observed with the model membrane

surface containing GM2 as the only glycolipid receptor, the strongly binding receptors seemed to have activated GM2 receptors which led to a higher CTB binding. However, no significant cooperativity was observed when GM3 was mixed with strongly binding receptors. In addition, cooperative action between strong receptors was negligible.

**Possible causes of heterogeneous cooperativity**

To the best of our knowledge, positive cooperativity between GM2 and other glycolipid receptors has not yet been reported. Several possible reasons may cause this heterogeneous cooperativity, including induced glycolipid cluster formation, allosteric regulation, and reduction of dimensionality. Each hypothesis has been considered and discussed in the following.

Cremer and his coworkers have demonstrated that increasing GM1 density in a model membrane induces the formation of GM1 clusters, leading to weaker CTB binding.[91] If mixing GM2 had induced the disturbance of glycolipid clusters leading to increased CTB binding, the addition of other glycolipids should have altered the clustering of glycolipid receptors and caused some change in binding cooperativity. However, we observed cooperative interactions only between GM2 and other strongly binding glycolipids. Furthermore, the glycolipid concentration was kept relatively low (less than 2 mol%) to minimize any heterogeneous distribution of glycolipids on the membrane surface. Therefore, we believe that it is less likely for induced heterogeneity to be the major cause of positive cooperativity.

Allosteric regulation is another possible cause of positive cooperativity. The bound glycolipids (GM1/fucosyl-GM1/GD1b) could have enhanced the binding energy between GM2 and its adjacent binding sites, enabling GM2 to participate in the CTB binding process and leading to a higher binding capacity (Figure. 6a). To test this hypothesis, we modified the saturation binding assay developed by Leach et al. for detection of allosteric interactions.[92]

Klassen and his coworkers have reported that at the equilibrium state CTB forms a binding complex with GM1 oligosaccharide (GM1os), an allosteric modulator that contains the same glycan structure as the GM1 glycolipid without its ceramide tail.[93] We first incubated CTB with various concentrations of GM1os oligosaccharide Then, we measured the binding of GM1os-CTB complex to a model membrane containing 2 mol% glycolipid (GM2 or fucosyl-GM1) at a fixed CTB concentration (345 nM) (Figure. 6b). If the bound GM1os had altered the energetics of the adjacent CTB binding subunit, the allosteric effect should have initiated the attachment of GM1os-CTB complex to the membrane containing GM2. Instead, negligible CTB binding to the lipid bilayer having GM2 was still observed. For the lipid bilayer containing 2 mol% of fucosyl-GM1, the amount of bound GM1os-CTB complex decreased with increased GM1os concentration (Figure. 6b). This is due to competitive binding between GM1os and fucosyl-GM1 receptors. In addition, three different research groups independently evaluated the allosteric effect of GM1os-CTB binding and found that the affinity constants increased by only twofold when the neighboring binding sites were occupied.[32,93,94] Turnbull et al. have estimated the dissociation constant for CTB binding with GM2 to be 2 mM. Thus, even twofold enhancement of affinity constant (leading to ~1mM dissociation constant) is not sufficient to promote CTB binding to GM2 at the physiological concentrations. Although we cannot completely exclude the allosteric regulation between GM2 and other strong receptors, it is probably not the major cause for the observed positive cooperativity.

Another possible cause for positive heterogeneous cooperativity is the influence of reduced dimensionality. Searching for reaction partners is much more efficient on a two-dimensional membrane surface than in 3D space. In 1968, Adam and Delbrück first proposed that organisms can shorten the diffusion time of dilute reactants by adsorption to cell membrane

surfaces in order to enhance the reaction rates of the biological processes.[95] Many researchers have validated this concept and provided a comprehensive theory to describe this mechanism.[96-101] Recently, Sengers et al. also reported that reduced dimensionality can improve the binding efficiency of a bivalent monoclonal antibody interaction with membrane bound targets by about $10^4$-fold.[102] Thus, it is possible that reduction of dimensionality enhanced the CTB binding to GM2.

**The influence of reduced dimensionality**

We hypothesized that CTB first moves from the solution phase to the membrane surface and attaches to one of the strongly binding receptors (GM1, fucosyl-GM1, and GD1b). Jobling et al. have shown that a single active binding site on CTB pentamer is sufficient for cell binding and intoxication;[103] therefore, we expected CTB could form a relatively stable membrane-bound state with a single strongly binding receptor (Figure. 1). Once CTB is anchored to the surface, the effective concentration of GM2 on 2-D membrane surface dramatically increases for subsequent bindings. Although the weak binding between GM2 and CTB implies a short lifetime of the CTB-GM2 complex, the enhanced effective concentration allows GM2 to continuously participate in the process to bind to CTB leading to an increase in binding capacity. This hypothesis requires the presentation of a strongly binding receptor in order to anchor CTB to the membrane surface.

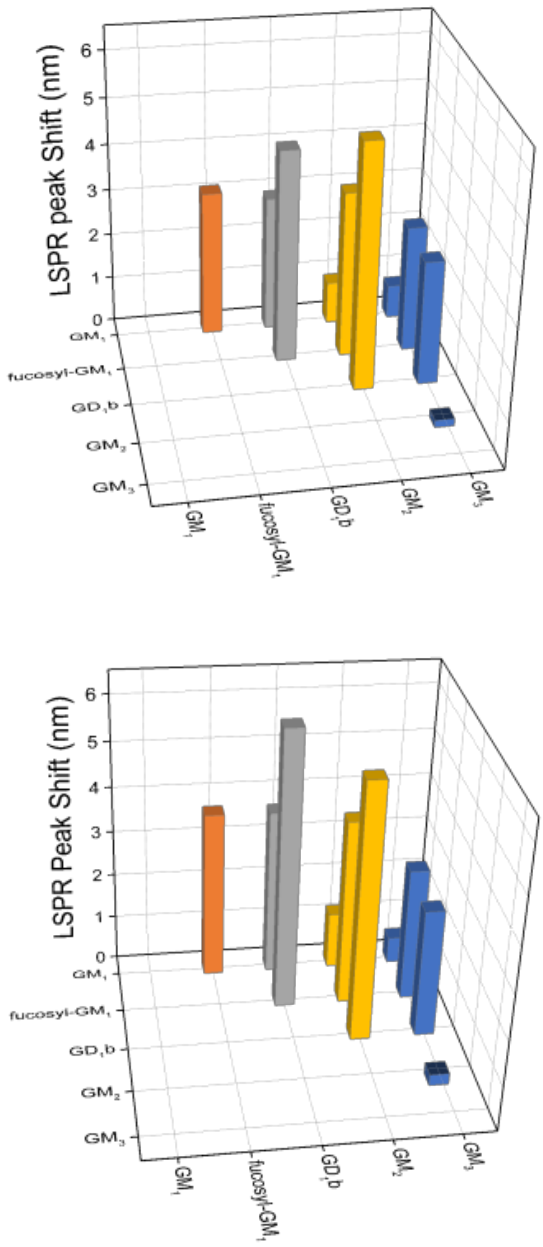


Figure 5: Equilibrium binding of CTB to membrane surfaces containing two glycolipids in a 1:1 mole ratio (1 mole% of each glycolipid). The CTB concentration used was (a) 706 nM, (b) 1726 nM. Reprinted from reference 26.

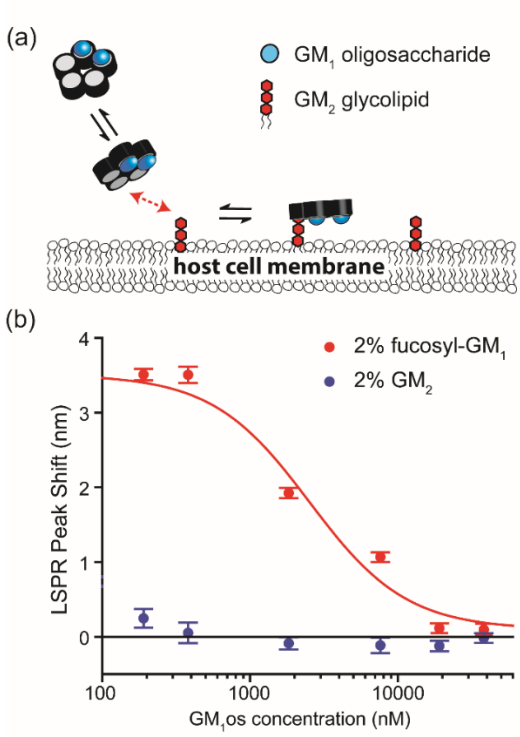


Figure 6: Evaluation of allosteric effect. (a) A schematic of the allosteric regulation hypothesis. CTB was incubated with $GM_1$os to form a $GM_1$os-CTB complex. Then, this $GM_1$os-CTB complex was bound to a model membrane containing $GM_2$. If $GM_1$os modulated the energetics of the adjacent CTB binding pocket, the attachment of $GM_1$os-CTB complex to the membrane containing $GM_2$ should be detectable. (b) Binding of CTB-$GM_1$os complex to membrane surfaces containing 2 mol% fucosyl-$GM_1$ and 2 mol% $GM_2$. Binding of CTB-$GM_1$os complex to the $GM_2$ surface was still negligible; thus, allosteric regulation may not be a major cause of the enhanced CTB binding. Data are reported as mean ± S.D. (n=8). Reprinted from reference 26.

In order to verify this hypothesis, we first evaluated the 2D and 3D reaction rates using the established theoretical models.[99-101] The reaction rate, $\phi$, can be written as[100]:

$$\phi = k_{obs} C_A C_B \qquad \text{Equation 2}$$

Where $C_A$ and $C_B$ are the number densities of the two reactants, and $k_{obs}$ is the empirical rate constant. In diffusion controlled reactions, $k_{obs}$ is a function of diffusion coefficients ($D_{3D\ or\ 2D}$), the radius of diffusion spaces ($b$), and the encounter radius of the target receptor ($a$). Based on our experimental conditions, the bulk concentration of CTB (species A) and glycolipid

(species B) were estimated as: $C_A = 3 \times 10^{-7}\ mol/L$, $C_B = 3 \times 10^{-7}\ mol/L$. 3D diffusivities of CTB and glycolipid containing liposome were estimated using the Stokes-Einstein equation as $D_{A,3D} = 9.77 \times 10^{-11}\ m^2/s$ and $D_{B,3D} = 4.88 \times 10^{-12}\ m^2/s$. The measured diffusivity of bound CTB was acquired from literature ($D_{A,2D} = 2.5 \times 10^{-13}\ m^2/s$).[104,105] The DOPC lipid diffusivity was $D_{B,2D} = 8.25 \times 10^{-12}\ m^2/s$.[106] Using different fluorescent labeling approaches, previous researchers have also reported the diffusivity of GM1 in DOPC bilayer to be around $3.6\sim8 \times 10^{-12}\ m^2/s$.[107,108]

We estimated the 3D reaction rate using Smoluchowski's relation which gives a steady-state rate constant for fast reactions,[100]

$$k_{obs,3D} = 4\pi a(D_{A,3D} + D_{B,3D}) \qquad \text{Equation 3}$$

Prior studies derived the approximate solution of $k_{obs}$ for 2D membrane reactions using Smoluchowski theory, mean-passage time theory, and statistical thermodynamic theory (the models are summarized in Supplementary Note).[99-101] Based on our experimental conditions, we found that the 2D reaction rate can be up to $10^4$ higher than 3D reactions. The increased reaction rate implies that effective concentration of reactants on the membrane surface is enhanced by about $10^4$-fold. This calculated enhancement factor has the same order of magnitude of the value in antibody system reported by Sengers et al.[102] In such a case, the reduction of dimensionality could raise the effective GM2 concentration close to or higher than the dissociation constant of CTB-GM2 (2mM). Thus, it is possible that this significant enhancement of reaction rate between bound CTB and GM2 led to higher CTB binding.

To further verify this hypothesis, we altered the diffusivity of glycolipids by replacing DOPC with DMPC that has a gel phase transition temperature near room temperature (24 °C). We conducted the measurements of CTB binding to DMPC model membranes with 1 mol%

GM1 and GM1:GM2 mixture (1 mol%:1 mol%) at 15 °C and 45 °C. In the DOPC bilayer, which has transition temperature at -20 °C,[109] the cooperativity between GM1 and GM2 at 15 °C was quite similar to what we obtained at room temperature, which implies that such a temperature change does not alter CTB binding much (Figure 7). However, the diffusion of glycolipids in DMPC gel phase is two orders of magnitude lower when compared to the fluidic DMPC membrane.[110,111] Goins et al. reported GM1 diffusivity to be approximately 1-2 x $10^{-13}$ $m^2/s$ in DMPC below 20 ℃.[112] Under this condition, the 2D reaction rate is only 400-500 times higher than the 3D reaction rate in DMPC gel phase. Thus, we expected that the rate enhancement via reduced dimensionality would be minimized in the DMPC system at 15 °C. Figure. 7 shows that mixing GM2 with GM1 in a DMPC bilayer did not enhance the overall CTB binding at 15 °C; in contrast, binding enhancement was observed in fluidic DMPC bilayer at 45 °C. This result further corroborates our hypotheses that reduction in dimensionality is influencing the binding of CTB with heterogeneous mixtures of glycolipids.

In addition, 10 mol% of cholesterol was added to DOPC bilayer in order to alter the fluidity and the heterogeneity of model membranes. Similar to the DMPC system, changing the membrane environment altered the heterogeneous binding cooperativity (Figure. 7). This result is not surprising because many studies have shown the compositions of fatty acids and cholesterol in host cells can influence the toxin potency.[113,114] Previous studies have also reported that surface diffusion and heterogeneity can influence the homo-multivalent CTB-GM1 binding.[115] Our result indicated that the membrane environment is also essential in hetero-multivalent binding process.

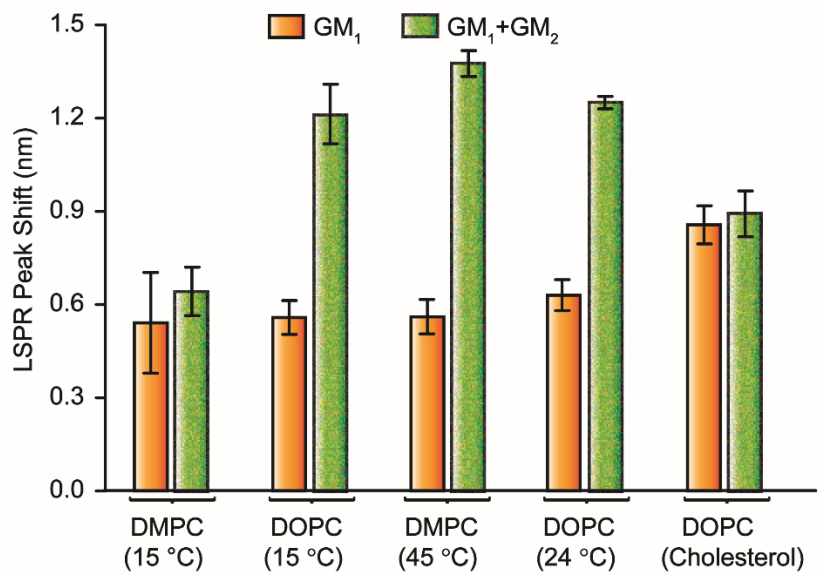


Figure 7: CTB binding to single glycolipid (orange) or paired glycolipids (green) in different membrane environments. DMPC/DMPS (15 °C), DOPC/DOPS (15 °C), DMPC/DMPS (45 °C), DOPC/DOPS (room temperature) or DOPC/DOPS/cholesterol (room temperature)) The heterogeneous binding cooperativity between $GM_1$ and $GM_2$ depends on the fluidity and heterogeneity of membranes. Data points are reported as mean ± S.D (n = 11). Reprinted from reference 26.

The other question is why mixing GM3 with the other receptor did not enhance CTB binding. The only difference in the structure of GM2 and GM3 is that GM2 contains an additional N-acetyl galactosamine (GalNAc) in its glycan portion. The crystal structure of CTB-GM1 complex indicates that the sugar groups of galactose (Gal), GalNAc, and sialic acid (Neu5Ac) in GM1 were buried in the CTB binding subunit and contribute to 39%, 17%, and 43% of the contact surface area respectively.[116] CTB binding to GM3 that has only one Neu5Ac epitope should be weaker than GM2 receptor. In fact, Turnbull et al. estimated the dissociation constant for α-methyl sialoside, which contains only Neu5Ac epitope, to be 210 mM[32]. Even though the mechanism of reduced dimensionality could increase the reaction rate around $10^4$-fold, the effective concentration of GM3 on membrane surfaces is still far below the dissociation

constant between CTB and sialic acid residual. Therefore, it wasn't surprising that no cooperativity was found between GM3 and the other binding receptors.

**A new perturbation protocol for screening glycolipid receptors**

One of the difficulties in observing hetero-multivalency is that some receptors, such as GM2, only exhibit significant binding when they form a partnership with other receptors. Traditional ligand-receptor binding assays (e.g. microarray technology) cannot reflect such hetero-multivalency because they screen only one specific receptor at a time. Thus, the contribution of GM2 was often ignored since CTB binding to pure GM2 was only detected at the CTB concentration far beyond physiologically relevant conditions. To address this issue, previous studies have developed combinatorial arrays that mix two different receptors in 1:1 ratio[77]. However, this labor-intensive method cannot observe hetero-multivalent binding involving more than two receptors.

In order to efficiently discover receptor candidates for multivalent binding proteins, we designed a new membrane perturbation protocol. This protocol first involves constructing a membrane that contains all receptor candidates with known compositions as a reference. The reference membrane is then perturbed by increasing the density of a desired glycolipid receptor. If a specific receptor can either directly bind to the target protein or indirectly form a binding complex with the assistance of other glycolipids; the perturbation will alter the overall protein binding irrespective of the mechanism.

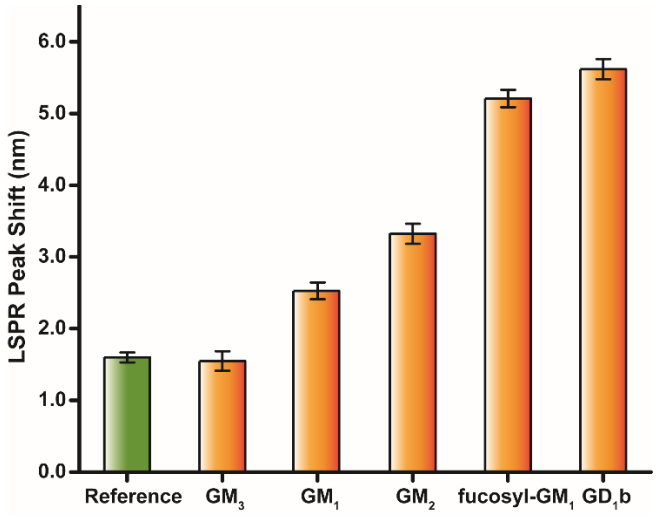


Figure 8: The demonstration of membrane perturbation protocol. 1726 nM CTB was bound to the reference and perturbed membranes that preserved all receptor candidates. The reference membrane contained 88.75 mol% DOPC, 10 mol% DOPS, 0.25 mol% of each GM1, GM2, GM3, GD1b and fucosyl-GM1. The reference membrane was perturbed by increasing the density of a specific glycolipid to 2 mol%. Data points are reported as mean ± S.D (n = 11). Reprinted from reference 26.

As a proof-of-concept, we constructed a reference membrane consisting of GM1, GM2, GM3, fucosyl-GM1, and GD1b (0.25 mol% of each glycolipid). We then perturbed the reference membrane by increasing one of the glycolipid receptor to 2 mol%. The CTB binding to the reference membrane and each perturbed membrane is shown in Figure. 8. As expected, CTB binding was significantly enhanced when the densities of GM1, fucosyl-GM1, and GD1b were increased. The positive binding cooperativity between GM2 and the other glycolipids present in the reference membrane also enhanced the overall CTB binding. In addition, increasing GM3 density did not enhance CTB binding. Thus, we could exclude GM3 as a CTB receptor candidate without conducting the entire combinatorial array measurement. In order to identify receptors of multivalent protein from a large library of molecules, this perturbation method can be more efficient than combinatorial glycolipid arrays.

## Discussion

In this study, significant enhancement of CTB binding was observed when a strongly binding receptor was mixed with a weakly binding receptor (GM2). When investigated further, the reduction of dimensionality looks like the most likely cause. If this mechanism is valid, a fraction of bound CTB should simultaneously bind to GM2 and other strong binding receptors. Most recently, Klassen and his coworkers demonstrated the same heterogeneous binding cooperativity using catch-and-release electrospray ionization-mass spectrometry (CaR-ESI-MS) assay.[62,63] Mass spectrometry allows identifying the types of receptors binding to CTB. Using CaR-ESI-MS assay, Klassen and his coworkers observed that CTB could bind to very weak binding receptors GM2 and GM3 when 7 different glycolipids (GM1, GM2, GM3, $GD_1a$, GD1b, GD2, and GT1b) were mixed in either picodiscs or micelles systems, but no binding was observed when GM2 or GM3 was the only receptor. Their results provide evidence that CTB can directly bind to weakly binding receptors when they are mixed with strongly binding receptors. It is worth noting that we did not observe binding cooperativity between GM1 and GM3, but Klassen and his coworkers observed CTB binding to GM3. This is probably due to the difference of lipid bilayer conditions. In our experiment, surface density of glycolipid receptor was maintained at 1mol%. CaR-ESI-MS assay mixed 7 glycolipid receptors equally resulting in 14 mol% of each glycolipid. The reaction enhancement via reduced dimensionality was higher in CaR-ESI-MS assay; thus, it is not surprising that Klassen and his coworkers observed CTB binding to GM3.

Reduction of dimensionality provided a potential mechanism to answer a long-standing question, why CTB binding does not correlate with GM1 level on cell surfaces.[117] Yanagisawa et al. observed strong reactivity between CTB and embryonic neuroepithelial cells in the absence of

GM1.[36] Kirkeby stained GM1 with CTB and anti-GM1 antibody, and found that both labeling reagents were not co-localized.[39] In addition, GM1 is of very low abundance (0.0015-0.003 mol% of glycosphingolipids) in human small intestinal epithelial cells[37]; thus, a recent publication raised a question, whether GM1 is sufficient to induce cholera toxin attachment.[38] In the reduction of dimensionality model, high-affinity receptors can serve as initiators, and then activate weak receptors, leading to higher retention of CTB on the cell surface. Thus, the overall CTB binding is not simply controlled by a single GM1 receptor; the weakly binding receptors can contribute to CTB binding via reduction of dimensionality. Surface diffusion and local density of membrane receptors can influence the 2D reaction rate, membrane fluidity and heterogeneity (i.e. lipid raft) which can also play essential roles in CTB binding process.

The mechanism of reduced dimensionality has also been used to explain unexpected phenomena in various multivalent binding studies.[85,87,102] For example, Mazor et al. observed that the binding avidity of a bispecific antibody to receptors confined in cell membrane surfaces were significantly higher than the binding avidity to free receptors in solution.[60] Sengers et al. established a mathematical model based on the reduced dimensionality hypothesis to describe the mechanism of bivalent antibody binding to heterogeneous membrane targets, and estimated that the effective affinity of bivalently bound antibody can be enhanced by approximately 4 orders of magnitude.[102] These studies, combined with our own CTB binding measurements suggest the importance of the role of reduced dimensionality in multivalent protein-cell membrane recognition. Further kinetic studies are necessary in order to verify the hypothesis and establish a comprehensive model of hetero-multivalent recognition.

Since the complex interplay between multiple membrane receptors is critical, we also developed a new membrane perturbation protocol to efficiently screen receptor candidates. This

protocol measured CTB binding to perturbed membranes that preserve all receptor candidates; therefore, the interplay between different receptors can be monitored. This new protocol is more efficient in screening the potential receptors than the combinatorial array, which detects proteins binding to the binary mixture of glycolipids. For example, if we plan to screen 20 receptor candidates, the membrane perturbation protocol required only 21 measurements instead of 190 measurements in a combinatorial array.

## Supplementary Information

### Calculation of Reduction of Dimensionality

As described in the main text, the reaction rate, $\phi$, can be written as equation 2[100]. The reactant concentrations are measured in either units of $mol/m^3$ for bulk reactions or $mol/m^2$ for surface reactions. Thus, the 3D reaction rates ($\phi_{3D}$) are in units of $mol/(m^3 \cdot \sec)$; on 2D membrane surface, the unit of reaction rate ($\phi_{2D}$) is $mol/(m^2 \cdot \sec)$. To evaluate the difference between 3D and 2D reactions, the 2D reaction rate was multiplied by a constant $S/V$ in order to covert the surface concentration to volume concentration. $S$ is the total surface area of the outer leaflet of liposome confined in volume $V$. Using the DOPC lipid footprint in bilayer of 0.72nm$^2$,[106] the total surface area of outer leaflet of liposome containing 1 mol % of glycolipid can be estimated:

$$\frac{S}{V} = \left(\frac{C_{B,3D}}{1\%}\right) \cdot N_A \cdot 0.72nm^2/2 = 6.5 \times 10^3 m^{-1} \qquad \text{Equation 4}$$

Thus, the reaction events per volume per time occurring on 2D membrane surfaces is: $\phi_{2D} \cdot (S/V)$

In order to consider the influence of diffusion processes, we estimated the reaction rate in diffusion controlled reactions. For 3D reactions, Smoluchowski equation gives equation 3[95,100].

Here, we assumed the encounter radius is equivalent to the head group size of DOPC in bilayer ($\sqrt{0.72nm^2/\pi} = 0.48nm$). 3D diffusivities of CTB and glycolipid containing liposome were estimated using Stokes-Einstein equation. ($D_{A,3D} = 9.77\,\text{x}10^{-11}\ m^2/s$ and $D_{B,3D} = 4.88\,\text{x}10^{-12}\ m^2/s$)

For 2D reactions, prior studies derived several analytical solutions using various approaches. We selected three classic models to evaluate the approximate reaction rate on 2D membrane surfaces. [99-101] Hardt employed the approximate solution of mean diffusion time derived by Adam and Delbrück[95] and calculated the 2D reaction rate[99]:

$$k_{obs,2D} = 2\pi N_A \left( \frac{D_{A,2D}}{ln\frac{1}{a\sqrt{\pi N_A C_{B,2D}}}} + \frac{D_{B,2D}}{ln\frac{1}{a\sqrt{\pi N_A C_{A,2D}}}} \right) \qquad \text{Equation 5}$$

where $D_{A,2D}$ and $D_{B,2D}$ are the 2D diffusivity of CTB and glycolipid obtained from the literatures ($D_{A,2D} = 2.5 \times 10^{-13}\ m^2/s$ and $D_{B,2D} = 8.25 \times 10^{-12}\ m^2/s$).[104-106] $C_{A,2D}$ and $C_{B,2D}$ are the surface densities (unit:$mol/m^2$).

Szabo et al. applied the first passage time approach to evaluate the surface reaction rate.[101] Keizer showed the solution for diffusion controlled reactions:[100]

$$k_{obs,2D} = 2\pi D'/(ln(b/a) - 3/4) \qquad \text{Equation 6}$$

where $D' = D_{A,2D} + D_{B,2D}$, and $b$ represents the diffusion distance. If CTB serves as the sink for the glycolipid, we can obtain $b = \sqrt{1/\pi N_A C_{A,2D}}$.[99]

Keizer reported a similar formula for $k_{obs,2D}$ using a statistical thermodynamic theory:

$$k_{obs,2D} = 2\pi D'/(ln(b/a) - \gamma + ln\sqrt{2})$$ Equation 7

where $\gamma$ is the Euler's constant = 0.5772. In our experiments, the glycolipid concentration ($C_{B,3D}$) was controlled at 300 nM. Considering 300 nM of CTB, the 2D reaction rate is around $10^4$ higher than 3D reaction rate. ($\phi_{2D} \cdot (S/V)/\phi_{3D} =$ ~8,000 for equation 5, ~13,000 for equation 6, and ~9,000 for equation 7. Even if we consider the diffusivity value of $GM_1$ reported in literature [107,108], the 2D reaction rate is still 5000-10000 times higher than the 3D reaction rate. At higher CTB concentrations ($C_{A,3D} = 700nM$), the 2D reaction rate could be up to 20,000 times higher than the 3D reaction rate. In general, the reduction of dimensionality mechanism can enhance 2D reaction rate by 3~4 orders of magnitude.

## Conclusion

In summary, we elucidated the essence of hetero-multivalency in CTB-cell membrane recognition using a high-throughput and easy-to-use nanocube sensors. We believe that the detection protocols presented here can provide a systematic and efficient strategy to investigate multivalent protein-cell membrane recognition.

# CHAPTER III

# HETERO-MULTIVALENCY OF *PSEUDOMONAS AERUGINOSA* LECTIN LECA BINDING TO MODEL MEMBRANES[‡]

## Chapter Summary

A single glycan-lectin interaction is often weak and semi-specific. Multiple binding domains in a single lectin can bind with multiple glycan molecules simultaneously, making it difficult for the classic "lock-and-key" model to explain these interactions. We demonstrated that hetero-multivalency, a homo-oligomeric protein simultaneously binding to at least two types of ligands, influences LecA (a *Pseudomonas aeruginosa* adhesin)-glycolipid recognition. We also observed enhanced binding between *P. aeruginosa* and mixed glycolipid liposomes. Interestingly, strong ligands could activate weaker binding ligands leading to higher LecA binding capacity. This hetero-multivalency is probably mediated via a simple mechanism, Reduction of Dimensionality (RD). To understand the influence of RD, we also modeled LecA's two-step binding process with membranes using a kinetic Monte Carlo simulation. The simulation identified the frequency of low-affinity ligand encounters with bound LecA and the bound LecA's retention of the low-affinity ligand as essential parameters for triggering hetero-multivalent binding, agreeing with experimental observations. The hetero-multivalency can alter lectin binding properties, including avidities, capacities, and kinetics, and therefore, it likely occurs in various multivalent binding systems. Using hetero-multivalency concept, we also offered a new strategy to design high-affinity drug carriers for targeted drug delivery.

[‡] Reproduced from Ref. 29 with permission from Scientific Reports

## Introduction

*Pseudomonas aeruginosa* is a ubiquitous and opportunistic bacterium. The increase of antibiotic resistance worldwide limits therapeutic options, leading to high morbidity and mortality of *P. aeruginosa* infections.[118,119] One mechanism that *P. aeruginosa* uses to cause disease is adhesion to epithelial cells.[120-123] Adhesion of *P. aeruginosa* is mediated by surface adhesins, including LecA (i.e. PA-IL), LecB (i.e. PA-IIL), and Type IV Pilus (T4P), which bind to glycan ligands on epithelial cell surfaces.[124-128] In addition to their role in adhesion, LecA and LecB can influence host cell functions.[128-133] Thus, it is essential for us to understand the binding mechanisms for *P. aeruginosa* adhesins to host cell ligands in order to gain insight into strategies to combat infections.

In this article, we first focus on LecA, a homotetrameric lectin, where each monomer has a single glycan binding site.[134] LecA contains two adjacent binding site pairs facing in opposite directions. (Figure.1) This conFigureuration allows adhesion of *P. aeruginosa* to epithelial cells and may also contribute to linkages between bacteria, subsequently leading to biofilm formation.[126,135] It is known that LecA prefers binding to α-galactose terminated glycolipids; typically, globotriaosylceramide (i.e. Gb3, Galα1-4 Galβ1-4 Glc ceramide) is considered a major ligand for LecA.[134,136-141] However, it is known that LecA can bind to other types of glycolipids (e.g. β-galactose (Galβ) and N-acetylgalactosamine (GalNAc) terminated glycolipids), but the binding affinities are lower than with Gb3.[139,142]

We recently reported a hetero-multivalent binding phenomenon for cholera toxin subunit B (CTB) in an environment that mimics the natural cell membrane.[26,27] Interestingly, we found that strong binding ligands could activate weak binding ligands via a fundamental mechanism,

Reduction of Dimensionality (RD).[26] We illustrate the concept of RD in Figure. 9. The reaction rates of the subsequent binding events on the membrane surface are at least $10^4$ times higher than the first binding event.[26] Thus, even a weak binding ligand can now participate in the second or higher order binding events resulting in higher protein attachment. This intrinsic mechanism suggests that the binding of multivalent proteins is not simply controlled by a single type of ligand; instead, the cooperative actions between strong and weak ligands can greatly influence the overall attachment of proteins and bacteria.

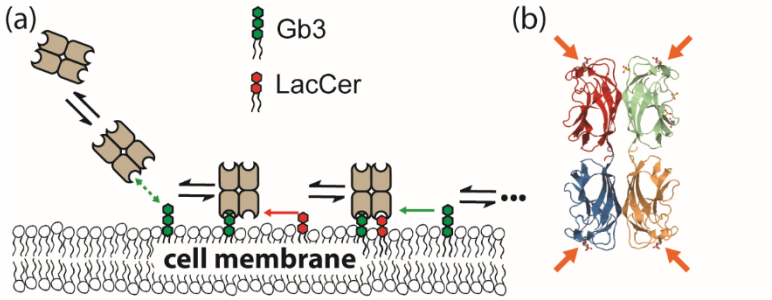


Figure 9: Schematic for the Reduction of Dimensionality (RD) model. a) A schematic representation of RD influencing LecA interactions with the cellular membrane. LecA first diffuses from solution to a membrane surface and attaches to the high-affinity ligand, Gb3. Then, free membrane ligands move two dimensionally, enabling subsequent binding. The reduced dimensionality of diffusion enhances the effective concentrations of membrane ligands; thus, a weak ligand, such as LacCer, can contribute to LecA binding. (**b**) Graphical representation of LecA complexed with galactose as observed in the crystal structure (PDB code 1OKO)[136]. Four binding sites are indicated by arrows. Protein and carbohydrate are displayed in a cartoon representation with coloring done by subunit using JSmol. Reprinted from reference 29.

We hypothesized that the RD mechanism plays a key role in *P. aeruginosa* adhesion by influencing many different multivalent proteins, including LecA. Although Gb3 is the major LecA ligand, Gb3 is at low levels in human intestinal epithelial cells and murine lungs.[37,143] We suspect that Gb3 can activate abundant but weaker glycolipid ligands, influencing LecA

attachment via the RD mechanism. We examined hetero-multivalency in LecA binding through analysis of hetero-multivalent binding cooperativities between major and minor LecA binding ligands. We were excited to find that high-affinity ligands were able to activate weak binding ligands, leading to positive hetero-multivalent cooperativity. Moreover, we designed a high-affinity liposome containing mixed ligands to target *P. aeruginosa* using the concept of the RD mechanism. Our study suggests that the inherent RD mechanism may play an essential role in various multivalent recognition systems.

## Materials and methods

### Materials

Ammonium hydroxide, bovine serum albumin Fraction V (BSA), copper (II) chloride dihydrate, ethanol, Pluronic F-127, polyvinylpyrrolidone (MW ~55,000) (PVP), tetraethyl orthosilicate (TEOS), silicone oil (useable range -50°C to +200°C) and tris-buffered saline (TBS) obtained as a 10x solution (1x working solution 20 mM Tris 0.9% NaCl pH ~7.4) were purchased from Sigma-Aldrich (St. Louis, Missouri). Silver(I) nitrate Premion® grade and the agar used for the LB agar plate, obtained as a powder, were purchased from Alfa-Aesar (Tewksbury, Massachusetts). 2-Propanol (iPA) and Texas Red™ 1,2-dihexadecanoyl-sn-glycero-3-phosphoethanolamine, triethylammonium salt (TR-DHPE) was purchased from Fisher Scientific (Pittsburgh, Pennsylvania). 1,5-Pentanediol (PD) was purchased from Acros Organics (Geel, Belgium). PA-IL from *Pseudomonas aeruginosa* (also known as LecA) was purchased from Elicityl (Crolles, France). 5.04 μm silica beads were purchased from Bangs Laboratories, Inc. (Fishers, Indiana). Calcium chloride was from BDH VWR Analytical (Radnor, Pennsylvania). The TBS solution used in bacterial binding was made using Tris from Research Products International, Corp. (Mt. Prospect, Illinois). The NaCl used to make the bacterial

binding TBS solution along with the powder for Luria-Bertani (LB) broth were from Amresco (Solon, Ohio). HCl, ACS guaranteed reagent, for the bacterial binding TBS solution was obtained from EMD (Billerica, Massachusetts). Globotriaosylceramide, Gb3 and Lactosylceramide, LacCer, (Galβ1-4Glc-Ceramide) were purchased from Matreya, LLC. (State College, PA). 1-palmitoyl-2-oleoyl-sn-glycero-3-phosphocholine (POPC) and 1-palmitoyl-2-oleoyl-sn-glycero-3-phospho-L-serine (sodium salt) (POPS) were purchased from Avanti Polar Lipids (Alabaster, AL).

**Nanocube Synthesis**

The nanocube synthesis procedure is originally from Tao et al.[144] The silver nanocubes were synthesized via the polyol method which uses PVP as a structure-directing agent. In brief, the procedure was as follows. First, 0.2 g of $AgNO_3$ was dissolved into 10 mL of PD along with 30 μL of 82 mg/L $CuCl_2$ in PD. Next, 20 mL of PD was added to a 100 mL round bottom flask that was then heated to 130 °C with stirring in a 190°C silicon oil bath. After reaching 130 °C in the flask, 250 μL of the $AgNO_3$ solution along with 500 μL of a 20 g/L PVP in PD solution was added to the flask followed by a second addition of 500 μL from both the $AgNO_3$ and PVP solutions 35 seconds later. Then every following minute, 500 μL of each solution was added to the reactor until the solution turned a deep red color, about 15 minutes. After achieving a deep red color, the reaction was then allowed to cool and was washed by centrifugation using 200 proof ethanol.

The silica coating procedure was originally described in Wu et al.[81] and modified by Worstell et al.[27] First, 20 mL of the silver nanocube solution was washed into iPA via centrifugation and then added to a 250 mL round bottom flask along with 55 mL of iPA, 22.1 mL of MilliQ® water, 6.8 mL of TEOS, and 3.4 mL of 0.84% ammonium hydroxide. Next, the

mixture was stirred at room temperature for 60 minutes before 50 mL of ethanol was added to stop the reaction. After stopping the reaction, the silica coated cubes were centrifuged and reconstituted in 75 mL of iPA. The solution was then returned to the round bottom flask along with 22.1 mL of MilliQ® water, and 6.8 mL of TEOS. This solution was incubated at 60 °C for 10 hours before being washed with MilliQ® water. The silica coated nanocubes were stored in MilliQ® water at room temperature until use.

**Vesicle Preparation**

Small unilamellar vesicles (SUVs) were prepared via extrusion.[27] The procedure, in brief, is as follows. First, the desired compositions of lipids in chloroform solutions, prepared as per manufacturers recommendations, were mixed in a 25 mL round bottom flask and, then, dried using a rotary evaporator (Heidolph Hei-VAP Value®). Next, the dried lipids were reconstituted using MilliQ® water and extruded through a 100 nm polycarbonate filter (Whatman®) using a mini-extruder (Avanti Polar Lipids) resulting in a 3 g/L SUV solution.

**Supported Lipid Bilayer Formation on Ag@SiO2 Nanocubes**

Supported lipid bilayers were formed on the nanocubes using a modified vesicle fusion method.[27] 100 μL of the 3 g/L SUV solution was added to a 0.5 mL Eppendorf ® tube and vortex mixed for 20 seconds. Then, 10 μL of a concentrated nanocube solution was added to the tube and the tube was vortex mixed for 1 second. Following this, 110 μL of 2x TBS was added to the tube and vortex mixed for one second. These last two steps were repeated pipetting 10 μL of concentrated nanocube solution and 10 μL of 2x TBS each time until 100 μL of the nanocube solution was consumed. Then, the tube was vortex mixed for an additional 10 seconds and diluted with 1x TBS with 100 μM $CaCl_2$ to the desired nanocube concentration.

**Nanocube Protein Binding Measurement**

Bilayer coated nanocubes were incubated for 1 hour with 31.3 μL of 0.5 g/L BSA per 1250 μL of nanocube solution to reduce nonspecific binding. Then, the desired amount of LecA was added. For these experiments, 10 mol% POPS/90 mol% POPC lipid bilayer was used as a control. After addition of LecA, the test, control, and blank solutions were vortex mixed for 10 seconds each and pipetted as 20 μL aliquots into wells of a 384 well plate, 8 wells for the test, 4 wells for the control, and 4 wells for the blank solutions for each LecA concentration tested. Finally, the plate was read using a UV/Vis microplate reader spectrophotometer equipped with a CCD (FLUOstar Omega®, BMG-Labtech) to collect the extinction spectra every 13.3 minutes for a total of 80 minutes at room temperature. The resulting spectra were the results of averaging 200 flashes per well at a 1 nm resolution. The location of the quadrupole LSPR (Localized Surface Plasmon Resonance) peak (LSPR peak) was determined by 5$^{th}$ order polynomial fitting. The resulting LSPR peak shift was calculated from the average LSPR peak location of the 8 wells and then subtracted by the LSPR shift of the control lipid bilayer to give the total LSPR shift. It is worth noting that in contrast to single-molecule imaging technique, the solution phase nanocube sensors measure the ensemble average of LecA binding events by collecting averaged binding profiles from nearly a million of nanocubes in the solution[81]. This nullifies the effect of variation in LecA distribution over nanocubes.

The saturation binding curves were fit by the Hill-Waud binding model[91]

$$\Delta\lambda_{LSPR} = \frac{V_m[LecA]^n}{K_h^n + [LecA]^n} \qquad \text{Equation 8}$$

where $K_h$ is the Hill's equation apparent dissociation constant, $n$ is the Hill cooperativity coefficient, [LecA] is the concentration of LecA, and $V_m$ is the maximum $\Delta\lambda_{LSPR}$ of the fully bound state. $\Delta\lambda_{LSPR}$ is the observed LSPR peak shift, which corresponds to the attachment of

LecA on the lipid bilayer surface. To quantify the cooperative binding effect, we modified the heterogeneous cooperativity defined in our recent paper[26]:

$$\text{heterogeneous cooperativity } (\phi) = \Delta\lambda_{mix} - \sum_i \Delta\lambda_{pure,i} \quad \text{Equation 9}$$

where $\Delta\lambda_{mix}$ is the LSPR shift when LecA binds to a bilayer containing two different glycolipids, and $\Delta\lambda_{pure,i}$ is the LSPR shift when LecA binds to a bilayer containing the correspondent individual glycolipid, $i$. If no enhancement is observed between two different glycolipids, the $\phi$ value should be approximately zero. A positive (or negative) $\phi$ value indicates positive (or negative) cooperativity.

**P. aeruginosa Liposomal Targeting**

Four kinds of fluorescent liposomes were prepared, i) 99 mol% POPC /1 mol% TR-DHPE, ii) 89 mol% POPC/10 mol% Gb3/1 mol% TR-DHPE, iii) 89 mol% POPC/10 mol% LacCer/1 mol% TR-DHPE and iv) 89 mol% POPC/5 mol% Gb3/5 mol% LacCer/1 mol% TR-DHPE. Lipids stored in organic solvents (chloroform for POPC or a chloroform/methanol/water mixture for glycolipids) were mixed to obtain the desired final composition. They were then dried using a rotary evaporator (Heidolph Hei-VAP Value®), followed by rehydration with Milli-Q® water. SUVs were prepared by the standard extrusion protocol described in our prior publications.[26,27] The filters used for extrusion were Whatman® Track-Etched Nucleopore™ membrane having 19 mm diameter and 100 nm pore size.

*P. aeruginosa* strains PAO1/pJDC233 and Xen41 were cultured overnight in 3 ml LB medium at 37°C with shaking at 200 rpm and grown to an $OD_{600}$ = 1.0. Cells were diluted 100 fold in LB, and 100 µl of this was added into 96 well plates (Greiner Bio-One µClear® product number 655096) and incubated at 37°C without shaking for 48 hours. Planktonic cells were carefully pipetted out, and attached cells were washed twice with TBS buffer (50 mM Tris-HCl,

pH 7.6, 150 mM NaCl). After the washes, 100 µl of TBS buffer with 100 µM $CaCl_2$ containing Gb3, POPC, LacCer or Gb3/LacCer liposomes at different concentrations (0.3, 0.15, 0.0725 and 0 g/L) was added into 96 well plates and incubated at 37°C for 2 hours to facilitate liposome binding to bacterial cell membranes. Gentle rinsing with TBS buffer, twice, washed unbound liposomes away and bacterial cells were re-suspended in 100 µl of TBS with 100 µM $CaCl_2$ and mixed by through pipetting. The fluorescent signals of the liposome bound bacteria were detected using fluorescent spectrophotometer (EnVision™ 2104 Multilabel Reader, PerkinElmer®) at an Excitation/Emission wavelength of 580nm/620nm, respectively. Bacterial enumeration was performed by using 10-fold serial dilutions and plating on solid media (LB agar plate made from LB broth and 1.5% agar) to establish bacterial cell count (CFU/mL). The bacterial-liposome binding was represented as fluorescence signal per total number of bacteria. Each experiment was done in triplicate and the average value and standard error are reported.

**Statistical Analysis and Regression**

The data comprising each binding curve is given as a mean ± standard deviation (S.D.) where n = 8. The Hill-Waud model was then fit to the data for each binding curve via the Levenberg Marquardt algorithm in OriginPro 9.1® (OriginLab). This returned the calculated value, standard error, and $R^2$ value as well as the residuals, studentized residuals, and studentized deleted residuals. The parameter values and standard errors are reported in Table 2.

The *P. aeruginosa* liposomal binding data sets were tested for normality using the Kolmogrov-Smirnov test in OriginPro 9.1®. In all cases, we could not reject the null hypothesis that the data came from normal distributions. Therefore, it was reasonable to apply Welch's unequal variances t-test to the data.

Table 2: Hill's equation parameters obtained by fitting in OriginLab. A * indicates that fitting was highly uncertain due to the data not reaching a plateau and – indicates fitting did not converge. The values are represented as a mean±SE (where the standard error of the fit is based on fitting through 96 points for each curve). Reprinted from reference 29.

| **Lipid Compositions (mol%)** | | | | **Fitted Parameters** | | | |
|---|---|---|---|---|---|---|---|
| **Gb3** | **LacCer** | **POPS** | **POPC** | **$V_m$ (μM)** | **$K_h$ (μM)** | **n** | |
| 1 | 0 | 10 | 89 | 1.53 ± 0.02 | 0.09 ± 0.00 | 2.68 ± | |
| 0 | 4 | 10 | 86 | - | - | - | * |
| 0 | 8 | 10 | 82 | $6.41*10^3$ ± | $3.76*10^6$ ± | 0.65 ± | * |
| 1 | 1 | 10 | 88 | 1.83 ± 0.04 | 0.12 ± 0.01 | 1.08 ± | |
| 1 | 2 | 10 | 87 | 2.81 ± 0.04 | 0.11 ± 0.01 | 1.39 ± | |
| 1 | 4 | 10 | 85 | 3.18 ± 0.04 | 0.17 ± 0.01 | 1.16 ± | |
| 1 | 8 | 10 | 81 | 3.75 ± 0.04 | 0.13 ± 0.00 | 1.35 ± | |

**Kinetic Monte Carlo (kMC) Simulation**

The kMC algorithm was implemented to model the kinetics of LecA binding to a membrane containing both high-affinity and low-affinity ligands.[145,146] The surface of lipid bilayer is modelled as a 250-by-250 square lattice sites (i.e. 212x212 $nm^2$) with a periodic boundary condition, and ligands are randomly distributed on the surface. The details of the kMC simulation are described below.

*Microscopic Phenomena of kMC*: The LecA-ligand binding kinetics are described by five microscopic phenomena as follows:

- Ligands and LecA-ligand complexes on a lipid bilayer surface migrate due to the fluidity of the lipid bilayer
- LecA proteins diffuse within the solution.
- If a LecA is sufficiently close to a ligand on the surface, LecA can attach to the surface by binding to the ligand.

- A membrane-bound LecA binds to an additional ligand if the bound LecA has an unfilled binding site and a ligand is sufficiently close to the LecA.
- A ligand can dissociate from a membrane-bound LecA, and the LecA will detach from the lipid bilayer after all ligands dissociate from it.

For the purpose of this study, the above descriptions are simplified with the following two assumptions. First, the simulation domain is restricted to two-dimensions. To this end, the transport of LecA proteins to and from the surface via diffusion is described by effective association and dissociation rate constants from the literature. Second, because the diffusivity of membrane-bound lectins is almost two orders of magnitude lower than the glycolipid ligand,[105] we assume LecA-ligand complexes on the surface are immobile.

*Surface kinetics:* As a LecA molecule has two binding sites facing a membrane surface, the LecA molecule will bind to or dissociate from ligands in a stepwise manner, which results in 12 reactions to be considered in the kMC simulation (Figure. 10). The steps from solution-phase LecA to membrane-bound LecA were treated by the effective rate constants $k_{f,H}$, $k_{f,L}$, $k_{r,H}$, and $k_{r,L}$ (the second subscripts, H and L, represent the rate constant corresponding to high-affinity and low affinity ligands). First, the attachment and detachment rates are defined as:

$$r_{a,H} = 2k_{f,H}CR_H, \qquad r_{a,L} = 2k_{f,L}CR_L, \qquad r_{d,H} = k_{r,H}B_{1,0}, \qquad r_{d,L} = k_{r,L}B_{0,1} \qquad \text{Equation 10}$$

where $r_a$ is the attachment rate from solution to the surface, $C$ is the LecA concentration in solution, $r_d$ is the LecA detachment rate from the membrane to solution, $R$ is the number of ligand, and $B_{i,j}$ is the number of LecA binding to $i$ and $j$ number of high-affinity and low-affinity ligands. Here, a factor of two is multiplied because a LecA protein is symmetric molecule with two identical binding sites.

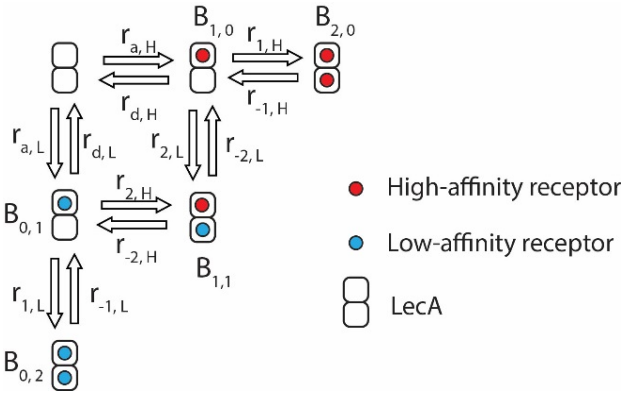


Figure 10: The schematic diagram for LecA- ligand binding kinetics. Bi,j is a LecA bound to i and j number of high-affinity and low-affinity ligands, respectively. Reprinted from reference 29.

Since a LecA can take up to two ligands in a membrane, a membrane-bound LecA can associate with or dissociate from additional ligands, which are termed as forward and backward reactions, respectively, hereafter (Figure. 10). The reaction rates of these surface binding events on the membrane are computed as follows

$$\mathrm{r_{1,H}} = \mathrm{k_{1,H}B_{1,0}R_H}, \quad \mathrm{r_{1,L}} = \mathrm{k_{2,L}B_{0,1}R_L}, \quad r_{-1,H} = 2\mathrm{k_{-1,H}B_{2,0}},$$

$$r_{-1,L} = 2\mathrm{k_{-1,L}B_{0,2}}$$

$$\mathrm{r_{2,H}} = \mathrm{k_{1,H}B_{0,1}R_H}, \qquad \text{Equation 11}$$

$$\mathrm{r_{2,L}} = \mathrm{k_{1,L}B_{1,0}R_H}, \; r_{-2,H} = \mathrm{k_{-1,H}B_{1,1}}, \; r_{-2,L} = \mathrm{k_{-1,L}B_{1,1}}$$

where $\mathrm{k_1}$ and $\mathrm{k_{-1}}$ are the forward and backward reaction rate on membrane surface.

Finally, the ligand migration rate is defined as[145,146]

$$\mathrm{r_{m,k}} = \mathrm{R_k}\frac{\mathrm{k_{m,k}}}{\mathrm{l^2}}, \forall\, k \in \{\text{'H', 'L'}\} \qquad \text{Equation 12}$$

where $\mathrm{k_{m,k}}$ is the migration rate constant of ligand $k$, and l is the distance between two lattice sites.

*Kinetic Monte Carlo Implementation:* An event is selected based on a random number and the total reaction rate, $r_t$, which is defined as

$$r_t = \sum_{k\in H,L} r_{a,k} + r_{d,k} + r_{-2,k} + r_{-1,k} + r_{1,k} + r_{2,k} + r_{m,k} \quad \text{Equation 13}$$

In order to execute an event, a uniform random number, $\xi_1 \in [0,1)$, is sampled. If $\xi_1 \leq r_{a,L}/r_t$, the attachment event with low-affinity ligand is selected. If $r_{a,L}/r_t < \xi_1 \leq (r_{a,L} + r_{d,L})/r_t$, the detachment event with low affinity ligand is selected. If $(r_{a,L} + r_{d,L})/r_t < \xi_1 \leq (r_{a,L} + r_{d,L} + r_{1,L})/r_t$, the forward reaction from $B_{0,1}$ to $B_{0,2}$ is selected. If $(r_{a,L} + r_{d,L} + r_{1,L})/r_t < \xi_1 \leq (r_{a,L} + r_{d,L} + r_{1,L} + r_{-1,L})$, the backward reaction from $B_{0,2}$ to $B_{0,1}$ is selected to occur; if , $(r_{a,L} + r_{d,L} + r_{1,L} + r_{-1,L})/r_t < \xi_1 \leq (r_{a,L} + r_{d,L} + r_{1,L} + r_{-1,L} + r_{-2,L})$, the backward reaction from $B_{1,1}$ to $B_{0,1}$ is selected; if $(r_{a,L} + r_{d,L} + r_{1,L} + r_{-1,L} + r_{-2,L})/r_t < \xi_1 \leq (r_{a,L} + r_{d,L} + r_{1,L} + r_{-1,L} + r_{-2,L} + r_{2,L})/r_t$, the forward reaction from $B_{1,0}$ to $B_{1,1}$ is selected; if $(r_{a,L} + r_{d,L} + r_{1,L} + r_{-1,L} + r_{-2,L} + r_{2,L})/r_t < \xi_1 \leq (r_{a,L} + r_{d,L} + r_{1,L} + r_{-1,L} + r_{-2,L} + r_{2,L} + r_{m,L})/r_t$, the migration event of lower affinity ligand is selected. Inequalities for selecting events related to high-affinity ligands can be written similarly, which are not shown here.

When an attachment event ($r_{a,k}$) is selected, a free ligand of type $k$ is randomly selected to associate with an incoming LecA protein. After a ligand for binding is selected, it is required to check whether there is enough free space around the selected ligand for the LecA molecule without overlapping with other LecA molecules that are already bound to the host cell membrane. If there is not enough space for an incoming LecA molecule, the attachment will be rejected. As the membrane becomes more crowded with an increasing number of membrane-bound LecA molecules, the available space for an additional LecA to attach to the host cell membrane decreases significantly; hence, the rejection rate will increase accordingly.

When a detachment event ($r_{d,k}$) is selected, one LecA molecule bound to one ligand of type $k$ is randomly selected and the LecA molecule dissociates from the ligand. Whenever

attachment or detachment events occur, the concentration of LecA in solution is updated via a mass balance by counting the number of proteins undergoing attachment and detachment processes.

When a forward reaction event on the membrane surface is selected, a free ligand of the corresponding type will bind to a LecA molecule attached to a ligand. Here, it is required to check whether there are any free ligands sufficiently close to the selected binding site, which is determined by the distance between the binding site and free ligands on the membrane. If the distance is smaller than the threshold distance ($l_c$), the corresponding ligand is classified as a free ligand that can bind with the LecA molecule. If there are no ligands close to the selected binding site, the forward reaction will not occur; if there is more than one available ligand, a ligand is randomly selected for the binding event.

Similarly, when a backward reaction event occurs, one bound LecA molecule is randomly selected, and one of its bound ligands is randomly chosen for dissociation.

When a migration event ($\mathrm{r}_{m,\mathrm{k}}$) happens, one free ligand of type $k$ is randomly selected and moves to one of its neighbouring empty sites.

After one event is selected and proceeds as described above, the time increment for the selected event is calculated by generating a new random number $\xi_2 \in [0,1)$, and the time increment is computed as follows[147]

$$\tau = -\frac{\ln \xi_2}{r_t} \qquad \text{Equation 14}$$

and the simulation will proceed by $t + \tau$ seconds. The kMC simulation is written in C#, and 50 trials are computed to calculate the average kinetics.

*Parameter Selection:* The distance between two lattice sites (l) is 0.85nm, which is equivalent to the head group size of DOPC in bilayer ($\sqrt{0.72nm^2} = 0.85nm$).[106] Because the size of a LecA subunit is ~2nm, we used 3nm for the value of the threshold radius ($l_c$). The nominal parameters for the high-affinity and low affinity ligands are listed in Table 3. The migration constant ($k_{m,k}$) of ligands was estimated by the average DOPC lipid diffusivity ($8.25 \times 10^{-12}\ m^2/s$).[106] The kinetic constants of LecA are not available. Lauer et al. analyzed the binding kinetics of cholera toxin subunit B (CTB) using the stepwise binding model, allowing us to estimate the kinetic constants. For the high-affinity ligand, $k_f$ and $k_r$ were acquired from the fundamental forward and reverse rate constants reported by Lauer et al. ( $k_1$ and $k_{-1}$ in the reference[84]). Because the dissociation constants are associated with releasing the binding between LecA and its ligands, we assume $k_r = k_{-1}$. $k_1$ is the surface forward rate constant without the contribution of reactants' surface diffusion; thus, we cannot use the fitted surface rate constant reported by Lauer et al. Instead, we used the parameter estimated by the interaction of membrane-bound antibody-antigen complexes reported by Sengers et al.[102] Because the equilibrium dissociation constant of the antibody-antigen system is an order of magnitude lower than LecA binding system, we chose $k_1 = 0.07\ \mu m^2 s^{-1} molecule^{-1}$, instead of the value ($0.7\ \mu m^2 s^{-1} molecule^{-1}$) reported by Sengers et al.[102] We reduced the forward rate constants ($k_f$ and $k_1$) 100-, 300-, and 1000-fold for the low-affinity ligands. The other rate constants of the low-affinity ligand remained same as the high-affinity ligands. It is worth noting that we have varied the rate constants two-orders of magnitude higher and lower to observe the influence of parameter selection. The results indicated that the qualitative phenomenon of hetero-multivalency remains the same as what was described in the main text.

Table 3: Nominal parameter values used in the kMC simulation. Reprinted from reference 29.

| | High-affinity ligand | Low-affinity ligand (100-fold weaker) | Low-affinity ligand (300-fold weaker) | Low-affinity ligand (1,000-fold weaker) |
|---|---|---|---|---|
| $k_f\ (M^{-1} \cdot s^{-1})$ | $2.8 \times 10^4$ | $2.8 \times 10^2$ | $9.3 \times 10^1$ | $2.8 \times 10^1$ |
| $k_r\ (s^{-1})$ | $3.2 \times 10^{-3}$ | $3.2 \times 10^{-3}$ | $3.2 \times 10^{-3}$ | $3.2 \times 10^{-3}$ |
| $k_1\ (\mu m^2 s^{-1})$ | $7 \times 10^{-2}$ | $7 \times 10^{-4}$ | $2.3 \times 10^{-4}$ | $7 \times 10^{-5}$ |
| $k_{-1}\ (s^{-1})$ | $3.2 \times 10^{-3}$ | $3.2 \times 10^{-3}$ | $3.2 \times 10^{-3}$ | $3.2 \times 10^{-3}$ |
| $k_m\ (m^2/s)$ | $8.25 \times 10^{-12}$ | $8.25 \times 10^{-12}$ | $8.25 \times 10^{-12}$ | $8.25 \times 10^{-12}$ |

## Results

Prior studies have shown that the presentation of glycan, such as oligosaccharides in solution, oligosaccharides on glycoarray surface, or glycolipids in cell membranes, can dramatically change the LecA binding.[138,139,148] In the glycoarray and glycolipid binding studies, LecA's preferred ligand is known to be Gb3, but LecA can also bind to βGal terminated glycans[19,21,139,142,148,149]. LecA significantly bound to the bilayer containing 1 mol% Gb3. At the same density, LecA-AGM1 and LecA-GM1 binding was much weaker[29]. We could not observe LecA binding to LacCer surfaces unless the LacCer density was increased to 8 mol%. Based on these results, Gb3 is a strong ligand LacCer is a weak ligand.

**Positive binding cooperativity between strong and weak ligands (Gb3 & LacCer)**

Based on the RD model, we expected that strong ligands will activate weak ligands, leading to higher binding capacity for LecA. To demonstrate this concept, we first measured LecA binding to the mixtures of Gb3 and LacCer. Keeping the density of Gb3 in the bilayer

fixed at 1 mol%, we performed telescoping concentrations of LacCer in the bilayer (Figure. 11a). LecA binding to pure 4 mol% surface density of LacCer was not measureable, and the binding at the highest LecA concentration (3μM LecA) to pure 8 mol% LacCer is minimal. (Figure. 11b) After mixing LacCer with 1 mol% of Gb3, LecA binding to mixtures of Gb3 and LacCer was significantly higher than LecA binding to 1 mol% of Gb3. We can use hetero-multivalent cooperativity ($\phi$ in equation 9) to quantify the enhanced binding capacity. In Figure. 11a, no obvious positive cooperativity was observed when 1 mol% Gb3 was mixed with 1 mol% LacCer, but cooperativity drastically increased at 2 mol% of LacCer. This result seems indicating that the surface density of the weak ligand has to reach a threshold value in order to contribute in LecA binding.

In addition to the threshold density of the weak ligand, we identified a second threshold of LecA concentration. Figure. 12 shows the changes in cooperativity at different LecA concentrations. The average cooperativity is minimal below 0.1 μM LecA but then increases until beginning to level off around 2 μM LecA. In the RD model, LecA has to first anchor to Gb3 in order to change from 3-D to 2-D diffusion, leading to an increased effective concentration of the weak ligand for the subsequent binding events. Thus, this hetero-multivalent binding process is limited by the first binding step, which corresponds to the dissociation constant of Gb3 (0.1 μM). This is probably the reason why the observed cooperativity significantly increased above the dissociation constant. Based on the RD mechanism, the same hetero-multivalent binding cooperativity was observed between Gb3 and other glycolipid ligands, GalβCer, GalNAc, GM1 and AGM1[29].

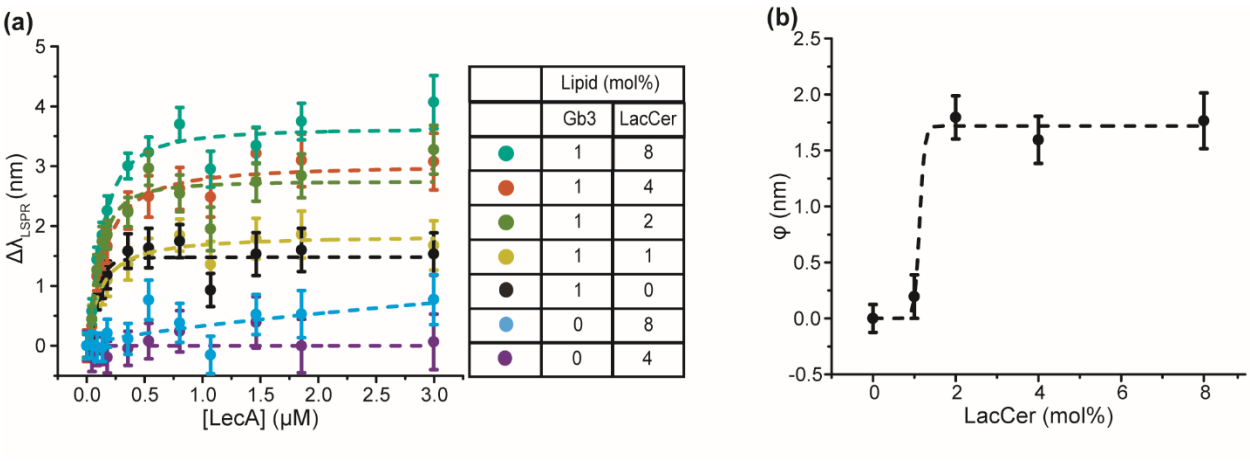


Figure 11: Saturation binding curves of LecA binding to common galactose terminated glycolipids and Gb3/LacCer mixtures that show positive cooperativity. The saturation binding curves' dash lines represent the curve fits to Hill's equation, fitted parameters are listed in Table 2. (a) Saturation binding curves of LecA binding to bilayers containing Gb3/LacCer mixtures. (b) $\phi$ values for 1 mol% of Gb3 mixed with different densities of LacCer. Dash line representing the fit of $\phi$ to the sigmoidal function is a guide to the eye. Data are reported as mean ± S.D. (n=8). Reprinted from reference 29.

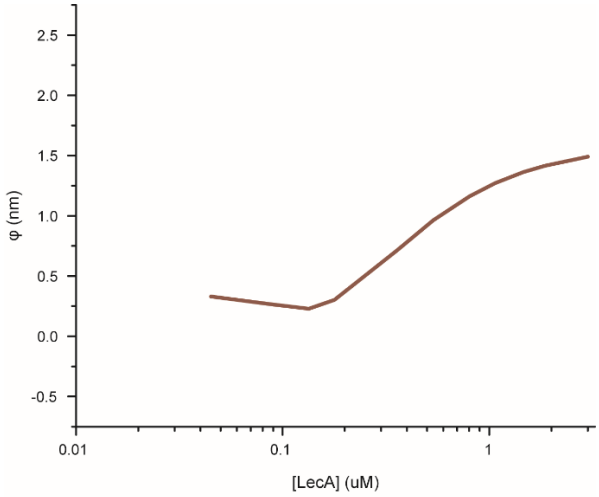


Figure 12: Calculated ϕ values at various [LecA] for a 1/4 mol% Gb3/LacCer mixture. Reprinted from reference 29.

**Explore the RD Mechanism Using Kinetic Monte Carlo (kMC) Simulation**

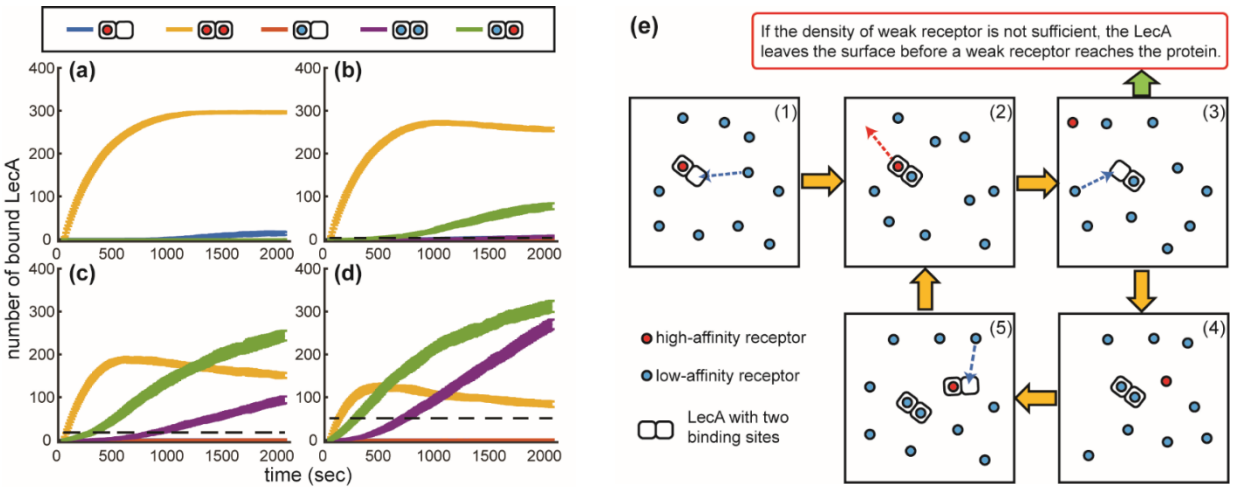


Figure 13: Modeling LecA binding kinetics using kMC simulation. LecA binding to a membrane surface containing 1 mol% of high-affinity ligands and various low-affinity ligand densities, (a) 0 mol%, (b) 0.5 mol%, (c) 3 mol%, and (d) 9 mol%. The affinity of the low-affinity ligand is 300-fold lower than the high-affinity ligand. ($K_{d,low}$=300$Kd_{,high}$ where $K_d$=$k_{-1}$/$k_1$) Each curve represents the number of bound LecA in different binding conFigureurations. The dashed line shows the maximum number of bound LecA at 2000 s without the high-affinity ligand at the same membrane density of low-affinity ligand. All data represented as average ± S.D from 50 kMC simulations. (**e**) A binding mechanism observed in the kMC simulation when the low-affinity ligand density is higher than the high-affinity ligand. (1) A LecA molecule moves from the solution phase to the membrane surface, and attaches to a high-affinity ligand. Then, a low-affinity ligand encounters the bound LecA completing the hetero-multivalent binding. (2) The high-affinity ligand dissociates from the bound LecA. (3) LecA binding to one low-affinity ligand is relatively unstable. At sufficient density, a low-affinity ligand can reach the free binding site before the LecA dissociates from the surface. (4) LecA binding to two low-affinity ligands is relatively stable. (5) The high-affinity ligand can facilitate the binding between LecA and low-affinity ligands by continuing the same process. (The Figure. shows only two binding sites that are participating in reactions happening on the surface. The other two binding sites facing in the opposite direction are not shown). Reprinted from reference 29.

We hypothesized that the RD mechanism is the cause of the observed hetero-multivalency.[26] To further understand the influence of the RD mechanism, we performed a kMC simulation to model the stepwise binding of LecA. (Figure. 13) The kMC simulation allows us to monitor the bound state of each individual LecA molecule; therefore, we can validate our

hypothesis. The kMC simulation conducted on a two dimensional square with 250-by-250 square lattice sites (i.e. 212x212 $nm^2$) represents the lipid bilayer. Glycolipid ligands are modeled as entities that can diffuse on a 2-dimensional membrane. Similar to the binding process shown in Figure. 11a, only two of the binding sites are exposed to one membrane surface at a time. Thus, the kMC simulation allows for two LecA binding sites attaching to and detaching from glycolipid ligands. The microscopic forward/reverse binding rate constants ($k_1$ and $k_{-1}$) between a high-affinity ligand (i.e. Gb3) and a LecA were estimated using literature values (parameter selection is described in the Supplementary information). The density of the high-affinity ligand was fixed at 1 mol%, and the density of the low-affinity ligand was varied from 0.5 to 9 mol%. The rate constants of low-affinity ligands were defined by reducing the forward rate constants of the high-affinity ligand 100-, 300-, and 1000-fold. (Figure. 14)

In most cases, we observed ~90% of bound LecA attaching to two ligands. Due to reduced dimensionality of diffusion, the frequency of a ligand encountering a bound LecA dramatically increases; thus, LecA could rapidly find a second ligand on the membrane surface and complete the second binding. When a membrane contained strong ligands without weak ligands (Figure. 13a), the number of total bound LecA reached an equilibrium at ~1000 s. When 0.5 mol% of the weak ligands were mixed with 1 mol% of the strong ligands (Figure. 13b), hetero-multivalent binding occurred. Initially, the majority of LecA bound to two strong ligands. After the density of the unbound high-affinity ligand was reduced to one-third of the density of the unbound low-affinity ligand (~500 s), we could observe a significant portion of the low-affinity ligands contributing to LecA binding, leading to the increased binding capacity. Obviously, when the densities of the low-affinity ligands were raised (Figure. 13c & 13d), the low-affinity ligands could participate in LecA binding at an early time point.

Most surprisingly, we also observed a significant number of LecA molecules simultaneously binding to two low-affinity ligands. Without the high-affinity ligand, we could not observe the same number of LecA binding to the bilayer at the same densities of low-affinity ligands. Figure. 13e shows the mechanism behind this phenomenon. A high-affinity ligand initiates attachment of LecA to the membrane surface; then, LecA can bind to an additional ligand or exchange bound ligands on the 2D membrane surface. However, a LecA molecule bound to only one low-affinity ligand will only maintain its bound state if it receives an unbound low-affinity ligand before the LecA molecule dissociates from the membrane.

It is obvious that the affinity of weak ligands can influence the hetero-multivalent binding process. (Figure. 14) When the affinity of weak ligands was decreased, the contribution of weak ligand to LecA binding reduced. For example, at 3 mol% density of weak ligand, weak ligands contributed 55%, 44%, and 31% of the LecA bound ligands for 100-, 300-, and 1000-fold reduced affinity, respectively. To enhance the contribution of the weak ligand, the density of weak ligand should be increased. This also corroborates our experimental observation that a threshold concentration of the weak ligand is required to enable its contribution in protein binding. Another noticeable phenomenon is that LecA binding to the mixed bilayer requires longer time to reach an equilibrium state. This is because the rearrangement of the bound ligands requires multiple stepwise reactions.

It is worth noting that the kMC simulation considers a simple two-step binding process without complex biological assumptions, such as ligand clustering, membrane curvature, or allosteric regulation. We still observed the same degree of hetero-multivalent binding cooperativity in the kMC simulation and the nanocube measurement, demonstrating the essence of the RD mechanism in hetero-multivalent binding systems.

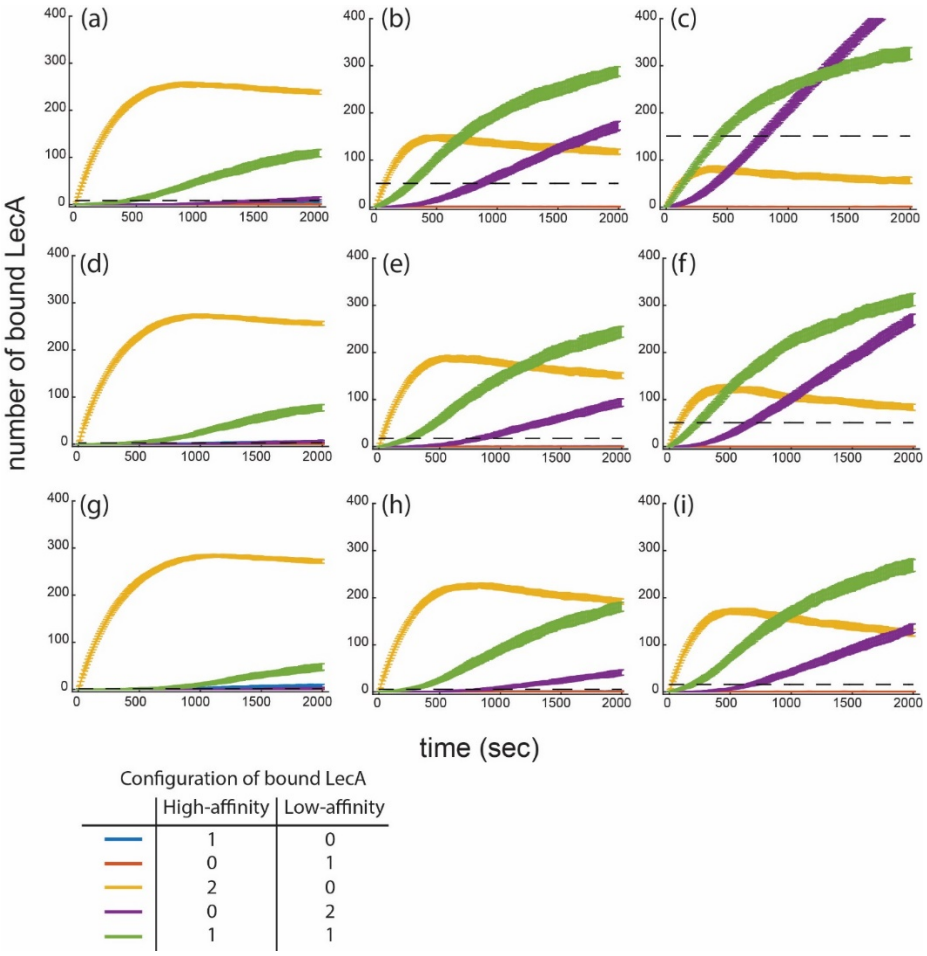


Figure 14: Modeling LecA binding kinetics using the kMC simulation. LecA binding to a membrane surface (250x250 sites) containing 1 mol% of high-affinity ligands and various densities of low-affinity ligand with different affinities: (a) 0.5 mol% ($\boldsymbol{K_{d,low} = 100K_{d,high}}$), (b) 3 mol% ($\boldsymbol{K_{d,low} = 100K_{d,high}}$), (c) 9 mol% ($\boldsymbol{K_{d,low} = 100K_{d,high}}$), (d) 0.5 mol% ($\boldsymbol{K_{d,low} = 300K_{d,high}}$), (e) 3 mol% ($\boldsymbol{K_{d,low} = 300K_{d,high}}$), (f) 9 mol% ($\boldsymbol{K_{d,low} = 300K_{d,high}}$), (g) 0.5 mol% ($\boldsymbol{K_{d,low} = 1000K_{d,high}}$), (h) 3 mol% ($\boldsymbol{K_{d,low} = 1000K_{d,high}}$), (i) 9 mol% ($\boldsymbol{K_{d,low} = 1000K_{d,high}}$). Each curve represents the number of bound LecA at different binding conFigureurations shown in the Figure. legend. The dash line shows the maximum number of bound LecA at 2,000 s when the membrane contains the same density of low-affinity ligands without any high-affinity ligands. All data represented as average ± S.D from 50 kMC simulations. Reprinted from reference 29.

**Hetero-multivalency between liposome and bacterium**

A key concept of the RD mechanism is that a strong ligand can activate weaker ligands, resulting in enhanced ligand binding. We observed this binding enhancement with two different bacterial lectins, LecA and CTB[26,27]. The same mechanism may occur in other types of multivalent binding systems, such as bacteria and viruses. We wondered if we could utilize the RD mechanism to design a high affinity liposome for targeting bacteria. A bacterium can have multiple surface adhesins that can bind to various host cell ligands with different affinities. Therefore, some ligands may exhibit relatively low binding affinities to bacterial adhesins. If we are able to fabricate a liposomal drug carrier containing both high- and low-affinity ligands, a liposome can simultaneously attach to multiple different surface adhesins in a bacterium, leading to higher retention of the drug carrier.

We fabricated fluorescent liposomes containing 10 mol% Gb3, 10 mol% LacCer, and an equal parts combination of the two (5 mol% Gb3/ 5 mol% LacCer) to target *P. aeruginosa*. As discussed above, Gb3 is a strong ligand, and LacCer is a weak ligand for LecA. Prior literature also reported that T4P of *P. aeruginosa* could attach to β-Gal terminated glycans.[127,150] Thus, we expected LacCer could serve as a ligand for both LecA and T4P. The control liposome contained only POPC lipid. The composition of control liposomes is similar to the formulation of liposomal antibiotics currently in phase 3 clinical trials[151-153]. We evaluated liposome targeting efficiencies in binding to two *P. aeruginosa* strains, PAO1 and Xen41, by measuring the retention of liposomes by the bacteria. The normalized fluorescence results of binding liposomes to 48 hour cultured bacteria are shown in Figure. 15.

The retention of the liposomes containing 10 mol% of LacCer was not higher than the control liposome. The retention of 10 mol% of Gb3 was slightly higher than the control system,

but the difference varied insignificance. Interestingly, for Gb3/LacCer liposomes (5 mol%+5 mol%), the retention was significantly greater than the other liposomal formulations tested. Compared to the control system, the retention of Gb3/LacCer liposomes was enhanced up to 4-fold (for Xen41, 2.5-fold for PAO1) at the lowest liposome concentration (0.0725g/L). Because the formula of the control liposome is similar to clinical liposomal antibiotics, this result indicated that we can improve the current drug formula by simply introducing two host cell molecules. These demonstrate the potential to use mixed host cellular ligands to improve liposomal targeting of *P. aeruginosa*.

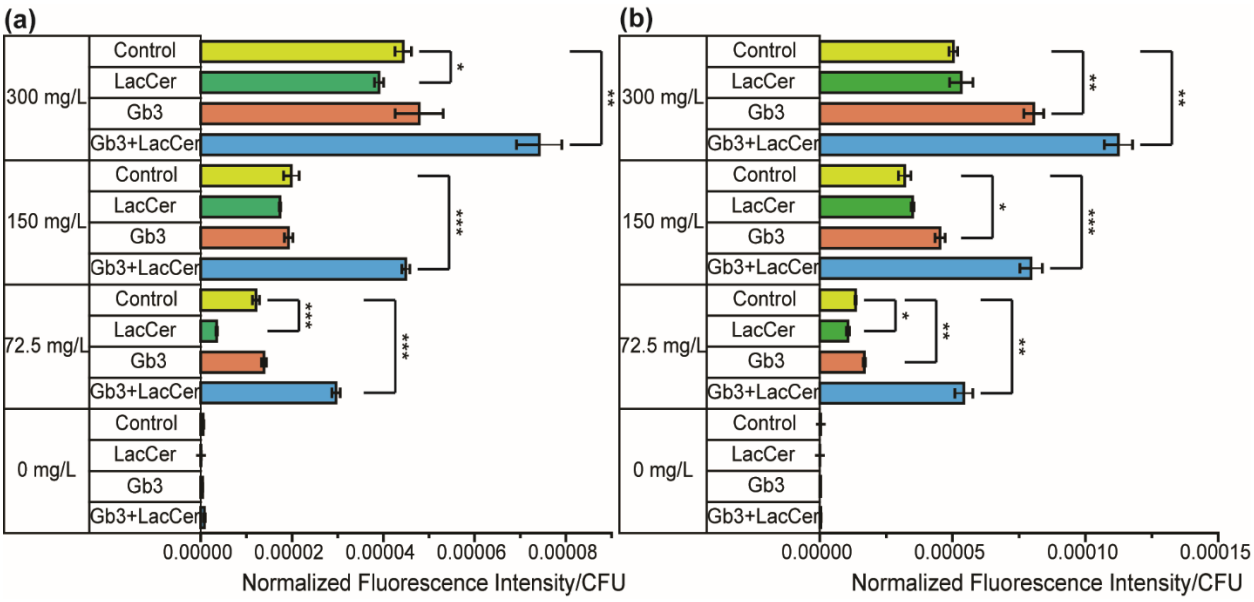


Figure 15: Liposome binding to P. aeruginosa. Retention of fluorescent liposomes on P. aeruginosa ((a) PAO1 and (b) Xen41) was quantified by normalized fluorescence intensity per colony forming unit (CFU). The liposome concentration given is mass concentration. Control (yellow) is 99.5 mol% POPC/0.5 mol% TR-DHPE. LacCer (green) is 10 mol% LacCer/89.5 mol% POPC/0.5 mol% TR-DHPE. Gb3 (orange) is 10 mol% Gb3/89.5 mol% POPC/0.5 mol% TR-DHPE. Gb3/LacCer (blue) is 5 mol% LacCer/5 mol% Gb3/89.5 mol% POPC/0.5 mol% TR-DHPE. The mean data have been reported. The error bars are standard deviation (n = 3). The stars indicate t-test unequal variance p-values of $p < 0.1$ (*), $p < 0.05$ (**), and $p < 0.01$ (***). Reprinted from reference 29.

## Discussion

Recent research on multivalent binding has suggested that total and relative densities of glycotopes in heterogeneous environment has an impact on carbohydrate-protein recognition events and cannot be explained by the simple on-off switch model.[154] In this paper, we have investigated LecA binding in heterogeneous glycolipid environment. Mixing high-affinity ligands with weakly binding ligands could alter the LecA binding behavior. The kMC simulations and experimental results indicated that the changes of binding capacity and avidity are probably induced by the RD mechanism. In order to initiate cooperative binding, we found two conditions must be satisfied. First, there is a minimum LecA concentration required before observing significant cooperativity. The minimum concentration corresponds to the dissociation constants of the highest affinity ligands present in the model membrane. This criterion is predicted by the RD mechanism. In the RD mechanism, the first binding event brings a ligand from the solution phase to the model membrane; then, the effective ligand concentrations increase for the subsequent binding events due to the reduced dimensionality of diffusion. Therefore, the occurrence of hetero-multivalent binding is limited by the first binding event, which corresponds to the dissociation constant between LecA and the highest affinity ligand.

The second criterion is that a sufficient amount of the weaker ligand is required to trigger hetero-multivalency. Through the analysis of the kMC simulation, the retention rate of LecA by the weak ligand and the frequency that weak ligands encounter membrane-bound LecA are two key parameters that determine the degree of hetero-multivalent binding. Thus, this threshold density is associated with the affinity of the weaker ligand. For Gb3/LacCer mixture, no obvious cooperativity was observed at 1 mol% of LacCer, but the cooperativity drastically increased at 2

mol% of LacCer. When the affinity of the weak ligand is reduced, a higher density of the weak ligand is required to observe the participation of weak ligand in LecA binding.

The threshold density of LacCer, approximately 2 mol%, is a noticeable portion of the total model membrane. This raises the question of whether LacCer in epithelial cells is present in sufficient quantities to play a role in LecA binding. To address this concern, we note that glycolipids are highly enriched in the apical plasma membrane of polarized epithelial cells.[155-157] Additionally, it has been shown that the glycolipid content can reach up to 30% of the total membrane lipids in microvilli.[158] This is significant as the typical total glycolipid fraction of the entire membrane for mammalian cells is ~5%.[159] Furthermore, Parkin et al. observed the microvillar membranes in porcine kidney cortex contain 3.53 mass% of LacCer, and LacCer was further enriched up to 7.26 mass% in detergent-resistant domains of microvilli.[160] Besides cell polarization, Gb3 can also cluster with galactosyl ceramide, glucosyl ceramide, and LacCer in cholesterol enriched domains.[161] These clustering processes could further concentrate local glycolipid abundance. Therefore, it is reasonable to expect that the threshold density of LacCer is biologically relevant on a local scale. In addition, we expect that the localized enrichment of membrane ligands induced by phase separation, dynamics of the cell cytoskeleton, cell polarization, and lipid asymmetry can influence the effect of the RD mechanism. Further studies are required to dissect the role of the RD mechanism in biological systems.

It should be noted that binding capacity (total amount of bound proteins) is not directly correlated with binding avidity (total binding energy between a protein and ligands) in multivalent binding systems. According to the kMC results, strong ligand can facilitate LecA binding to weak ligands, resulting in increased binding capacities. In the same situation, a significant portion of LecA can bind to both Gb3 and LacCer ligands or to two LacCer ligands;

therefore, we expect that the binding avidity would be lower than that of LecA binding to two Gb3 ligands. The changes of binding capacity and binding avidity may affect downstream processes of LecA. For instance, Eierhoff et al. showed that LecA-Gb3 interaction is critical to induce *P. aeruginosa* invagination of giant unilamellar vesicles (GUVs) and H1299 cells.[133] Their experimental data demonstrated the threshold density of Gb3 to be 0.1 mol% for bacterial engulfment which is much higher than the Gb3 content in lung epithelium. Based on their theoretical model, a higher number of LecA-Gb3 binding events and higher adhesion energy can enhance membrane engulfment of *P. aeruginosa*. Therefore, it is reasonable to hypothesize that the potential hetero-multivalent binding of LecA influences the invagination process. Another example is that Gb3 serves as a signaling ligand for LecA to induce CrkII phosphorylation.[128] The participation of weak ligands, such as LacCer, may change the LecA-Gb3 interactions, altering the signaling response. Additionally, it has also been reported that ligands binding to LacCer can activate Src family kinase Lyn.[162] Thus, the hetero-multivalent binding of lectins may introduce a possible secondary role of lectins in the Lyn signaling pathway. Further investigation is required to understand the potential role of hetero-multivalency in various biological systems.

Besides demonstrating a LecA binding mechanism, we showed the potential of using hetero-multivalent binding to improve targeted drug delivery. Traditionally, targeted drug delivery schemes have tended to decorate the drug carrier with the highest affinity ligands[163,164]; however, this strategy often leads to higher off-target binding. A recent computational study suggests that using a combination of multiple weaker affinity ligands can improve selectivity, and that selectivity can be further optimized by varying the ligand surface densities.[165] This theoretical study brings light to a new aspect of targeted drug delivery. However, using a set of

low affinity ligands may reduce the targeting efficiency of drug carriers. A potential solution is to decorate weak-affinity ligands on fluidic liposome surfaces along with a moderate ligand that can facilitate weak ligand-ligand binding via the RD mechanism. Thus, we believe liposomal carriers are an attractive approach for the design of multivalent-targeted drug delivery systems.

Our liposome-bacterium studies demonstrated the applicability of glycolipid mixtures to achieve improved liposome targeting to *P. aeruginosa*. Specifically, our results yielded two main conclusions. First, adding multiple types of glycolipids can significantly improve liposome binding beyond single glycolipid liposomes. Given the observed binding pattern, LecA is probably not the only actor at work in liposome binding to *P. aeruginosa*. We believe other galactose binding adhesins, such T4P, contribute to the observed liposome targeting. Second, the binding between *P. aeruginosa* and liposomes containing only LacCer ligand was negligible. Therefore, LacCer has to form a partnership with Gb3 ligand in order to exhibit improved liposome retention. This phenomenon is consistent with the LecA and CTB binding systems. Weak ligands need the assistance of high-affinity ligands to initiate hetero-multivalent binding. This phenomenon presents an issue to conventional ligand-ligand screening assays (e.g. microarray technology) because they screen ligands one by one. As a result, conventional methods may miss the essential weak binding ligands, which could exhibit high binding selectivity to the target pathogens. Thus, our previously published membrane perturbation protocol could provide a more efficient strategy to screen potential weak ligands involving *P. aeruginosa* binding.[26] In summary, the proof-of-concept liposome-targeting test has demonstrated the application of a hetero-multivalent targeting strategy. However, there is much work to be done to create a rational basis for *a priori* targeting design in terms of both affinity and selectivity.

## Conclusion

RD is an intrinsic mechanism that seemingly occurs in all multivalent binding processes. The low-affinity ligands can also contribute to the binding process via this simple mechanism. As such, the high-affinity molecule is not the only ligand to consider in multivalent binding processes; the multivalent recognition is determined by the cooperativity among high-affinity and low-affinity ligands. The simple RD mechanism adds another level of complexity to biological systems. Further studies are required to dissect the role of the RD mechanism in various biological systems. Besides LecA binding, we also demonstrated the application of hetero-multivalency to target whole bacteria. Our preliminary studies demonstrate the potential of improved efficiency in targeted drug delivery.

# CHAPTER IV

# EVALUATION OF HETERO-MULTIVALENT LECTIN BINDING USING A TURBIDITY-BASED EMULSION AGGLUTINATION ASSAY[§]

## Chapter Summary

Lectin hetero-multivalency, binding to two or more different types of ligands, has been demonstrated to play a role in both LecA (a *Pseudomonas aeruginosa* adhesin) and Cholera Toxin subunit B (a *Vibrio cholerae* toxin). In order to screen the ligand candidates that involve in hetero-multivalent binding from large molecular libraries, we present a turbidity-based emulsion agglutination (TEA) assay that can be conducted in a high-throughput format using the standard laboratory instruments and reagents. The benefit of this assay is that it relies on the use of emulsions that can be formed using ultrasonication, minimizing the bottleneck of substrate surface functionalization. By measuring the change in turbidity, we could quantify the lectin-induced aggregation rate of oil droplets to determine the relative binding strength between different ligand combinations. The TEA results are consistent with our prior binding results using a nanocube sensor. The developed TEA assay can serve as a high-throughput and customizable tool to screen the potential ligands involving in hetero-multivalent binding.

## Introduction

The exterior surface of cell membranes is densely populated with glycans (also called carbohydrates, saccharides, and sugars) in what is known as the "glycocalyx"[34]. This glycocalyx forms the foundation for interactions as diverse as cell-cell recognition, host-pathogen recognition, and cell signaling[34,166]. These interactions are mediated by binding of glycans with

[§] Reproduced from Ref 82 with permission from Colloids and Surfaces B: Biointerfaces

proteins, also called lectins. Because the interaction between a glycan and a single binding site in a lectin is typically weak and semi-specific, a lectin often binds several glycans simultaneously[34,166-168]. These multivalent interactions give rise to not only a stronger overall binding, but also enable modulation of affinity and selectivity of the binding lectin[154,169-171].

We recently demonstrated that a homo-oligomeric lectin could simultaneously bind to at least two types of glycan ligands (i.e. hetero-multivalent binding) via an inherent Reduction of Dimensionality (RD) mechanism, altering the binding behavior of lectins to cell membranes [26,27,29,172,173]. The binding valency and the fluidity of cell membrane are the essential characteristics influencing hetero-multivalency. This presents a critical issue to conventional ligand-receptor screening assays, such as microarray technology, because they often screen immobilized ligands one-by-one. To address the issue, we recently introduced a novel nanocube sensor that enables label-free detection of lectins binding to a cell membrane mimicking surface using a standard laboratory spectrophotometer[26,27,29]. Although the nanocube system encompasses many unique advantages (e.g. high-throughput utility, absolute quantification without daily calibration, easy-to-use, high sensitivity, etc.), these special nanocube sensors are not yet accessible for a wide range of scientific communities [26,27,29]. This limits biologists' ability to study hetero-multivalent binding phenomena [26]. Therefore, a highly accessible and high-throughput assay for determining potential ligands involved in hetero-multivalent binding is desirable.

A promising system for high-throughput screening of lectin interactions with glycolipids is an agglutination based assay. The lectin-glycan interactions are detected by monitoring the lectin-induced aggregation of glycan-coated particles. A classic agglutination assay is the hemagglutination assay in which the lectins that induce red blood cell aggregation indicate the

donors' blood group type [174-177]. The agglutination of antigen-coated latex particles has also been used for detection of antibodies [178]. In addition, Vico et al. have used glycan decorated liposomes to study lectin-glycan interactions [179]. Another potential system for the agglutination assay is oil-in-water emulsions. Compared to other agglutination assays, emulsified oils, which are stabilized by monolayers of lipids, have several advantages. First, in contrast to cells, the types and densities of ligands on oil droplets are controllable. Second, unlike latex particles, the lipids and the glycolipids presented at the oil-water interface maintain the similar two-dimensional fluidity as on the native cell membranes [180,181]. Third, compared to the liposome agglutination assay, the higher refractive index of oil droplets improves the sensitivity of agglutination measurements at smaller particle sizes [182-184]. Fourth, the preparation of these emulsions can be done using common laboratorial equipment via ultrasonication or high-pressure homogenization [185]. Both well-established emulsion methods can generate stable nano-sized droplets, typically about 100 nm [185-188]. The ease-of-preparation will allow scientists to customize a large number of hetero-multivalent binding systems in-house.

In this paper, we have presented a turbidity-based emulsion agglutination (TEA) assay to assist biology society in determining potential glycolipid candidates involved in lectin hetero-multivalency. TEA assay only requires common laboratory instruments and reagents; thus, it is immediately accessible for the scientific community. The emulsion aggregation induced by lectins could result in a change of solution turbidity which could be measured by a UV/Vis spectrophotometer, graphically represented in Figureure 16. Prior works have determined the relationship between the turbidity of the solution at various wavelengths and the particle size, allowing us to quantify the degree of agglutination using turbidity [189-197]. We have also explored the light scattering theory to determine the optimal working conditions of the TEA assay. A

*Pseudomonas aeruginosa* lectin, LecA, was used to validate the TEA assay. Our recent publication has systematically evaluated the hetero-multivalency of LecA [29]; and the results of the TEA assay correlate well with our prior study. In addition, we have validated our results using kinetic measurements of particle size by dynamic light scattering (DLS) and found excellent agreement.

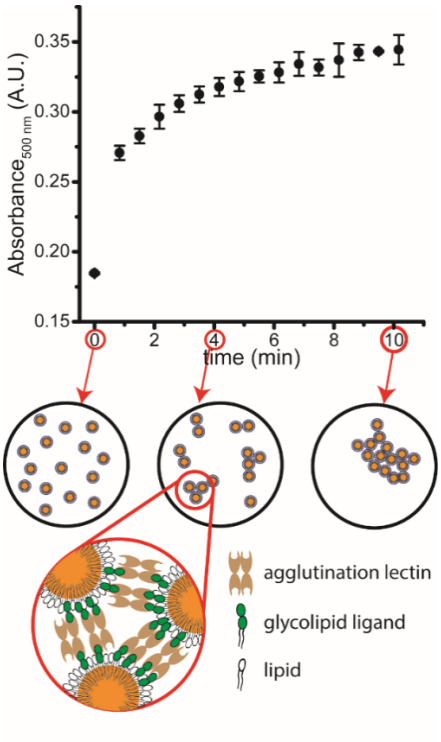


Figure 16: Schematic of oil droplet aggregation relative to observed changes in absorbance at 500 nm. The lipid-stabilized o/w emulsions are prepared by ultrasonication. The lipids presented at the oil-water interface maintain the same two-dimensional fluidity as on native cell membranes. The binding between the agglutination lectins and the glycolipid ligands induces the particle aggregation, resulting in the change of turbidity. Reprinted from reference 82.

## Emulsion Turbidity Theory

For a monodisperse system, the turbidity can be expressed as a function of emulsion concentration and particle size [190,192,193,196,198]:

$$\tau = \frac{\ln\left(\frac{I_0}{I}\right)}{l} = \frac{2.303\text{Abs}}{l} = K\pi r^2 N \qquad \text{Equation 15}$$

where $\tau$ = the turbidity; $\text{Abs} = \log\left(\frac{I_0}{I}\right)$ = the absorbance measured by UV-vis spectrometer; $I_0$ = intensity of the incident light; $I$ = intensity of the transmitted light; $l$ = scattering path length; $r$ = the particle radius; $N$ = the concentration of particles; and $K$ = scattering efficiency factor which depends on relative refractive index of the medium, $m$, and $\alpha = \frac{2\pi r}{\lambda}$ and $\alpha$ typically varies between 0 and 5 [182]. The wavelength, λ, is actually $\lambda_{vacuum}/n_2$, where $n_2$ is the refractive index of the emulsion solution. Using Mie scattering theory for spheres of arbitrary size, Hulst [199] has derived *K* as:

$$K = \frac{2}{\alpha^2}\sum_{n=1}^{\infty}(2n+1)\{|A_n|^2 + |B_n|^2 \qquad \text{Equation 16}$$

However, when $|m-1| \ll 1$ and $\alpha|m-1| \ll 1$, the equation for *K* could be simplified using Rayleigh-Gans scattering theory [199]. (The detailed equations of Mie and Rayleigh scattering theories are summarized in the supplementary information).

The coagulation theory given by Smoluchowski [200] could be related to condensation polymerization where any colloidal monomer or aggregate could stick with any monomer or aggregate size [195]. After aggregation is induced, the emulsion becomes poly-disperse and turbidity can thus be defined as:

$$\tau = \sum_j K_j \pi (r_j)^2 N_j \qquad \text{Equation 17}$$

where $K_j$ is the scattering efficiency factor and $N_j$ is the concentration of the j-mer aggregates with hydraulic radius $r_j$. For condensation polymerization, Flory [201] has described $N_j$ as:

$$N_j = N_0(1-p)^2\, p^{j-1} \qquad \text{Equation 18}$$

$N_0$ is the initial concentration of the particles and $p$ is the extent of the reaction given by $p = \frac{\frac{1}{2}kt}{1+\frac{1}{2}kt}$ where $k$ is the rate constant of the condensation polymerization/coagulation [197]. Using Rayleigh scattering theory, Oster developed the following approximation for coagulating system [195]:

$$\tau = \frac{24\pi^3}{\lambda^4} n_1^4 \left(\frac{m^2-1}{m^2+2}\right)^2 V_0^2 N_0(1+kt) \qquad \text{Equation 19}$$

and hence,

$$\frac{d\tau}{dt} = \frac{24\pi^3}{\lambda^4} n_1^4 \left(\frac{m^2-1}{m^2+2}\right)^2 V_0^2 N_0 k \qquad \text{Equation 20}$$

where $n_1$ is the refractive index of the solvent, and $V_0$ is the volume of the initial particle [195]. Under Rayleigh scattering assumption, $\frac{d\tau}{dt}$ is linearly proportional to the aggregation rate constant, $k$ [197].

## Methods and Materials

### Materials

Silicone oil (refractive index of 1.403), PA-IL from *Pseudomonas aeruginosa* (also known as LecA), tris-buffered saline (TBS) obtained as a 10x solution (1x working solution 20 mM Tris 0.9% NaCl pH ~7.4), and silicone oil were purchased from Sigma-Aldrich (St. Louis, Missouri). Calcium chloride was purchased from BDH VWR Analytical (Radnor, Pennsylvania). Globotriaosylceramide, Gb3, (Galα1-4Galß1-4Glc-Ceramide), and Lactosylceramide, LacCer,

(Galβ1-4Glc-Ceramide) were purchased from Matreya LLC (State College, PA). 1-palmitoyl-2-oleoyl-sn-glycero-3-phosphocholine (POPC) was purchased from Avanti Polar Lipids (Alabaster, AL).

**Preparation of O/W Emulsion**

The desired compositions of lipids in chloroform solutions were mixed in a 25 mL round bottom flask and, then, dried using a rotary evaporator (Heidolph Hei-VAP Value®). The dried lipids were reconstituted using 1X TBS with 100 μM $CaCl_2$, forming multilamellar vesicles (MVs) in aqueous solution. The emulsions were prepared by mixing 5 μL of silicone oil, 474.18 μL of 1X TBS with 100 μM $CaCl_2$, and 220 μL of MV solution. The mixture was then sonicated using a Qsonica Q125 tip sonicator at 60% amplitude for 1 hour cycling 10 seconds on and 10 seconds off in an ice bath. The size distributions of oil droplets were determined by DLS.

**Kinetic Turbidity Measurement**

The 20 μL of emulsion was diluted into 80 μL of 1X TBS with 100 μM $CaCl_2$ in six wells of a 96 well plate (Costar® 3370) to maintain turbidity in a range of 0.5 to 0.8 in order to ensure the UV/Vis was in the linear response region and to minimize multiple scattering. The turbidity of the emulsions was detected by an ultra-fast UV/Vis microplate spectrophotometer equipped with CCD camera (FLUOstar Omega®, BMG-Labtech). Because the biological analytes do not significantly absorb light at a wavelength of 500 nm, the turbidity was determined at this wavelength. 10 μL of 3.227 g/L LecA was added to three wells of the emulsion to induce agglutination. 10 μL of the buffer was added to the remaining three wells as the negative controls. All of the solutions were mixed by pipetting in the well plate. After mixing, the turbidity of the emulsions was detected using the microplate spectrophotometer. The extinction spectra were collected in the range of 300-1000 nm wavelengths every ~30-60 s for 60

minutes and then every 30 minutes for 2 more hours at room temperature. Each spectrum was the result of averaging 200 flashes per well at a 1 nm resolution. The time lag between LecA additions from the start of turbidity detection was 50s. The $OD_{500\ nm}$ value over the course of 2 min was fit with a line to obtain the change in turbidity vs time, $\frac{d\tau}{dt}$.

**Kinetic DLS and Zeta Potential Measurements**

Batch mode hydrodynamic size (diameter) measurements were performed on a Malvern Zetasizer Nano ZS90 (Malvern Instruments, Southborough, Massachusetts) with detection occurring at 90° to the light source. The emulsion was diluted 10 μL of emulsion into 90 μL of 1X TBS with 100 μM $CaCl_2$ followed by equilibration (typically 2 minutes) in the DLS at 25°C before a minimum of three measurements per sample were made. After dilution, the system was checked for multi-particle scattering by testing 10 μL of emulsion diluted into 190 μL of 1x TBS with 100 μM $CaCl_2$ to ensure that it gave the same particle diameter. Then 5 μL of 3.227 g/L LecA was added to the cuvette and mixed by pipetting the solution 10 times. A measurement of hydrodynamic size (determined by cumulants average or Z- average) via three measurements was then taken every 10 minutes for 2 hours. Only results with a polydispersity index (PDI) less than 0.3 were used for fitting to minimize errors in calculating particle diameter by method of cumulants. Zeta potential was also measured on the Malvern Zetasizer Nano ZS90 via three measurements. This measurement was conducted twice for each emulsion system.

**Statistical Analysis**

The turbidity testing for each lipid composition was repeated on 3 different days with 3 technical replicates on each day for a total of 9 replicates. The turbidity data sets were tested using Welch's t-test in OriginPro 9.1®. The DLS data set is represented as mean ± SE (n=3 runs over each 10 min interval) per lipid composition.

## Results and Discussion

To ensure that sufficient time was given to allow for droplet aggregation, we calculated the diffusion limited mean first pass time using the Hardt's analysis[202]:

$$\tau_{diffusion} = \frac{1}{4\pi r N_0 D} \quad \text{Equation 21}$$

where $D$ is the droplet diffusivity that can be calculated using the Stokes-Einstein equation:

$$D = \frac{k_b T}{6\pi\mu r} \quad \text{Equation 22}$$

$k_b$ is the Boltzmann constant; $T$ is temperature; and $\mu$ is the dynamic viscosity**.**

The $\tau_{diffusion}$ for our system is about 1.14 seconds and thus can be sure that the aggregation rate observed in the following DLS and turbidity measurements is not diffusion limited.

**Dynamic Light Scattering (DLS) measurement**

To validate the TEA assay, we first conducted a LecA binding experiment with DLS (Figure 17). The o/w emulsions were fabricated via ultrasonication and stabilized by lipids. Before the LecA addition, there was not much change in the droplet size, indicating stability of the emulsions (Figure. 18). However, droplets aggregated after LecA addition because of the binding of proteins to various glycolipid ligands on oil droplet surfaces. We have reported the average diameter of oil droplet as a function of time in Figure. 17. 1 mol% Gb3 / 4 mol% LacCer aggregates the fastest at 5.8 ± 0.3 nm/min (mean ± S.E., n=6). 1 mol% Gb3 aggregates about five times slower at 1.16 ± 0.05 nm/min (mean ± S.E., n=14). Although the aggregation rate of 4 mol% LacCer is minimum (0.084 ± 0.0045 nm/min (mean ± S.E., n=8)), it is still greater than the control system of 100 mol% POPC that corresponds to essentially constant particle size,

indicating no aggregation. To ensure that the electrostatic interactions were not influencing the aggregation of droplets, we measured zeta potential of all the emulsion systems (Table 5). The zeta potential values are comparable for all emulsion compositions, indicating that the electrostatic interaction is not the major contributor to particle aggregations.

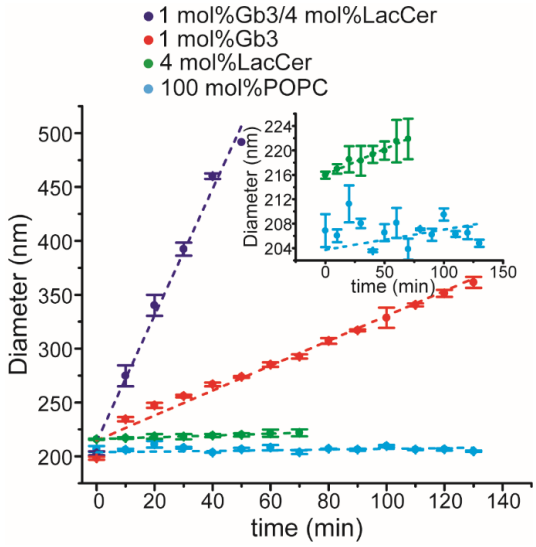


Figure 17: DLS data of average diameter as a function of time since LecA addition. Data points represent the average diameter determined from cumulants Z-average mean ± S.E. (n = 3) of three tests for each 10 minutes time interval. The dashed line represents the fitted slope for each bilayer composition. Inset is a zoomed-in view of 4% LacCer and 100% POPC bilayers. Reprinted from reference 82.

In our prior work with LecA, we observed that lipid bilayer surfaces containing mixture of Gb3 and LacCer bound to more LecA proteins than either Gb3 or LacCer individually [29]. This is because Gb3 ligands activate the weak LacCer ligands via the RD mechanism, leading to hetero-multivalency (i.e. a protein simultaneously binding to at least two different types of ligands) [29]. The hetero-multivalency phenomenon increases the available binding sites on a membrane surface. The result of DLS measurements is consistent with our prior observations of

LecA hetero-multivalency. From our previous study, we found out that the binding between LecA and nanocube sensors coated with 1 mol% Gb3 or 1 mol% Gb3 / 4 mol% LacCer had saturated at 3 μM LecA concentration. In DLS experiments, the binding measurements were conducted at a high LecA concentration of 3 μM, leading to the saturated LecA binding to oil droplet surfaces.

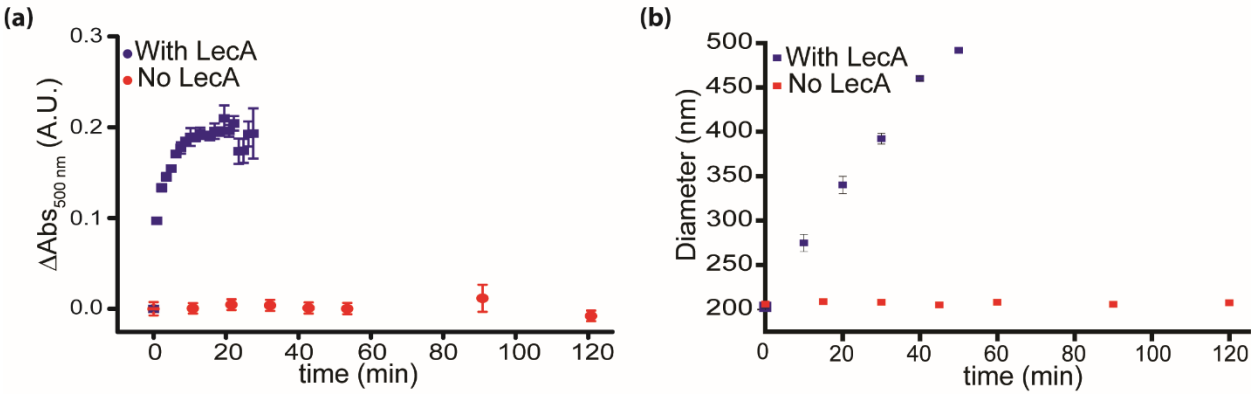


Figure 18: Kinetic measurements for the emulsions containing mixture of 1 mol% Gb3 and 4 mol% LacCer with and without LecA. a) TEA assay, (b) DLS measurements. Data is given as mean ± SE (n=3). In the absence of LecA, no aggregation was observed for about two hours, indicating the inherent stability of the droplets. Reprinted from reference 82.

Table 4: Zeta potential of different emulsion systems. Data is given as mean ± SE (n=6). Reprinted from reference 82.

| **Emulsion composition** | **Zeta Potential (mV)** |
|---|---|
| 100 mol% POPC | -0.61 ± 0.10 |
| 99 mol% POPC / 1 mol% Gb3 | -0.97 ± 0.22 |
| 96 mol% POPC / 4 mol% LacCer | -0.49 ± 0.14 |
| 95 mol% POPC / 1 mol% Gb3 / 4 mol% LacCer | -0.14 ± 0.09 |

Therefore, for Gb3/LacCer mixture, a higher number of LecA could be present in the interaction area between two oil droplets, increasing the attraction force. As such, a higher aggregation rate was observed in the Gb3/LacCer mixture system (Figure. 19).

**TEA assay**

For comparison, we conducted the same binding conditions of DLS in the TEA assay. In the following analysis, we use absorbance (Abs) measured by the UV-vis spectrometer to represent the turbidity. Because we did not change the scattering path length ($l$), only a constant factor is required to convert Abs to turbidity ($\tau = \frac{2.303\text{Abs}}{l}$).

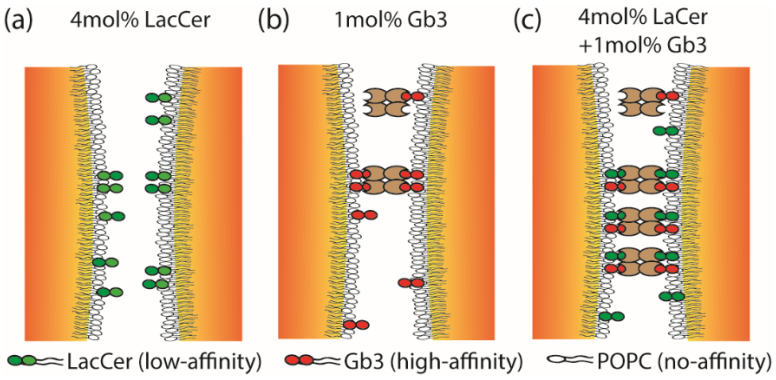


Figure 19: The schematic of hetero-multivalency in emulsions. (a) The binding affinity between a LacCer ligand and a binding domain of LecA is too weak to hold bound lectins. (b) The high-affinity ligands, Gb3, could bind to LecA, leading to the aggregation of oil droplet. (c) Via the RD mechanism, LacCer could participate in LecA binding with the assistance of Gb3. This phenomenon increases the available binding sites, resulting in the increased number of bound LecA between two oil droplets. Thus, a higher aggregation rate was observed. Reprinted from reference 82.

Figure. 20 provides curves of turbidity as a function of time after LecA addition. For Gb3/LacCer mixture system at 6 μM LecA concentration, we observed that the turbidity increased for about 10 minutes, and then seems to have reached a plateau region. Interestingly,

size of the oil droplets grew constantly in DLS data within 1 hour incubation (Figure. 17). As such, the plateau region of the turbidity data should not be assumed to be the steady state condition for binding. In fact, the decrease of turbidity slope ($\frac{d\tau}{dt}$) after some time is due to the shift in the scattering regime. Initially, the light scattering is in Rayleigh scattering region. Based on Oster approximation (equation 20), the $\frac{d\tau}{dt}$ value is proportional to the aggregation rate constant in the Rayleigh scattering region [195]. However, as time progresses, the oil droplets aggregate and thus grow in size and become comparable with the wavelength of the incident light, shifting from Rayleigh to Mie scattering region. In this case, the turbidity should be presented by equation 17. Thus, the turbidity can be written by combining equations 17 and 18:

$$\tau = \sum_j K_j \pi (a_j)^2 N_0 \left(\frac{1}{1+\frac{kt}{2}}\right)^2 \left(\frac{\frac{kt}{2}}{1+\frac{kt}{2}}\right)^{j-1} \qquad \text{Equation 23}$$

where $\tau$ is directly proportional to $K_j$ and $a_j$, but inversely proportional to $t^2$. Also, the scattering efficiency factor, $K_j$, depends on the cluster size.

Figure. 21 shows the scattering efficiency factor, $K_j$, calculated by the Rayleigh-Gans scattering theory and Mie theory (see supporting information) [199,203]. Compared with Rayleigh-Gans theory, the Mie scattering formula derived by Hulst is more general and valid in a wider range of particle size [199]. In Figure. 20b, the oscillation of the efficiency factor was observed. The efficiency factor reaches a maxima and then starts to decrease as particles aggregate further. Therefore, the turbidity might either become constant or even start to decrease, resulting in the decrease of turbidity slope ($\frac{d\tau}{dt}$) as time progressed. A number of previous theoretical and experimental investigations also reported the same phenomenon that turbidity increases with

coagulation in the Rayleigh scattering regime, whereas turbidity decreases when big particles coagulate [194,197,204-206].

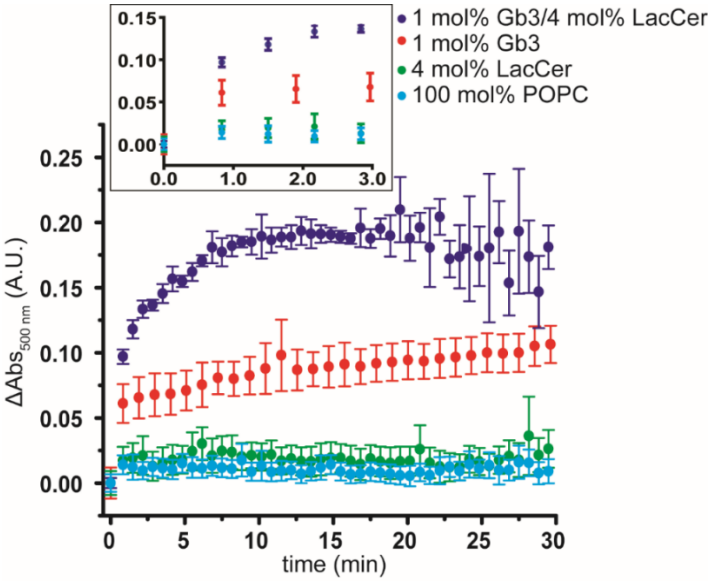


Figure 20: Turbidity data was subtracted by the initial turbidity value. Data is given as mean ± S.E. (n = 3). The inset is a zoomed-in view for the first two minutes, showing the change in turbidity (y axis) with time (x axis) for each emulsion system. Reprinted from reference 82.

Because the scattering behavior of the emulsion is highly nonlinear in the Mie scattering region, it is challenging to correlate turbidities and agglutination rates. To simplify the calculation, we limited the analysis of turbidity in the initial region that follows the predictions of Rayleigh scattering. Therefore, the linear correlations between agglutination rates and turbidity slopes ($\frac{d\tau}{dt}$) could be applied. To validate the Rayleigh scattering assumption at the initial time point, we compared the scattering efficiency factors calculated by Rayleigh-Gans and Mie scattering theories (Figure. 21). For our system, $m = 1.05$ and initial $\alpha = 1.726$, using 1.338 as refractive index of 1X TBS buffer [207]. The error in efficiency factor calculated using Rayleigh-

Gans scattering theory is about 2.26% compared to Mie theory. We could, hence, assume that the particles are in the Rayleigh scattering regime initially. Therefore, the $\frac{d\tau}{dt}$ value calculated from the initial slope of the turbidity data should be proportional to the particle aggregation rate. In addition, particle aggregations can induce greater changes of turbidity in Rayleigh scattering than in the Mie scattering, leading to higher sensitivity of the turbidity measurement. Thus, to ensure that the Rayleigh scattering equations were applicable, the analysis was conducted using data for 0-2 minutes, when the particle diameter is less than 275 nm, giving the threshold error to be 3% for the validity of Rayleigh-Gans scattering theory.

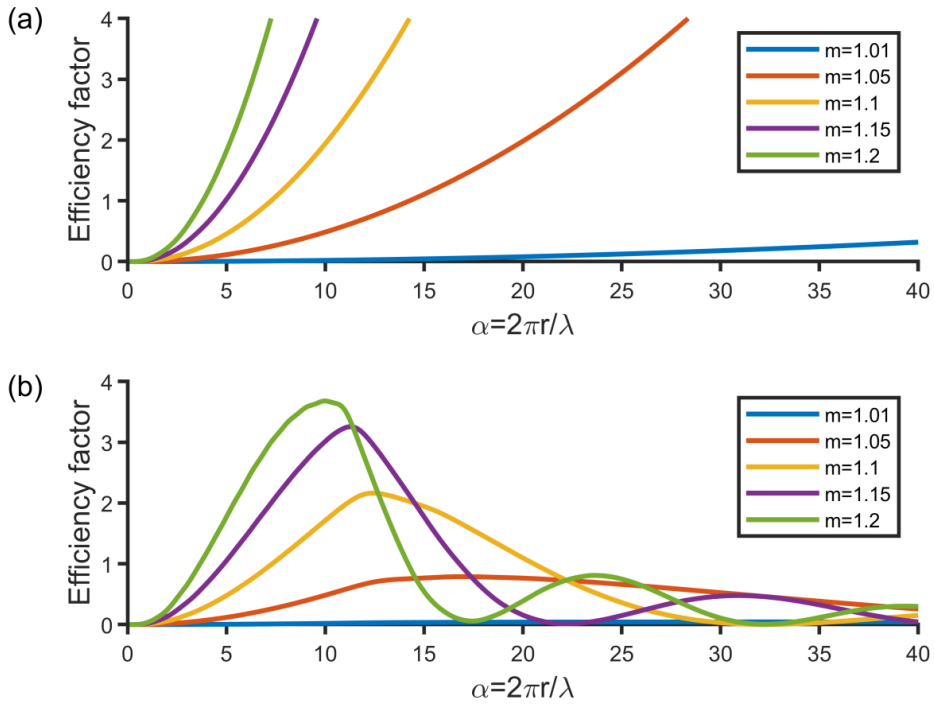


Figure 21: Scattering efficiency factor, K, as a function of size parameter, α. (a) Efficiency factor computed using Rayleigh-Gans scattering theory. (b) Efficiency factor computed using Mie scattering theory. Reprinted from reference 82.

**Reproducibility, Limitations, and Benefits of TEA assay**

As shown in equation (20), the turbidity slope depends on several experimental parameters, such as oil droplet size and concentration; therefore, the experimental variation may influence the quantification. To demonstrate the reproducibility of TEA assay, the inter-day results across three different days are shown in Figure. 22. There is no clustering of any day's three data points indicating the reproducibility of this method. This is confirmed in that each day's data was not significantly ($p < 0.05$) different from the total population and that the coefficients of variation (CV) of 9% and 4% for Gb3/LacCer mixture and Gb3 systems, respectively. The turbidity slope of Gb3 system ($6.6\times10^{-4}\pm0.3\times10^{-4}$ ($n = 9$)) is significantly greater ($p < 0.001$) than both LacCer (2.2×10-4±0.4×10-4(n = 9)) and POPC (1.7×10-4±0.3×10-4(n = 9)). Furthermore, the slope of Gb3/LacCer mixture (1.33×10-3±0.04×10-3 (n = 9)) is also significantly greater ($p < 0.001$) than Gb3 system. Both nanocube sensor data [29] and the DLS results are in close agreement with the turbidity data. This demonstrates the feasibility of using the TEA assay to study hetero-multivalency.

However, a few limitations remain with the TEA assay. First, the sensitivity of the TEA assay is lower than the DLS and nanocube assays. Although the affinity between LacCer and LecA is weak, we could detect LecA attaching to 4 mol% LacCer using the DLS and the nanocube sensor but not using the TEA assay. To improve the sensitivity, we can vary the experimental parameters to result in greater changes in the turbidity slope. Decreasing droplet size, using oil with a higher refractive index, or measuring turbidity at a lower wavelength would improve the sensitivity. However, changing these variables might make TEA assay shift from the Rayleigh to Mie scattering regions earlier, leading to lower sensitivity and inaccurate prediction

of aggregation rate. Therefore, the Rayleigh scattering criteria described above should be confirmed before changing the experimental protocol.

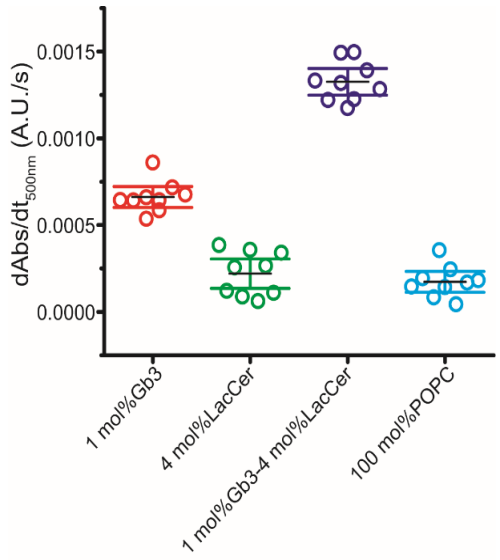


Figure 22: Reproducibility of the TEA assay. Dots represent individual data points across 3 days. Solid black lines represent the mean at each condition. Colored lines represent two standard errors (n=9) of each bilayer. Reprinted from reference 82.

A second limitation is that the TEA assay is semi-quantitative. The values of turbidity slope are dependent on the working conditions. To obtain the absolute value of rate constant, the concentration and the size of oil droplet should be measured. Therefore, we prefer using TEA assay for ranking the relative binding strength among various ligand compositions, instead of measuring the absolute binding energy.

A third limitation is that the current analysis only works for the Rayleigh scattering regime. Rayleigh scattering is chosen in the design of TEA assay so that it is unnecessary to determine the population distribution and the ranking of relative binding strength can be done without needing additional measurements of particle size and concentration [197]. This enables measurements using only the UV/Vis spectrometer. If the oil and aqueous phases are kept the

same, the size of the oil droplets is the major factor that determines the type of scattering regime. The experimental parameters that influence the size of droplets are a) relative concentration of total lipids to the amount of oil, b) interfacial tension, and c) emulsification process. (See the supplementary information) By maintaining a constant molar ratio of oil and total lipid, relatively low densities of glycolipids and same emulsification process, we were able to obtain a consistent droplet size at different glycolipid compositions. This is evidenced by our DLS measurements. The droplet size for all the glycolipid compositions is maintained at 206 ± 8 nm.

Despite some drawbacks, the TEA assay solves current problems with the tools used to study multivalent lectins. First, the TEA assay solves the problem of high-throughput screening of multivalent protein binding to heterogeneous systems. For example, the glycoarray, developed by the Consortium for Functional Glycomics (CFG), currently contains over 600 unique glycan molecules [208]. To evaluate the hetero-multivalent lectin binding to two types of ligands, at least 179,700 conditions have to be evaluated in a combinatory binding assay [77]. Although we have developed a membrane perturbation protocol to improve the ligand screening efficiency [26], the intrinsic complexity of hetero-multivalency still presents an issue for all the existing assays. The TEA assay is compatible with a commercial microwell plate reader equipped with automated reading and injection accessories, enabling quick detection of multiple formulations simultaneously. Second, the TEA assay provides a second way to determine relative hetero-multivalent binding that is easy-to-use, utilizes only inexpensive and commercially available reagents, and uses only common laboratory equipment. The result of this is that the TEA assay can easily be adopted in a wide range of biological laboratories. Thus, combined with its established reproducibility, the TEA assay is a tool that is customizable to screening of large molecular libraries without requiring specialized equipment.

## Supplementary Information

### Calculation of the scattering efficiency factor, K

As described in the main text, the turbidity for a mono disperse system can be expressed as [190,192,196,198,209]:

$$\tau = \frac{\ln\left(\frac{I_0}{I}\right)}{l} = \frac{2.303\text{Abs}}{l} = K\pi r^2 N \qquad \text{Equation 24}$$

where $\tau$ = the turbidity; $\text{Abs} = \log\left(\frac{I_0}{I}\right)$ = the absorbance measured by UV-vis spectrometer; $I_0$ = intensity of the incident light; $I$ = intensity of the transmitted light; $l$ = scattering path length; $r$ = the particle radius; $N$ = the concentration of particles; and $K$ = scattering efficiency factor which depends on relative refractive index of the medium, $m$, and $\alpha = \frac{2\pi r}{\lambda}$. Since the refractive index of the emulsion solution, $n_2$, is >1, the wavelength, λ is actually $\lambda_{vacuum}/n_2$.

### Calculation of scattering efficiency factor (*K*) using Mie scattering theory

Hulst derived a general formula of *K* for spheres of arbitrary size [199]:

$$K = \frac{2}{\alpha^2}\sum_{n=1}^{\infty}(2n+1)\{|A_n|^2 + |B_n|^2\} \qquad \text{Equation 25}$$

$A_n$ and $B_n$ can be estimated from [198,199]

$$A_n = \frac{\varphi_n'(m\alpha)\,\varphi_n(\alpha) - m\,\varphi_n(m\alpha)\,\varphi_n'(\alpha)}{\varphi_n'(m\alpha)\,£_n(\alpha) - m\,\varphi_n(m\alpha)\,£_n'(\alpha)} \qquad \text{Equation 26}$$

$$B_n = \frac{m\varphi_n'(m\alpha)\,\varphi_n(\alpha) - \varphi_n(m\alpha)\,\varphi_n'(\alpha)}{m\,\varphi_n'(m\alpha)\,£_n(\alpha) - \varphi_n(m\alpha)\,£_n'(\alpha)} \qquad \text{Equation 27}$$

$$\varphi_n(z) = (\pi z/2)^{1/2}\,J_{n+1/2}(z) \qquad \text{Equation 28}$$

$$\chi_n(z) = -(\pi z/2)^{1/2}\,N_{n+1/2}(z) \qquad \text{Equation 29}$$

Where $J_{n+1/2}(z)$ is the Bessel function of the first kind and $N_{n+1/2}(z)$ is the Neuman function or the Bessel function of the second kind.

$$\pounds_n(z) = (\pi z/2)^{1/2}\, H^{(2)}_{n+1/2}(z) \qquad \text{Equation 30}$$

$$H^{(2)}_n(z) = J_n(z) - \mathrm{i}\, N_n(z) \qquad \text{Equation 31}$$

$$\pounds_n(z) = \varphi_n(z) + \mathrm{i}\, \chi_n(z) \qquad \text{Equation 32}$$

Equation (25) ~ (32) are used to compute the scattering efficiency factor shown in Figure. 21b.

**Calculation of scattering efficiency factor (*K*) using Rayleigh-Gans scattering theory**

When $|m-1| \ll 1$ and $\alpha|m-1| \ll 1$, the equation for *K* could be simplified using Rayleigh-Gans scattering theory [198,199].

$$K = |m-1|^2\, \omega(\alpha) \qquad \text{Equation 33}$$

When $\alpha < 1$,

$$\omega(\alpha) = \frac{4}{9}\alpha^4 \int_0^{\pi} G^2\left(2\alpha\, \sin\frac{\theta}{2}\right) \cdot (1 + \cos^2\theta)\, \sin\theta\, d\theta \qquad \text{Equation 34}$$

$$G(u) = \frac{3}{u^3}(\sin\, u - \cos\, u) \qquad \text{Equation 35}$$

When $\alpha \geq 1$,

$$\omega(\alpha) = \frac{5}{2} + 2\alpha^2 - \frac{\sin\, 4\alpha}{4\alpha} - \frac{7}{16\alpha^2}(1 - \cos\, 4\alpha) + \left(\frac{1}{2\alpha^2} - 2\right)\{\gamma + \log\, 4\alpha - Ci(4\alpha)\}$$

Equation 36

$$\gamma = Euler's\ constant = 0.577 \qquad \text{Equation 37}$$

$$Ci(x) = Cosine\ integral = -\int_x^{\infty} \frac{\cos\, u}{u}\, du \qquad \text{Equation 38}$$

Equation (33) ~ (38) are used to calculate the efficiency factor shown in Figure. 21a.

**Design Parameters for the TEA assay**

The size of the oil droplets is the major factor influencing the future binding experiments using the TEA assay, if the oil and the aqueous phases are kept same. To compare the binding data at different experimental conditions, the size of oil droplets should be consistent. Few experimental parameters that can affect the droplet size are:

*Ratio of the amount of oil and total lipids (phospholipids and glycolipids):* Increasing the concentration of total lipids will lead to the formation of smaller sized droplets. To obtain consistent results, the molar ratio of oil and total lipids should be kept constant.

*Oil / water interfacial tension*: The glycolipid compositions can influence the interfacial tension, leading to the change in droplet sizes. When the glycolipid composition is kept at a low density (<5 mol%), the interfacial tension is majorly dominated by the phospholipids. In such a case, the alternation of glycolipid composition has minimum impact on the interfacial tension and, hence, the droplet size. This is evidenced by our DLS measurements. In each of the four different glycolipid compositions, the oil droplet sizes are maintained at 206 ± 8 nm.

*Emulsification process:* Power and duration of homogenization or ultrasonication can influence the droplet size. The consistency of emulsification process can be verified by comparing the inter-day data. For example, in the positive binding systems (Gb3 or Gb3/LacCer system), the inter-day CV was under 9%. This demonstrates that the reported emulsification protocol can produce consistent O/W emulsions.

The TEA assay is a semi-quantitative method. It cannot precisely measure the binding energy or the number of bound lectins, but the TEA assay can still be used to rank the binding strength among different combinations of glycolipids for a high throughput screening. The TEA assay offers the qualitative information of lectin binding, such as (1) identification of ligands

which can directly contribute to lectin binding, and (2) identification of ligands which can indirectly contribute to lectin binding by forming partnership with the other ligands. For example, Gb3 was considered a high-affinity ligand because it could induce detectable aggregation without other ligands. In contrast, the low-affinity LacCer required the assistance of Gb3 to induce detectable aggregation. Our prior publication has demonstrated that changing the lectin concentrations would not influence the relative binding strength [29]. Although higher lectin concentrations could induce higher degree of aggregation and thus improve the sensitivity of turbidity measurement, it is, however, preferred to conduct measurements near physiological conditions.

## Conclusion

We have applied scattering and coagulation theories to develop the TEA assay for studying complex hetero-multivalency of agglutinating lectins. The TEA assay followed the expected results from our prior work, reiterating the concept of heterogeneous cooperativity in LecA binding to lipid mixtures of Gb3 with LacCer. In conclusion, the TEA assay enables the semi-quantitative detection of multivalent protein binding to heterogeneous lipid surfaces. Its high-throughput utility will significantly accelerate the ligand screening process of hetero-multivalency. Because TEA assay can conduct the analysis in a highly accessible, flexible, and inexpensive manner, it will immediately improve the biological community's ability to study hetero-multivalency of agglutinating lectins.

# CHAPTER V

# MULTIVALENT TARGETED LIPOSOMAL DRUG DELIVERY AGAINST *PSEUDOMONAS AERUGINOSA* [**]

## Chapter Summary

*P. aeruginosa* is a multi-drug resistant bacterium which is in a critical need of new antibiotics because of increasing resistance against existing antibiotics. One of the challenges in development of new drugs is their toxicity to the healthy host cells. An effective targeted drug delivery technique can reduce the drug toxicity while increasing the drug efficacy. Inspired by the mechanism of bacterial adhesion to host cells, we used host cell glycans as targeting ligands on liposomal drug carriers. LacCer is a low-affinity ligand for *P. aeruginosa*. However, targeted liposomes (containing LacCer with a high-affinity ligand, Gb3) had higher retention on bacteria compared to the non-targeted liposomes. This is because of the fluidic membrane that glycolipids on liposome can self-organize to reach hetero-multivalent interactions with different adhesins on the bacterium. After the first ligand attachment, because of the reduced dimension of diffusion, the reaction rate of the subsequent bindings is at least $10^4$ times higher than the first binding. Thus, low-affinity ligands, can also significantly contribute to the bacterial attachment. In a thigh infected mouse model, the drug retention rate increased by up to 200% in the thigh. Furthermore, treatment with targeted liposomal ciprofloxacin led to an 83% and 33% higher survival rate in mice compared to free ciprofloxacin and non-targeted liposomal ciprofloxacin, respectively. We envisage that the techniques used in this study can be more broadly applied to design drug carriers for treatment against other multi drug resistant pathogens.

[**] Article submitted to Antimicrobial Agents and Chemotherapy Journal

## Introduction

Bacterial resistance to existing antibiotics has become a serious public health problem[3,6-8,210]. Approximately 2.8 million antibiotic resistant infections occur in the United States every year, leading to more than 35,000 deaths[9]. Multi-drug resistant (MDR) *Pseudomonas aeruginosa* is one of the bacteria posing serious threats. Due to intrinsic low permeability of its outer membrane, mutational mechanisms[211-215], additional penetration barrier by biofilm formation[129,216], and adaptation to environment conditions and stresses[16], *P. aeruginosa* has developed resistance to many existing antibiotics. *World Health Organization* listed *P.* aeruginosa among the top three pathogens which are in a critical need of new antibiotics[5]. As a result, an extensive research is being done on the development of new antibiotics. However, besides being effective against the bacteria, many of the newly developed drugs could also be toxic to the healthy host cells. Continuous and frequent drug dosing for long periods to treat MDR pathogen further leads to adaptive resistance to antibiotics[16]. Therefore, an effective targeted drug delivery technique which can increase the local drug concentrations at the site of infection is an ideal tool to reduce drug toxicity and enhance drug efficacy.

In this paper, we have developed a liposome-based drug delivery system with glycans as targeting ligands for an effective treatment against *P. aeruginosa*. Prior research has demonstrated that liposomal antibiotics have superior efficacy leading to a shorter course of treatment at lower cumulative doses compared to free antibiotics as a treatment against MDR pathogens such as *Streptococcus pneumoniae* and *Klebsiella pneumoniae*[217-221]. Encapsulation of antibiotics in liposomes can improve pharmacokinetics and biodistribution as well as enhance the activity against extracellular pathogens, particularly to overcome the bacterial drug resistance[217,222,223]. In addition to these known advantages, we prefer liposomes over other types

of drug carriers because liposomes can offer the unique two-dimensional ligand fluidity to enable the multivalent interactions between a drug carrier and a bacterium[28,29,82].

It is known that *P. aeruginosa* adhesion to host cells is mediated by binding of several surface adhesins, including LecA (i.e. PA-IL), LecB (i.e. PA-IIL), and Type IV Pilus (T4P), to glycan ligands on epithelial cell surfaces[124-128]. If different ligands on a drug carrier can simultaneously bind to multiple bacterial adhesins, the increase in ligand-receptor affinities should improve the targeting efficiency and specificity[165]. To achieve this goal, we investigated the binding mechanism of *P. aeruginosa* adhesins to various glycolipids from human epithelia[29,82]. We discovered a new glycolipid, lactosylceramide (LacCer), which could improve the attachment of liposomes to *P. aeruginosa*. Interestingly, LacCer is a low-affinity ligand of *P. aeruginosa*. When liposomal drug carriers were prepared with 10 mol% of LacCer alone, no improvement of liposome retention was observed. However, by mixing LacCer with the other known *P. aeruginosa* ligand, globotriaosylceramide (Gb3), on the same liposome surface (5 mol% LacCer / 5 mol% Gb3), we could observe contribution of LacCer to the *P. aeruginosa* binding, leading to an increased liposomal retention rate[29]. The mechanism of this hetero-multivalent binding phenomenon is shown in Figure. 23. The first binding between liposomes and bacteria is initiated by a high affinity glycolipid (e.g. Gb3). After the first attachment, the unbound glycolipids can freely diffuse and rearrange on the surface of liposomes and bind to the other bacterial adhesins in the vicinity of the attached liposomes. Due to the reduced dimension of diffusion, the effective reaction rate of subsequent bindings on the 2D surface are at least $10^4$ times higher than the first binding in 3D space[26]. This intrinsic rate enhancement mechanism, called reduction of dimensionality (RD), facilitates the binding between bacterial adhesins and low-affinity glycan ligand, leading to an enhanced retention of liposomes on the bacteria.

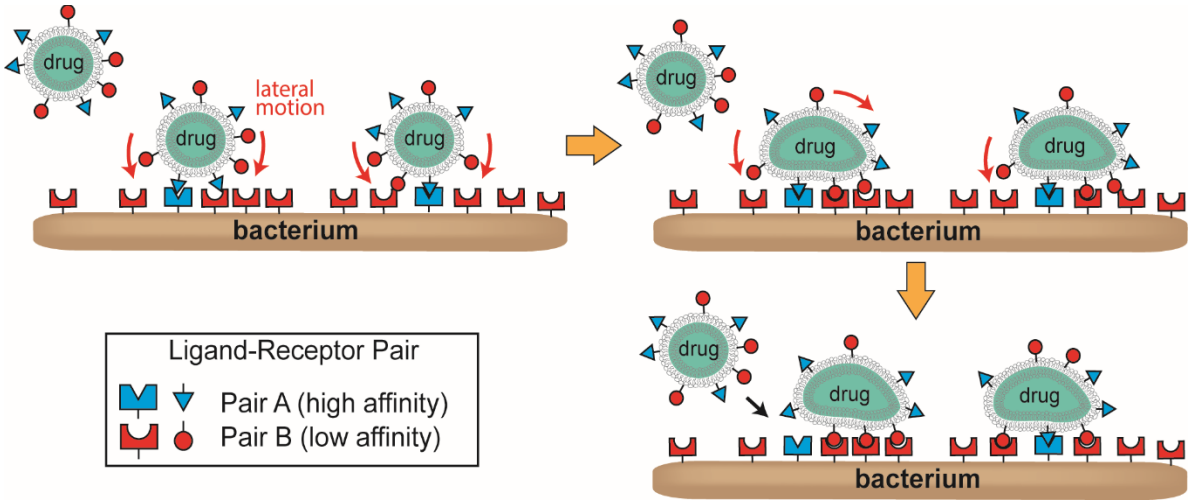


Figure 23: Reduction in dimensionality (RD) mechanism with liposomes. The first binding between liposomes and bacteria essentially happens in a 3D space. Liposomes diffuse from the solution phase to a bacteria surface and the first binding is initiated by a high affinity glycolipid (on the liposome) and receptor (on the bacterial surface) pair. After the first attachment, the unbound glycolipids can diffuse two dimensionally on the liposome surface, encounter with their respective receptors and enable subsequent binding. The reaction rate on a 2D surface is $10^4$ times higher than the reaction rate in 3D space. Thus, low-affinity glycolipids can also contribute in subsequent bindings. This hetero-multivalent binding between liposomes and bacteria causes higher retention of liposomes on the bacteria surface, leading to attachment of more number of liposomes.

This hetero-multivalent binding mechanism offers a new strategy to enhance the targeting efficiency of the drug carrier. Two-dimensional mobility of the ligands on the drug carrier surface is the key to activate the binding pairs with lower binding affinities. Liposomes provide the critical two-dimensional membrane fluidity and, hence, are an ideal tool to enhance multivalent targeting efficiencies. In this paper, therefore, we have examined the efficacy of liposomal antibiotics against *P. aeruginosa*. We have compared the biodistributions of targeted and non-targeted liposomes in the murine *P. aeruginosa* thigh infection model. Additionally, we have encapsulated a common antibiotic, ciprofloxacin, in liposomes and have evaluated the efficacy of the drug in three different drug delivery systems, a) ciprofloxacin encapsulated in

targeted liposomes, b) ciprofloxacin encapsulated in non-targeted liposomes, and c) free ciprofloxacin. Results indicate that this hetero-multivalent liposomal drug has a great potential for an effective treatment against *P. aeruginosa*.

## Methods

### Liposome preparation and size determination

The liposomes or small unilamellar vesicles (SUVs) were prepared via extrusion 27. The desired compositions of phospholipids and glycolipids in chloroform were mixed in 25 mL round bottom flask and then dried using a rotary evaporator (Heidolph Hei-VAP Value®). The non-targeted liposomes contain 100 mol% 1-palmitoyl-2-oleoyl-glycero-3-phosphocholine (POPC) and the targeted liposomes contain 90 mol% POPC, 5 mol% globotriaosylceramide, Galα1-4Galß1-4Glc-Ceramide, (Gb3) and 5 mol% lactosylceramide, Galβ1-4Glc-Ceramide, (LacCer). To prepare the ciprofloxacin encapsulated liposomes, the dried lipids were rehydrated with 9 g/L ciprofloxacin in 0.1 N hydrochloric acid (HCl) solution. The overall liposome concentration was maintained at 5 g/L. The liposome solution was then extruded through 100 nm polycarbonate filters (Whatman®) using a mini-extruder (Avanti Polar Lipids) to prepare SUVs. The liposome solution was then incubated at 4°C for 20-24 hours to stabilize the liposomes-ciprofloxacin formulation. In this technique, the ciprofloxacin drug gets encapsulated in the aqueous core of the liposomes. To remove the un-encapsulated drug, the liposome solution was filtered using MilliporeSigma Amicon Ultra 0.5 mL vials with pore size 50 kDa and centrifuging at 16000 xg for 20 minutes and the volume is reconstituted with 0.1 N HCl to maintain the liposome concentration at 5 g/L. The un-encapsulated ciprofloxacin concentration in the filtrate was estimated by measuring the absorbance OD of ciprofloxacin at 278 nm using a UV-VIS

spectrometer. The concentration of ciprofloxacin encapsulated in liposomes, encapsulation efficiency and drug loading are estimated as follows:

$$Encapsulated\ ciprofloxacin, Ci_{liposomes}, \left(\frac{g}{L}\right) = \frac{Ci_{total} \times V_{total} - Ci_{filtrate} \times V_{filtrate}}{V_{total}} \quad \text{Equation 39}$$

$$Encapsulation\ efficiency\ (\%) = \frac{Ci_{total} - Ci_{filtrate}}{Ci_{total}} \times 100 \quad \text{Equation 40}$$

$$Drug\ loading\ (g/g) = \frac{Ci_{liposomes}}{C} \quad \text{Equation 41}$$

Where $Ci_{total}$ is the initial ciprofloxacin concentration in the liposome solution before filtration, $Ci_{filtrate}$ is the ciprofloxacin concentration in the filtrate and $C$ is the liposome concentration, and $V_{total}$ and $V_{filtrate}$ are the volume of the liposome solution and filtrate solution respectively.

For the preparation of fluorescent labeled liposomes for bio-distribution and phagocytosis study, the dried lipids were reconstituted using MilliQ® water and, then, extruded. The composition of non-targeted liposomes was 99 mol% POPC and 1 mol% Texas Red™ 1,2-dihexadecanoyl-sn-glycero-3-phosphoethanolamine, triethylammonium salt (TR-DHPE) and targeted liposomes was 89 mol% POPC, 5 mol% Gb3, 5mol% LacCer and 1 mole% TR-DHPE.

Particle sizes of the liposomes were measured by dynamic light scattering (DLS) using Malvern Zetasizer Nano ZS90 (Malvern Instruments, Southborough, Massachusetts) with detection occurring at 90° to the light source.at room temperature. The liposomes were diluted 10 times followed by equilibration at 25 °C. After dilution, the solution was checked for multi-particle scattering by further diluting the liposome solution 2 times. A minimum of three measurements per sample was taken.

**Drug release rate estimation**

The ciprofloxacin encapsulated liposome solution stored in Thermoscientific slide-A-Lyzer G2 dialyses cassettes, 10 kDa was kept in a sink of 1X phosphate buffered saline (PBS). The amount of drug released in the PBS solution was estimated by measuring the absorbance OD at 278 nm at different time points. The sink solution was replaced every 4 hours.

**Flow Cytometry**

J774.A1 murine macrophage (MØ) were maintain in a humidified condition at 5% CO2, 37℃. Cells were maintained in Dulbecco's Modified Eagles's Medium (DMEM-high glucose supplemented with 10% (v/v) fetal bovine serum, 1 % (v/v) sodium pyruvate, 1 %(v/v) non-essential amino acids and 1% (v/v) penicillin-streptomycin. When cells were passed in 75 flask Becton Dickinson (BD), J774.A1 MØ reached 90% confluence. MØ cells were seeded into 12 wells plate at roughly 1x106 cells/well and incubated overnight in pen-strep free culture media. After an overnight adherence, old medium was replaced 1 mL of free pen-strep free media containing 10, 15, and 20 µg/mL of PE-Texas-Red dyed liposomes and incubated for 1 hr, at 100 rpm, 37ºC, 5% CO2. After incubation, media was removed and cells were washed at least twice with 1X cold PBS to stop liposome internalization. Cells were scraped and centrifuged at 1500 rpm for 10 min at 4ºC. The supernatant was removed and the cells were fixed 4% paraformaldehyde (PFA) for 15 min at room temperature. Liposomal uptakes were analyzed using BD LSRFortessa™X-20 flow cytometry equipped with air-cooled argon ion laser emitting at 561 nm excitation and emission spectra for PE-Texas Red at 610/20, 600LP and DB FACSDiva software. We counted 10,000 events and analysis was performed using Flowjo software.

**Bacterial strain, media, cell culture**

Wild-type *PAO1* strain of *Pseudomonas aeruginosa* and *PAO1-GFP* expressing green fluorescence protein (GFP) on plasmid pMEP9-1 strain were utilized for our studies. Wild-type *PAO1* was cultured in Mueller-Hinton broth and *GFP-PAO1* was cultured in MH-broth with 500 μg/mL carbenicillin to select for plasmid pMEP9-1. Murine macrophage, J774.A1, were maintained in 37°C, 5% CO2 humidified incubator in Dulbecco's Modified Eagles's Medium (DMEM-high glucose supplemented with 10% (v/v) fetal bovine serum, 1 % (v/v) sodium pyruvate, 1 %(v/v) non-essential amino acids and 1% (v/v) penicillin-streptomycin with and without.

**In vitro antimicrobial activity of liposomal ciprofloxacin**

A single colony of *PAO1* bacteria were isolated by streaking from frozen glycerol stock onto tryptic soy agar (BD) and incubated overnight at 37 °C A single colony was inoculated in 5 mL Mueller- Hinton (MH) broth, grown at 37 °C, 200 rpm in a shaking incubatory to mid-log phase OD650 = 0.4 corresponding to 0.5 McFarland. The bacterial culture was then diluted to a density of 5x105 CFU/mL in MH broth. Ciprofloxacin encapsulated liposomes were prepared as described above and a 10 mg/mL of free ciprofloxacin was prepared by dissolving in 0.1 N HCl aqueous solution. The antimicrobial activity of ciprofloxacin-loaded liposome was performed in comparison to ciprofloxacin free drug were done using the standard broth microdilution in accordance to CLSI guideline. A two-fold serial dilution of free ciprofloxacin and liposomal ciprofloxacin were prepared in MH broth containing 0.1 N HCl 5% (v/v) and plated in triplicate in 96 well plate. A 95:5% (v/v) MHB to 0.1 N HCl, MHB to 90 mol% POPC + 5 mol% Gb3 + 5 mol% LacCer targeted liposomes, and MHB to 95 mol% POPC non-targeted liposome with ciprofloxacin plus bacteria were used as positive control and the negative control using MH

broth only. The 96 well plate was then sealed in Breatheasy® membrane and incubated for 18-24 hrs at 37℃. The lowest concentration of free drug or liposome that inhibited the bacterial growth was defined as minimum inhibitory concentration (MIC) and concentration higher than MIC were then plated on tryptic soy agar with 5% sheep blood and incubate at 37℃ for 18-24hr. The lowest concentration where no bacterial growth was defined as minimum bactericidal concentration (MBC). The experiment was done in triplicate at least three times for reproducibility.

**Time-kill kinetics**

Time-kill kinetics was performed using known MIC value for free drug and liposome encapsulated ciprofloxacin are 0.125 μg/mL respectively. *PAO1* was cultured to mid-exponential phase in MH-broth to OD650 = 0.4 and diluted down to 5x105 CFU/mL and seeded quadruplicate in a 96 well plate at 0X MIC, 0.5X MIC, 1X MIC, 2X MIC and 4X MIC concentrations. The 96 well titer plate was then incubated at the following time point: 1, 2, 6, 12 and 24 h at 37 ° C, 140 rpm. At each time point, 1:10 serial dilution was performed in phosphate buffered solution 1X PBS and 50 μL of dilution were then suspended on TSA plate with 5% sheep blood via sterile beads and incubate for 18-24 h. Bacterial colonies were counted and time-kill curves were generated and normalized to the starting inoculum.

**Murine P. aeruginosa thigh infection model**

Male CD-1 mice weighing 22-24 g were acquired from Charles Rivers Laboratory were used for all studies. The studies were approved by *Texas A&M University Institutional Animal Care and Use Committee* (IACUC). Ciprofloxacin encapsulated targeted and non-targeted liposome as well as empty targeted liposomes were prepared as prescribed above, free ciprofloxacin-HCl was dissolved in 1:1 (v/v) of 0.1 N HCl and prepared in 0.9% sterile saline

solution for injection. *P. aeruginosa* (*PAO1*) and *PAO1* expressing green fluorescent protein (*PAO1*-GFP) on plasmid pMRP9-1 were grown on TSA plates as described above. Single colony of PA01 and PA01-GFP was suspended in Luria broth (LB; 50 mL) and Luria Broth supplemented with 500 µg/mL carbenicillin (VWR) (LB+500 µg/mL) respectively and grown in a shaking incubator (37°C, 200rpm) to an OD650 of 0.4 which correspond to 0.5 McFarland. The bacterial was then washed three times with 0.9% saline via centrifugation at 2500 rpm, 15 min for 4 °C and 1.0 x $10^9$ CFU/mL bacterial inoculum was prepared in LB and confirmed by serial dilution and plating. Full sedation was induced in mice by intraperitoneal administration of 60 mg/kg ketamine and 8 mg/kg xylazine solution. At t = 0 all mice were inoculated by intramuscular thigh injection with 0.1 mL of *PAO1* inoculum at 1.0x$10^9$ CFU/mL. Mice were then scored for weight, tagged and assorted into a randomized treatments group. Liposomal drug and free drug treatment were administered two hours after the initial infection (dose 1) and every 12 h after the initial dose 1. Sham and empty targeted liposomes were treated with 0.1 mL of sterile 0.9% saline solution, and % targeted liposome in sterile 0.9% saline respectively. Encapsulated and non-encapsulated ciprofloxacin were dissolved and prepared at pediatric dose of 10mg/kg concentration and 10% of mice weight were used as concentration basis for treatment targeted, non-targeted ciprofloxacin liposomes and free ciprofloxacin based on preliminary dose finding study. At each treatment interval blinded investigator assigned clinical score to all treatment groups. The survival studies were performed in duplicate and the result were pooled.

**Liposomal bio-distribution in murine model**

*In vivo* liposomal bio-distribution was carried out in the same infection model described above and treated with PE-Texas red dye tagged targeted and non-targeted liposomes two hours

after infection. Four hours after infection, 2 h after treatment, the mice were anesthetized, blood exsanguinated via cardiac puncture, dissected lung, heart, liver, spleen and thigh muscle and homogenized in 1X PBS, except the lung which was homogenized in 0.9% saline solution. Tissue homogenate were then plated in black 96 well titer plate and GFP and PE-Texas red fluorescence were read at excitation and emission and bacterial were quantified 488/511 nm and 580/620 nm, respectively using BioTek Cytation 5.

## Results

### Characterization of liposomal ciprofloxacin

The literature has shown that 100 nm liposomes have longer blood circulation time and better penetration into physiological barriers, such as skin, sputum, mucus, and P. aeruginosa biofilms[224-230]. Thus, we fabricated 100 nm ciprofloxacin loaded liposomes by the extrusion method with 100 nm size polycarbonate filters and then, characterized the size and drug encapsulation efficiency. The non-targeted liposomes contain 100 mol% POPC lipids, and the targeted liposomes contain 5 mol% Gb3, 5 mol% LacCer, and 90 mol% POPC. In our previous study [29], *in vitro* results demonstrated that this composition of targeted liposomes had up to 2.5 times and 4 times higher attachment with *P. aeruginosa* strains PAO1 and Xen41 respectively, compared to the non-targeted liposomes. The average diameters of non-targeted and targeted liposomes were measured to be 108 ± 0.3 nm and 118 ± 4.2 nm respectively using dynamic light scattering (Figure 24a). Forier et al. determined the apparent penetration levels to be about 50% in the *P. aeruginosa* biofilms for liposomes in this size range [224]. The drug encapsulation efficiency and drug loading are very similar for both non-targeted and targeted liposomes (Figure 24b and 24c). Additionally, the release rate of ciprofloxacin from liposomes was measured using

a dialysis cassette within a sink of 1X PBS buffer (Figure 24d). The release kinetics for non-targeted and targeted liposomes were similar.

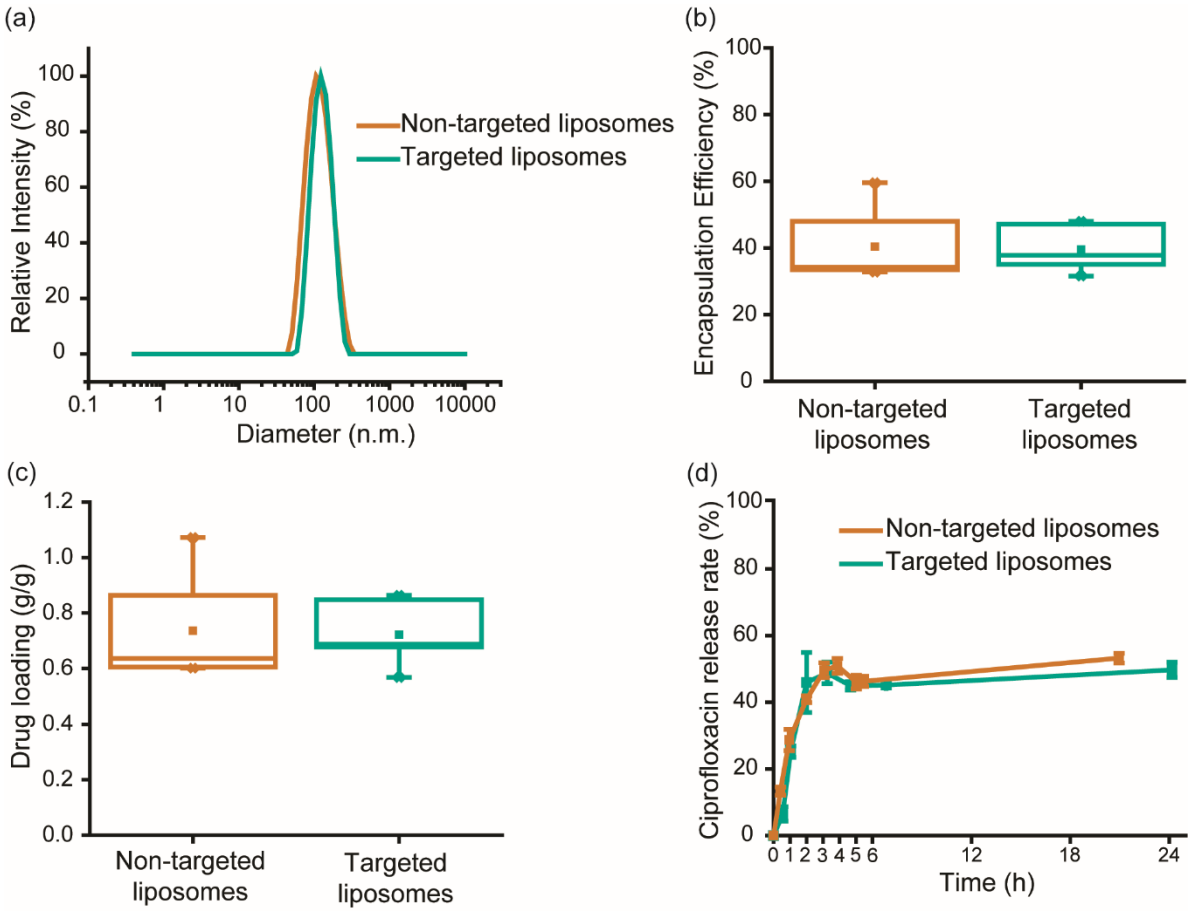


Figure 24: Characterization of ciprofloxacin encapsulated targeted (containing 5 mol% Gb3 and 5 mol% LacCer and non-targeted (containing no ligand) liposomes. a) Hydrodynamic diameter of the liposomes measured using DLS, b) encapsulation efficiency of ciprofloxacin in liposomes for n = 6 measurements, c) drug loading in liposomes for n = 6 measurements, and d) release rate of ciprofloxacin from liposomes in a sink of 1X PBS buffer solution measured using dialysis cassettes. For the box plots in (b & c), the box encompasses the 'interquartile range 25%~75%', dot inside the box represents 'mean', horizontal bar inside the box represents 'median' and the whiskers are determined by the 5$^{th}$ and 95$^{th}$ percentiles. Data in release rate measurements are reported as mean ± S.E. (n=5).

**Macrophage uptake**

Direct interaction of liposomes with macrophages plays an important role in liposome clearance [228]. To evaluate the influence of macrophage uptake, we determined the phagocytosis of liposomes with *J774.A1* murine macrophage using flow cytometry (Figure 25). Both targeted and non-targeted liposomes had similar phagocytosis. Their uptake rates are lower than the positive control liposomes containing 30 mol% POPS, but slightly higher than the stealth liposomes (PEGylated liposomes).

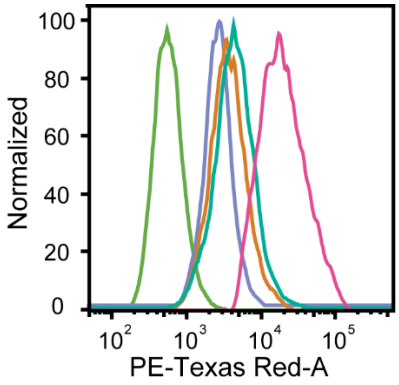


| | Sample | Mean | Geometric Mean |
|---|---|---|---|
| | Macrophages only | 651 | 584 |
| | PEGylated liposomes | 2906 | 2668 |
| | Non-targeted liposomes | 4324 | 3654 |
| | Targeted liposomes | 5240 | 4359 |
| | POPS lipsomes | 24828 | 19446 |

Figure 25: Phagocytosis of different liposomes by J774.A1 murine macrophages measured by flow cytometry. Control liposomes, containing 30 mol% POPS, have higher uptake by the macrophages than the PEGylated liposomes. There is not much difference in phagocytosis of targeted (5 mol% Gb3 and 5 mol% LacCer) and non-targeted liposomes by the macrophages, which indicates that the difference in the bio-distribution with the targeted and non-targeted liposomes is because of the attachment of targeted liposomes with the bacteria.

**In vitro efficacy of liposomal ciprofloxacin**

The minimum inhibitory concentration (MIC) and the minimum bactericidal concentration (MBC) of ciprofloxacin in three delivery systems, a) free drug, b) drug encapsulated in targeted liposomes, and c) drug encapsulated in non-targeted liposomes against

*PAO1* strain of *P. aeruginosa* were determined by following CLSI microdilution protocol[231]. Free ciprofloxacin is very effective against *PAO1* strain, resulting in a low MIC of 0.125 μg/mL and MBC of 0.25 μg/mL.The MIC and MBC values of targeted and non-targeted liposomal ciprofloxacin were identical to the values of free ciprofloxacin. For the CLSI microdilution protocol, the free and liposomal drugs were incubated with the bacteria during the entire experiment. This result indicates that ciprofloxacin was sufficiently released from the liposomes and contacted with bacteria during the incubation period.

To examine the effect of drug release, we also measured the time-kill kinetics of bacteria at different drug concentrations. Figure 26 shows the growth of bacteria with time for different drug delivery systems at different drug concentrations. The rate of bacterial inhibition with liposomal ciprofloxacin was slower compared to the free drug. At a drug concentration of 0.25 and 0.5 μg/mL, the free ciprofloxacin killed all the bacteria within 2 hours, whereas there were some bacteria present with liposomal ciprofloxacin, albeit at inhibited growth. This is because the slow release of the drug from the liposomes delayed the drug response. Because the drug release rates of targeted and non-targeted liposome are similar (Figure. 24d), the time killing kinetics of the targeted and non-targeted liposomal drugs were comparable.

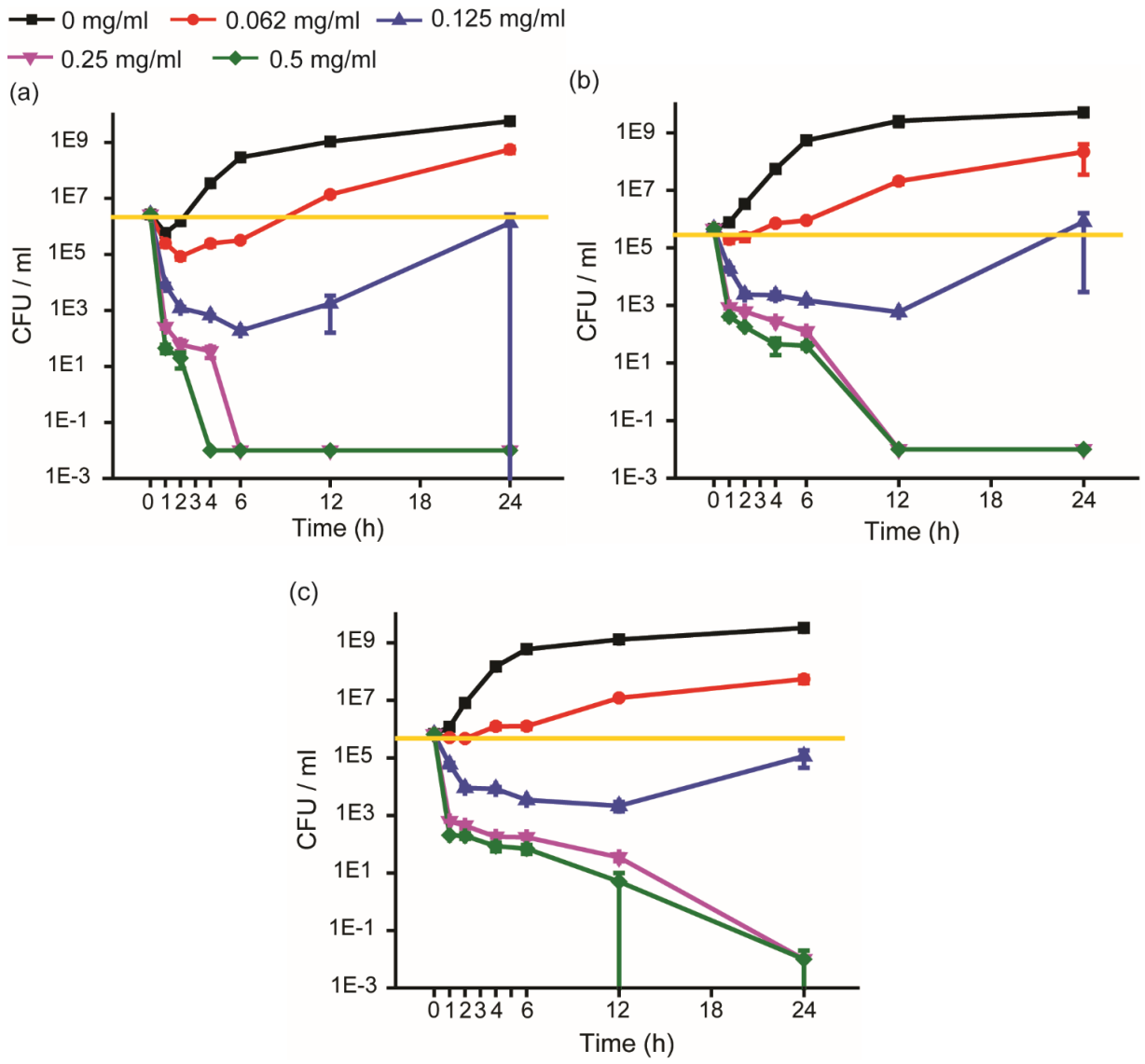


Figure 26: Time-dependent bactericidal activity of ciprofloxacin against P. aeruginosa PAO1 at different drug concentrations for different drug delivery systems. a) free ciprofloxacin i.e. drug administered directly without any drug carrier. b) Targeted liposomes carrying ciprofloxacin. c) Non-targeted liposomes carrying ciprofloxacin. Mycobacterial cultures were exposed to ciprofloxacin in different delivery systems for 24 h at 37 °C. At 1, 2, 4, 6, 12 and 24 h, 100 µL of samples were added on blood agar plates and incubated for 18 h at 37 °C to determine colony forming units (CFU). The yellow line represents the bacterial inoculum CFU, so any value below this line indicates inhibited bacterial growth. While there is inhibited or no bacterial growth at drug concentrations ≥ 0.125 µg/mL (MIC for ciprofloxacin) with both drug delivery systems, the rate of bacteria killing is slower with liposomes. This is because of the controlled release of drug from liposomes whereas bacteria is exposed to all the drug with free ciprofloxacin from time t = 0 h. All data points are reported as mean ± S.E (n = 4). Experiments were performed in triplicates. Results shown are from one representative experiment.

**In vivo biodistribution of liposomes**

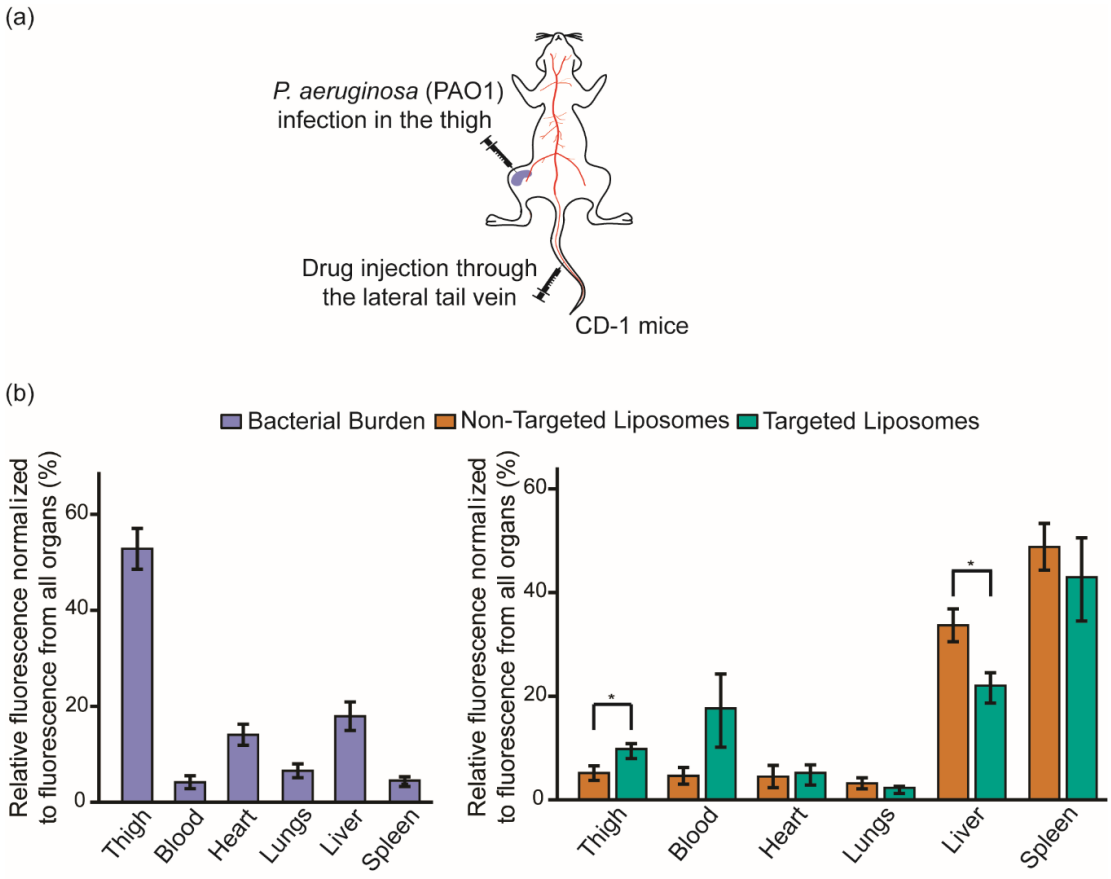


Figure 27: Biodistribution of targeted and non-targeted liposomes in a thigh infected mouse model. a) Mouse schematic showing bacterial infection in the thigh and liposomal administration through the lateral tail vein. b) Relative fluorescence in each organ tissue is presented as the percentage of total fluorescence in all the organs for targeted, non-targeted liposomes and bacteria. The left thigh of the mice were infected with the $1 \times 10^9$ CFU/ml of bacteria and 5 g/L concentration of respective liposomes were injected through the tail vein. Targeted liposomes contain 5 mol% Gb3, 5 mol% LacCer. Localized amount of targeted liposomes is two times higher than the non-targeted liposomes at the site of infection, thigh. All the data are reported as mean ± S.E. of n=15 mice.

In the MIC/MBC and time-killing kinetic experiments, free and liposomal ciprofloxacin were incubated with the bacteria during the entire experiment; thus, *in vitro* results could not demonstrate the advantage of the targeted liposomes. In addition, *in vitro* experiments did not

consider the influences of the reticuloendothelial system and drug clearance. To address these issues, we evaluated the efficacies of the three delivery systems in a thigh infected mouse model.

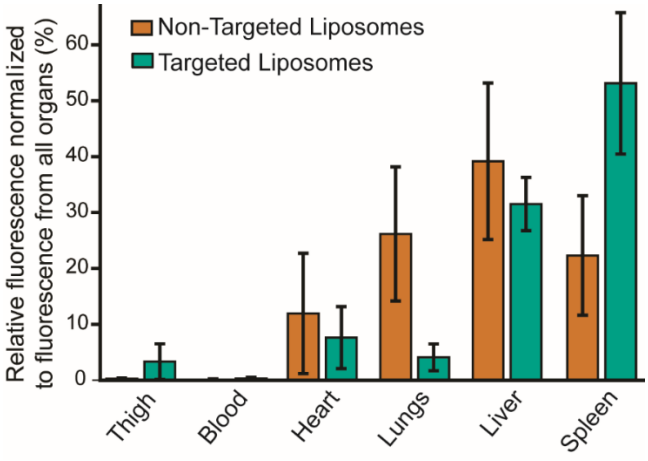


Figure 28: Bio-distribution of targeted and non-targeted liposomes in the absence of bacteria in the mice. Relative fluorescence in each organ tissue is the percentage of total fluorescence in all the organs for both targeted and non-targeted liposomes. 5g/L concentration of respective liposomes were injected through the tail vein. Targeted liposomes contain 5 mol% Gb3, 5 mol% LacCer. Localized amount of targeted and non-targeted liposomes are not statistically different at the site of infection, thigh. All the data are reported as mean ± S.E. of n=15 mice.

In our previous research, we demonstrated that the attachment of targeted liposomes was up to 2.5 times higher than the non-targeted liposomes *in vitro*. To cognize if the targeted liposomes have higher targeting efficiency *in vivo* as well, we explored the biodistribution of targeted and non-targeted liposomes in the thigh infected mice. We first infected the mice thigh with *PAO1* and, then, fluorescently labelled targeted and non-targeted liposomes were administered through the lateral tail vein. Figure. 27 shows the bio-distribution of liposomes in different tissues. We observed that the localization of targeted liposomes is two times higher than the non-targeted liposomes in the thigh tissue where the bacteria was infected ($p < 0.05$). This

implies that the targeted liposomes probably attached to bacteria present in the thigh. In the liver and spleen tissues, the amount of non-targeted liposomes were higher than the targeted liposomes. Because liver and spleen are the primary reticuloendothelial system organs for liposome clearance[228], this result indicates that non-targeted liposomes might be getting cleared more rapidly from the body. To verify that the difference in biodistribution of targeted and non-targeted liposomes is caused by the bacterial infection, we also measured the biodistribution of targeted and non-targeted liposomes in health mice. There was no statistical significance between biodistribution of targeted and non-targeted liposomes in the absence of bacterial infection (Figure. 28). This further corroborates that the accumulation of targeted liposomes in the thigh and the blood tissue might be caused by the interaction between the bacteria and targeted liposomes.

**Survival study for drug efficacy evaluation**

We also conducted a survival study using the thigh infected mice to further assess the efficacy of the three drug delivery systems. The mice thigh was infected with bacteria PAO1 and the free and liposomal ciprofloxacin were administered through the lateral tail vein (Figure. 29). Since, *PAO1* strain is extremely sensitive to ciprofloxacin, we first estimated an appropriate dose of free ciprofloxacin for the survival study (Figure. 30). To demonstrate that the targeted liposomes exhibit better drug efficacy, we chose ciprofloxacin dose of 1 mg/kg which is not sufficient to inhibit the bacteria in the free ciprofloxacin system. Figure. 29 shows that all the mice administered with free ciprofloxacin died after 28 hours of bacterial infection, whereas 42% and 73% of the mice administered with ciprofloxacin encapsulated non-targeted and targeted liposomes respectively were still alive.

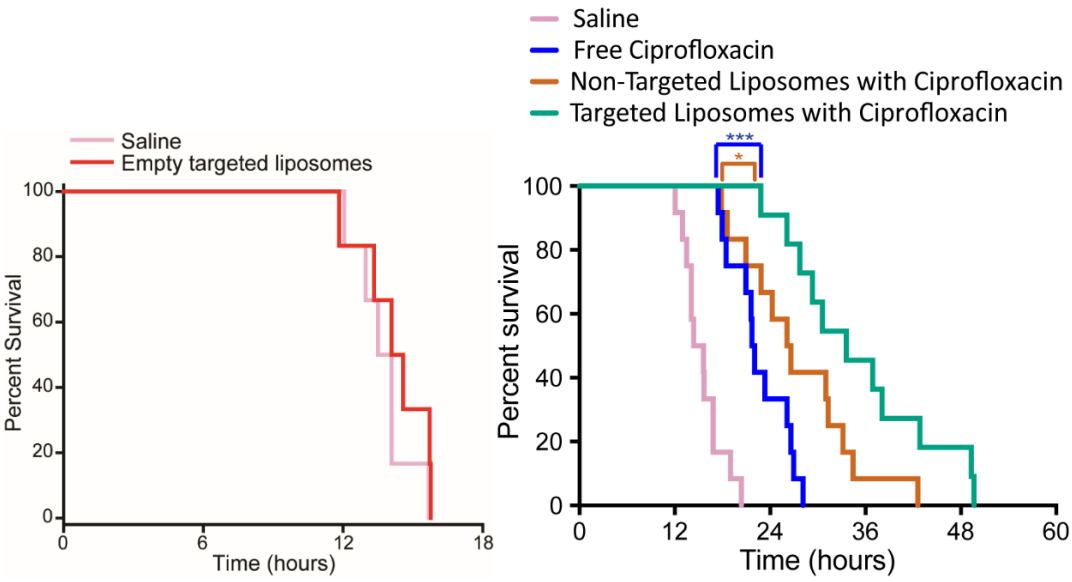


Figure 29: Survival rate of mice with drug delivery systems, targeted liposomes containing ciprofloxacin, non-targeted liposomes containing ciprofloxacin and free ciprofloxacin. The drug loading in the liposomes was 1 g/g. The left thigh of the mice was infected with the $1.0x10^9$ CFU/mL concentration of bacteria *PAO1* and ~32 µg/ml concentration of drug in different delivery systems was injected through the tail vein of n=12 mice per group. The mice administered with targeted liposomes have higher survival rate than with non-targeted liposomes and free ciprofloxacin.

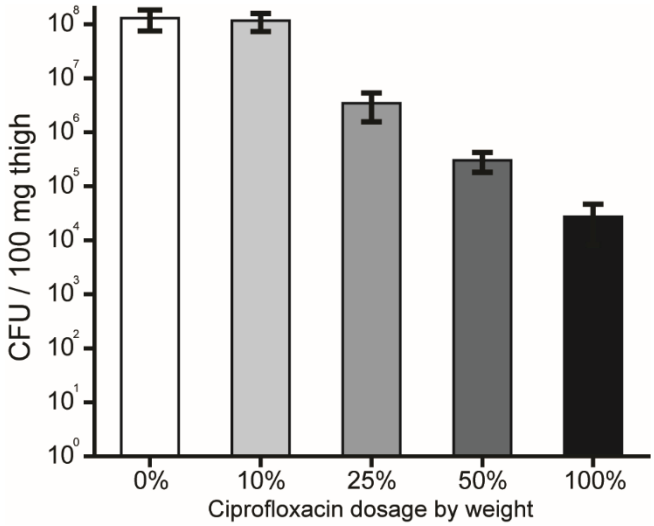


Figure 30: Estimation of ciprofloxacin dosage required for survival study. The left thigh of the mice was infected with the $1.0x10^9$ CFU/mL concentration of bacteria *PAO1* and free ciprofloxacin was injected through the tail vein of n=6 mice per group. 100% corresponds to the therapeutic dosage of ciprofloxacin for human i.e. 10 mg/kg. Data are reported as mean ± S.E.

## Discussion

Inspired by the nature of P. aeruginosa adhesion to epithelia, we incorporated two glycolipid ligands, Gb3 and LacCer, from host cells into liposomal drug carriers to achieve hetero-multivalent targeting. The hetero-multivalent binding strategy allows the accumulation of multiple ligand-receptor binding affinities, improving the overall targeting efficiency. Liposomes are better than other drug carriers because the targeting ligands can move two-dimensionally on the liposome surface, accelerating the hetero-multivalent binding process. In this paper, we fabricated multivalent targeted liposomal ciprofloxacin against *P. aeruginosa*. The increased mouse survival after treatment with targeted liposomal ciprofloxacin indicates that the hetero-multivalent targeting strategy is a promising approach for improving *P. aeruginosa* treatment.

One of the main challenges in liposomal drug delivery system is the liposome uptake by the macrophages that leads to removal from circulation. Liposome size and lipid saturation can influence the circulation half-life [232]. In addition, it has been demonstrated that some gangliosides can reduce the extent of uptake of liposomes by macrophages *in vivo* and thereby prolonging the circulation half-lives [232,233]. To address these concerns, we determined the phagocytosis of liposomes with *J774.A1* murine macrophage. Although, the addition of glycolipid ligands slightly increases the diameter of liposomes from 108 nm (non-targeted liposome) to 118 nm (targeted liposome), and changes the compositions of fatty acids, the phagocytosis of targeted and non-targeted liposomes were comparable. Moreover, in healthy mice, the accumulation of targeted and non-targeted liposome in liver and spleen tissue was not statistically significant (SI Figure 2). This result indicates that the decoration of glycolipids on the liposomal carriers does not strongly influence the interaction with reticuloendothelial system.

Thus, the circulation half-lives of liposomal carriers might not be the major factor influencing mouse survival rates.

In the thigh infected mice, the biodistribution shows that the liposome can cross the physical barriers and reach the infected site. The accumulation of the targeted liposomes in the thigh tissue was two-fold higher than the non-targeted liposomes. This enhancement value is similar to the value observed from *in vitro* experiment. Our prior *in vitro* experiment has shown that the same composition of the targeted liposome had up to 2.5 times higher attachment with *P. aeruginosa* strains PAO1, compared to the non-targeted liposomes [29]. The increased residence of targeted liposomes at the infected site was probably the major cause of increased mouse survival.

Although, the two-fold increase of drug residence is sufficient to improve the mouse survival, further enhancement of targeting efficiency is ideal. In this paper, for proof-of-concept, we only decorated two glycolipid ligands on liposome carriers. We anticipate an improved targeting efficiency by incorporating more host cell molecules as targeting moieties. For example, the other known *P. aeruginosa* adhesin, LecB, can bind to fucosyl molecules [124]. The addition of Lewis antigens to the current liposome composition should further improve the targeting efficacy [234]. Moreover, the other types of glycan molecules could also serve as potential ligands for targeting *P. aeruginosa* bacteria and biofilms. Glycans have been used as potential therapeutic agents to inhibit *P. aeruginosa* biofilm formation or facilitate biofilm dissolution *in vitro* [235-238]. Human milk glycans and fructo-oligosaccharides have been used to block the *P. aeruginosa* lectins and reduce the bacteria growth [239,240]. A small randomized trial in patients suffering from *P. aeruginosa* lung infection revealed reduction in bacteria counts with sugar inhalation and as well as combined therapy (sugar inhalation and antibiotics) treatment [241]. If we

could discover new glycan ligands interacting with *P. aeruginosa*, we can decorate these ligands on the drug carrier to improve the efficacy from the current composition.

It is worth noting that the discovery of new targeting ligands should be done with great care. Some ligand-receptor binding pairs may exhibit relative low binding affinities. To utilize the low-affinity binding pairs, the low-affinity ligand (e.g. LacCer) has to be activated by other high-affinity ligands (e.g. Gb3) in a fluidic membrane environment. Conventional ligand-receptor screening assays (e.g. microarray) often immobilize ligands and detect one ligand at a time. Thus, the essential low-affinity binding ligands, which could exhibit high binding selectivity to the pathogens, might get overlooked. Our previously published membrane perturbation method could provide a more efficient technique to discover the potential low-affinity ligands involving *P. aeruginosa* binding [26].

## Conclusion

In summary, we demonstrated the potential of multivalent targeted liposomal drug for *P. aeruginosa* treatment. This new drug delivery technique based on hetero-multivalent targeting should be able to be used against any other pathogen.

# CHAPTER VI

# CONCLUSION AND FUTURE WORK

In this dissertation, we explored the hetero-multivalent binding phenomenon between bacterial lectins and glycans. We systematically explored the lectin–glycan binding affinity (i.e. lectin's retention capability of a ligand), lectin-glycan binding capacity (i.e. the absolute number of bound lectins), and binding kinetics which are the major factors influence the hetero-multivalent binding. Although each of these mechanisms is individually straightforward, the collective influence of all of them together is extremely nonlinear. This results in complex effects on the overall lectin binding process, which may further affect the downstream biological functions of lectins. Additionally, glycan ligand surface densities (which influences the 2D collision probability between bound lectins and free ligands), the binding competition between different types of ligands (e.g. density ratio of different ligands), and molecular structures affect the pattern recognition process.

The low-affinity glycans, which have millimolar dissociation constants, are nearly undetectable using conventional assays such as microarrays with immobilized glycans. Therefore, these low-affinity glycans have often been overlooked as potential binding partners of their respective lectins. Our experimental observations and kMC simulations demonstrate that the low-affinity ligands can contribute significantly to the lectin binding with the assistance of high-affinity ligands in a fluidic cell membrane via the RD mechanism. We found that even a tiny amount of high-affinity ligands can be sufficient to trigger large amount of bound lectins if the density of the low-affinity ligands is adequate. Furthermore, we also determined that a bound lectin can be stabilized by the low-affinity ligands alone through the ligand-exchange process. As

such, the cooperative action between low-affinity and high-affinity glycan ligands is the major contributor in the lectin recognition phenomenon and is not governed by only one specific ligand. This observation explains how the fucosyl glycans, including fucosylated proteins, $Le^x$, and blood groups, could influence CT intoxication, instead of the high-affinity GM1 ligand[38,46-49]. In addition, ligand diffusion may influence lectin-staining assays. Prior studies have reported that lectin staining on live or fixed cells could result in different lectin binding patterns[242,243]. Cell fixation not only reduces glycan ligand diffusion but also perturbs local ligand densities on membrane surfaces. However, our results clearly demonstrate that ligand diffusion is the major essence of heteromultivalent binding.

Since, these low-affinity ligands are often available in abundance on the cell membrane, do the cells use them during lectin binding processes from the evolution standpoint? The participation of low-affinity ligands can modify the lectin binding behaviors, including binding capacity, kinetics and bound states. The variation of lectin bound states may further modulate the downstream processes. We hypothesize that these low-affinity ligands can serve as a modulator to gradually adjust the reaction rates and strengths of the lectin binding. Dennis and Brewer have suggested that pattern recognition of lectin is a paradigm for conditional regulation[65]. The same concept has been also discussed in a recent review paper[30]. Varki has indicated that many glycan functions are "analog", not digital; hence, a cell could escape pathogens by changing glycosylation without significantly manipulating the intrinsic glycan functions[30]. In addition to glycosylation, the analog alteration of lectin binding behaviors can also be achieved by changing local ligand densities on the cell membranes. Such alterations can be done by different biological processes, such as cell polarization, membrane perturbation by signaling transduction, cytoskeleton-induced membrane reorganization, etc. Heteromultivalent binding, hence, offers

cells a delicate approach to rapidly control glycobiology processes. Further investigation is required to understand how heteromultivalency influences lectin functions.

Similarly, we have demonstrated that the bacteria targeting can be enhanced with multiple glycans via the RD mechanism. Glycans are a good choice for targeted drug delivery because these molecules are biocompatible, less immunogenic, small enough to cross tissue barriers, and relatively inexpensive[244-248]. For this purpose, we chose liposomes as our drug carriers since they allow incorporation of multiple glycolipids at different compositions on their surface while maintaining the fluidity of the ligands[249-251]. Additionally, liposomes can accommodate both hydrophilic and lipophilic drugs, which makes them suitable for variety of drugs[252]. Prior clinical studies have shown liposomes carrying antibiotics can penetrate into biofilms leading to higher drug efficiency[225,253]. By decorating liposomal carriers with a collection of high affinity glycans, efficiency of liposomal antibiotics can be enhanced through the principle of hetero-multivalency. The different glycan ligands will bind with multiple receptors on the bacteria leading to high retention. Thus, even having multiple different moderate affinity ligands may have higher retention than one high affinity receptors. Additionally, this technique can be used for any other bacterial or pathogen system.

In this dissertation, we have shown enhanced targeting of *P. aeruginosa* bacteria using two glycan ligands, Gb3 and LacCer. While these ligands had at least two times better efficiency against the bacteria compared to the non-targeted liposomes, the liposomal composition can further be optimized to obtain even better results. Moreover, the accumulation of Gb3 in tissues containing lysosymes of people suffering from Fabry disease could lead to heart failure, dialysis or stroke[254]. Thus, Gb3 may not be the best choice to be used as a targeting ligand. The purpose of this dissertation was to mainly establish the functioning of hetero-multivalency in lectin

binding processes, bacterial interaction with the cell membrane and targeted drug delivery against the bacteria. Our analytical tools, discussed in this dissertation, can be used to identify potential high- and low-affinity ligands that can be used for targeted drug delivery. For example, fucosylated molecules, which are abundantly available on the cell membrane, could be investigated in a similar manner. More theoretical tools can be developed which can be used to optimize the desired composition of the liposomes. Furthermore, we used an antibiotic, ciprofloxacin, which is still effective against *PAO1* strain *P. aeruginosa*. However, there are other strains of this bacteria which have become resistant to ciprofloxacin. Researchers are developing new drugs but the toxicity of these new drugs to the healthy host cells have yet to be addressed. The efficacy and toxicity of these new drugs could be tested with targeted liposomes against the resistant strains.

In conclusion, we are the first group to methodically explain the mechanism behind hetero-multivalent binding based on the inherent physics principle, Reduction of dimensionality. In particular, the development of targeted drug delivery for its future applications could be a milestone in the research of antibiotic resistance. The work is not yet finished; there is more to be discovered on this topic. Although, the two-fold increase of drug residence is sufficient to increase the mouse survival time, further enhancement of targeting efficiency is desired. In this study, for proof-of-concept, we functionalized the liposomal carriers with only two glycolipid ligands. We anticipate improved targeting efficiency by incorporating more host cell molecules as targeting moieties. For example, the other known *P. aeruginosa* adhesin, LecB, can bind to fucosyl molecules [124]. Thus, the addition of Lewis antigens to the current liposome composition may further improve the targeting efficacy [234]. Recently, new lectins on the surface of *P. aeruginosa* were identified by reverse vaccinology and their potential glycan partners were

screened using glycan microarray [255,256]. Moreover, other types of glycan molecules may also serve as potential ligands for targeting *P. aeruginosa* planktonic bacteria and biofilms. For example, glycans have been used as potential therapeutic agents to inhibit *P. aeruginosa* biofilm formation or facilitate biofilm dissolution *in vitro* [235-238]. Human milk glycans and fructo-oligosaccharides have been used to block *P. aeruginosa* lectins and reduce the bacteria growth [239,240]. A small randomized trial in patients suffering from *P. aeruginosa* lung infection revealed reduction in bacteria counts with sugar inhalation, as well as combination therapy with both sugar inhalation and antibiotics [241]. If new glycan ligands interacting with *P. aeruginosa* are discovered, we could functionalize the liposomal drug carriers with these newly discovered ligands to improve the binding affinity compared with the current composition. The discovery of new targeting ligands likely requires novel approaches. Some ligand-receptor binding pairs may exhibit relatively low binding affinities.

To utilize the low-affinity binding pairs, the low-affinity ligand (e.g. LacCer) has to be activated by other high-affinity ligands (e.g. Gb3) in a fluidic membrane environment, as has been shown in our prior research [29,82]. Conventional ligand-receptor screening assays (e.g. microarray) often immobilize ligands and detect one ligand at a time. Thus, the essential low-affinity binding ligands, which may exhibit high binding selectivity to the pathogens, might get overlooked. Our previously published membrane perturbation method provides a more efficient technique to discover the potentially low-affinity ligands involved in *P. aeruginosa* binding [26].

# REFERENCES


1 Prevention, C. f. D. C. a. CDC on Infectious Diseases in the United States: 1900-99. *Population and Development Review* **25**, 635-640 (1999).

2 Runcie, H. Infection in a Pre-Antibiotic Era. *Journal of Ancient Diseases & Preventive Remedies* **03**, doi:10.4172/2329-8731.1000125 (2015).

3 Ventola, C. L. The antibiotic resistance crisis: part 1: causes and threats. *P T* **40**, 277-283 (2015).

4 Adedeji, W. A. THE TREASURE CALLED ANTIBIOTICS. *Ann Ib Postgrad Med* **14**, 56-57 (2016).

5 Organization, W. H. (ed WHO) (WHO, Geneva, 2017).

6 D'Andrea, M. M., Fraziano, M., Thaller, M. C. & Rossolini, G. M. The Urgent Need for Novel Antimicrobial Agents and Strategies to Figureht Antibiotic Resistance. *Antibiotics (Basel)* **8**, doi:10.3390/antibiotics8040254 (2019).

7 Martens, E. & Demain, A. L. The antibiotic resistance crisis, with a focus on the United States. *J Antibiot (Tokyo)* **70**, 520-526, doi:10.1038/ja.2017.30 (2017).

8 Rather, I. A., Kim, B. C., Bajpai, V. K. & Park, Y. H. Self-medication and antibiotic resistance: Crisis, current challenges, and prevention. *Saudi J Biol Sci* **24**, 808-812, doi:10.1016/j.sjbs.2017.01.004 (2017).

9 Prevention, C. f. D. C. a. (ed U.S. Department of Health and Human Services) (CDC, Atlanta, GA, 2019).

10 Coculescu, B.-I. Antimicrobial resistance induced by genetic changes. *J Med Life* **2**, 114-123 (2009).

11 Monserrat-Martinez, A., Gambin, Y. & Sierecki, E. Thinking Outside the Bug: Molecular Targets and Strategies to Overcome Antibiotic Resistance. *Int J Mol Sci* **20**, 1255, doi:10.3390/ijms20061255 (2019).

12 Dever, L. A. & Dermody, T. S. Mechanisms of Bacterial Resistance to Antibiotics. *Archives of Internal Medicine* **151**, 886-895, doi:10.1001/archinte.1991.00400050040010 (1991).

13 Cantón, R., Horcajada, J. P., Oliver, A., Garbajosa, P. R. & Vila, J. Inappropriate use of antibiotics in hospitals: The complex relationship between antibiotic use and antimicrobial resistance. *Enfermedades Infecciosas y Microbiología Clínica* **31**, 3-11, doi:https://doi.org/10.1016/S0213-005X(13)70126-5 (2013).

14 Khachatourians, G. G. Agricultural use of antibiotics and the evolution and transfer of antibiotic-resistant bacteria. *Canadian Medical Association Journal* **159**, 1129 (1998).

15 Perreten, V. *et al.* Antibiotic resistance spread in food. *Nature* **389**, 801-802, doi:10.1038/39767 (1997).

16 Fernández, L., Breidenstein, E. B. M. & Hancock, R. E. W. Creeping baselines and adaptive resistance to antibiotics. *Drug Resistance Updates* **14**, 1-21, doi:https://doi.org/10.1016/j.drup.2011.01.001 (2011).

17 Canaparo, R. *et al.* Recent Developments in Antibacterial Therapy: Focus on Stimuli-Responsive Drug-Delivery Systems and Therapeutic Nanoparticles. *Molecules* **24**, 1991, doi:10.3390/molecules24101991 (2019).

18 Szymanski, C. M., Schnaar, R. L. & Aebi, M. in *Essentials of Glycobiology* (eds Ajit Varki, Richard D. Cummings, & Esko Jeffrey D.) Ch. 42, (Cold Spring Harbor Laboratory Press, 2017).

19 Bernardi, A. *et al.* Multivalent glycoconjugates as anti-pathogenic agents. *Chemical Society Reviews* **42**, 4709-4727, doi:10.1039/C2CS35408J (2013).

20 Cecioni, S., Imberty, A. & Vidal, S. Glycomimetics versus multivalent glycoconjugates for the design of high affinity lectin ligands. *Chemical reviews* **115**, 525-561, doi:10.1021/cr500303t (2015).

21 Cecioni, S. *et al.* Rational Design and Synthesis of Optimized Glycoclusters for Multivalent Lectin–Carbohydrate Interactions: Influence of the Linker Arm. *Chemistry - A European Journal*, 6250-6263 (2012).

22 Jung, H., Robison, A. D. & Cremer, P. S. Multivalent ligand-receptor binding on supported lipid bilayers. *Journal of structural biology* **168**, 90-94, doi:10.1016/j.jsb.2009.05.010 (2009).

23 Zhang, R.-G. *et al.* The Three-dimensional Crystal Structure of Cholera Toxin. *Journal of Molecular Biology* **251**, 563-573, doi:http://dx.doi.org/10.1006/jmbi.1995.0456 (1995).

24 Karaveg, K. *et al.* Crystallization and preliminary X-ray diffraction analysis of lectin-1 from Pseudomonas aeruginosa. *Acta Crystallographica Section D* **59**, 1241-1242, doi:10.1107/S0907444903008710 (2003).

25 Tripathi, A. & Bankaitis, V. A. Molecular Docking: From Lock and Key to Combination Lock. *J Mol Med Clin Appl* **2**, 10.16966/12575-10305.16106, doi:10.16966/2575-0305.106 (2017).

26 Krishnan, P. *et al.* Hetero-multivalent binding of cholera toxin subunit B with glycolipid mixtures. *Colloids and Surfaces B: Biointerfaces* **160**, 281-288, doi:https://doi.org/10.1016/j.colsurfb.2017.09.035 (2017).

27 Worstell, N., Krishnan, P., Weatherston, J. & Wu, H. J. Binding Cooperativity Matters: A GM1-like Ganglioside-Cholera Toxin B Subunit Binding Study Using a Nanocube-Based Cell Membrane Array. *PLOS ONE* **11**, e0153265 (2016).

28 Choi, H.-K., Lee, D., Singla, A., Kwon, J. S.-I. & Wu, H.-J. The influence of heteromultivalency on lectin–glycan binding behavior. *Glycobiology* **29**, 397-408, doi:10.1093/glycob/cwz010 %J Glycobiology (2019).

29 Worstell, N. C. *et al.* Hetero-Multivalency of Pseudomonas aeruginosa Lectin LecA Binding to Model Membranes. *Scientific Reports* **8**, 8419, doi:10.1038/s41598-018-26643-7 (2018).

30 Varki, A. Biological roles of glycans. *Glycobiology* **27**, 3-49 (2017).

31 Leney, A. C., Fan, X., Kitova, E. N. & Klassen, J. S. Nanodiscs and Electrospray Ionization Mass Spectrometry: A Tool for Screening Glycolipids Against Proteins. *Analytical Chemistry* **86**, 5271-5277, doi:10.1021/ac4041179 (2014).

32 Turnbull, W. B., Precious, B. L. & Homans, S. W. Dissecting the Cholera Toxin−Ganglioside GM1 Interaction by Isothermal Titration Calorimetry. *Journal of the American Chemical Society* **126**, 1047-1054, doi:10.1021/ja0378207 (2004).

33 Branson, T. R. *et al.* A protein-based pentavalent inhibitor of the cholera toxin B-subunit. *Angewandte Chemie International Edition* **53**, 8323-8327 (2014).

34 Varki, A., Etzler, M., Cummings, R. D. & Esko, J. D. *Essentials of Glycobiology 2nd edition*. (Cold Spring Harbor Laboratory Press, 2009).

35 Dawson, G. Measuring brain lipids. *Biochimica et Biophysica Acta (BBA) - Molecular and Cell Biology of Lipids* **1851**, 1026-1039, doi:http://dx.doi.org/10.1016/j.bbalip.2015.02.007 (2015).

36 Yanagisawa, M., Ariga, T. & Yu, R. K. Cholera toxin B subunit binding does not correlate with GM1 expression: a study using mouse embryonic neural precursor cells. *Glycobiology* **16**, 19G-22G, doi:10.1093/glycob/cwl031 (2006).

37 Breimer, M. E., Hansson, G. C., Karlsson, K.-A., Larson, G. & Leffler, H. Glycosphingolipid composition of epithelial cells isolated along the villus axis of small intestine of a single human individual. *Glycobiology* **22**, 1721-1730, doi:10.1093/glycob/cws115 (2012).

38 Wands, A. M. *et al.* Fucosylation and protein glycosylation create functional receptors for cholera toxin. *eLife* **4**, e09545, doi:10.7554/eLife.09545 (2015).

39 Kirkeby, S. Cholera toxin B subunit-binding and ganglioside GM1 immuno-expression are not necessarily correlated in human salivary glands. *Acta Odontologica Scandinavica* **72**, 694-700 (2014).

40 Blank, N. *et al.* Cholera toxin binds to lipid rafts but has a limited specificity for ganglioside GM1. *Immunology and cell biology* **85**, 378-382 (2007).

41 Kuhlmann, F. M. *et al.* Blood group O–dependent cellular responses to cholera toxin: parallel clinical and epidemiological links to severe cholera. *The American journal of tropical medicine and hygiene* **95**, 440-443 (2016).

42 Glass, R. I. *et al.* Predisposition for cholera of individuals with O blood group possible evolutionary significance. *American journal of epidemiology* **121**, 791-796 (1985).

43 Harris, J. B. *et al.* Blood group, immunity, and risk of infection with Vibrio cholerae in an area of endemicity. *Infection and immunity* **73**, 7422-7427 (2005).

44 Harris, J. B. *et al.* Susceptibility to Vibrio cholerae infection in a cohort of household contacts of patients with cholera in Bangladesh. *PLoS neglected tropical diseases* **2** (2008).

45 Swerdlow, D. L. *et al.* Severe life-threatening cholera associated with blood group 0 in peru: implications for the latin american epidemic. *Journal of Infectious Diseases* **170**, 468-472 (1994).

46 Holmner, Å. *et al.* Novel binding site identified in a hybrid between cholera toxin and heat-labile enterotoxin: 1.9 Å crystal structure reveals the details. *Structure* **12**, 1655-1667 (2004).

47 Holmner, Å., Mackenzie, A. & Krengel, U. Molecular basis of cholera blood-group dependence and implications for a world characterized by climate change. *FEBS letters* **584**, 2548-2555 (2010).

48 Cervin, J. *et al.* GM1 ganglioside-independent intoxication by Cholera toxin. *PLoS pathogens* **14**, e1006862 (2018).

49 Wands, A. M. *et al.* Fucosylated molecules competitively interfere with cholera toxin binding to host cells. *ACS infectious diseases* **4**, 758-770 (2018).

50 Mandal, P. K. *et al.* Towards a structural basis for the relationship between blood group and the severity of El Tor cholera. *Angewandte Chemie International Edition* **51**, 5143-5146 (2012).

51 Heggelund, J. E. *et al.* High-resolution crystal structures elucidate the molecular basis of cholera blood group dependence. *PLoS pathogens* **12** (2016).

52 Heggelund, J. E. *et al.* Both El Tor and classical cholera toxin bind blood group determinants. *Biochemical and biophysical research communications* **418**, 731-735 (2012).

53 Vasile, F. *et al.* Comprehensive analysis of blood group antigen binding to classical and El Tor cholera toxin B-pentamers by NMR. *Glycobiology* **24**, 766-778 (2014).

54 Delguste, M. *et al.* Multivalent binding of herpesvirus to living cells is tightly regulated during infection. *Science Advances* **4**, eaat1273, doi:10.1126/sciadv.aat1273 (2018).

55 Schüller, S. Shiga Toxin Interaction with Human Intestinal Epithelium. *Toxins* **3**, 626-639 (2011).

56 Acheson, D. W. *et al.* Translocation of Shiga toxin across polarized intestinal cells in tissue culture. *Infection and immunity* **64**, 3294 (1996).

57 Hurley, B. P., Thorpe, C. M. & Acheson, D. W. K. Shiga Toxin Translocation across Intestinal Epithelial Cells Is Enhanced by Neutrophil Transmigration. *Infection and immunity* **69**, 6148, doi:10.1128/IAI.69.10.6148-6155.2001 (2001).

58 Schüller, S., Frankel, G. & Phillips, A. D. Interaction of Shiga toxin from Escherichia coli with human intestinal epithelial cell lines and explants: Stx2 induces epithelial damage in organ culture. *Cellular Microbiology* **6**, 289-301, doi:10.1046/j.1462-5822.2004.00370.x (2004).

59 Malyukova, I. *et al.* Macropinocytosis in Shiga toxin 1 uptake by human intestinal epithelial cells and transcellular transcytosis. *American Journal of Physiology-Gastrointestinal and Liver Physiology* **296**, G78-G92, doi:10.1152/ajpgi.90347.2008 (2009).

60 Mazor, Y. *et al.* Insights into the molecular basis of a bispecific antibody's target selectivity. *mAbs* **7**, 461-469, doi:10.1080/19420862.2015.1022695 (2015).

61 Sengers, B. G. *et al.* Modeling bispecific monoclonal antibody interaction with two cell membrane targets indicates the importance of surface diffusion. *mAbs* **8**, 905-915, doi:10.1080/19420862.2016.1178437 (2016).

62 Li, J. *et al.* Screening Glycolipids Against Proteins in Vitro Using Picodiscs and Catch-and-Release Electrospray Ionization-Mass Spectrometry. *Analytical Chemistry* **88**, 4742-4750, doi:10.1021/acs.analchem.6b00043 (2016).

63 Han, L., Kitova, E. N. & Klassen, J. S. Detecting Protein–Glycolipid Interactions Using Glycomicelles and CaR-ESI-MS. *Journal of The American Society for Mass Spectrometry* **27**, 1878-1886, doi:10.1007/s13361-016-1461-6 (2016).

64 Dam, T. K. & Brewer, C. F. Lectins as pattern recognition molecules: the effects of epitope density in innate immunity. *Glycobiology* **20**, 270-279 (2010).

65 Dennis, J. W. & Brewer, C. F. Density-dependent lectin–glycan interactions as a paradigm for conditional regulation by posttranslational modifications. *Molecular & Cellular Proteomics* **12**, 913-920 (2013).

66 Mellet, C. O., Nierengarten, J.-F. & Fernández, J. M. G. Multivalency as an action principle in multimodal lectin recognition and glycosidase inhibition: A paradigm shift driven by carbon-based glyconanomaterials. *Journal of Materials Chemistry B* **5**, 6428-6436 (2017).

67 Schnaar, R. L. Glycobiology simplified: diverse roles of glycan recognition in inflammation. *Journal of leukocyte biology* **99**, 825-838 (2016).

68 Purcell, S. C. & Godula, K. Synthetic glycoscapes: addressing the structural and functional complexity of the glycocalyx. *Journal of the Royal Society Interface Focus* **9**, 20180080 (2019).

69 Park, S., Gildersleeve, J. C., Blixt, O. & Shin, I. Carbohydrate microarrays. *Chemical Society Reviews* **42**, 4310-4326 (2013).

70 Wang, L. *et al.* Cross-platform comparison of glycan microarray formats. *Glycobiology* **24**, 507-517 (2014).

71 Zhu, X.-Y. *et al.* Quantitative glycomics from fluidic glycan microarrays. *Journal of the American Chemical Society* **131**, 13646-13650 (2009).

72 Tanaka, M. & Sackmann, E. Polymer-supported membranes as models of the cell surface. *Nature* **437**, 656-663 (2005).

73 Yamazaki, V. *et al.* Cell membrane array fabrication and assay technology. *BMC biotechnology* **5**, 18 (2005).

74 Castellana, E. T. & Cremer, P. S. Imaging large arrays of supported lipid bilayers with a macroscope. *Biointerphases* **2**, 57-63 (2007).

75 Ma, Y., Sobkiv, I., Gruzdys, V., Zhang, H. & Sun, X.-L. Liposomal glyco-microarray for studying glycolipid–protein interactions. *Analytical and bioanalytical chemistry* **404**, 51-58 (2012).

76 Briard, J. G., Jiang, H., Moremen, K. W., Macauley, M. S. & Wu, P. Cell-based glycan arrays for probing glycan–glycan binding protein interactions. *Nature communications* **9**, 880 (2018).

77 Rinaldi, S. *et al.* Analysis of lectin binding to glycolipid complexes using combinatorial glycoarrays. *Glycobiology* **19**, 789-796 (2009).

78 Gallegos, K. M. *et al.* Shiga toxin binding to glycolipids and glycans. *PloS one* **7** (2012).

79 Safina, G. Application of surface plasmon resonance for the detection of carbohydrates, glycoconjugates, and measurement of the carbohydrate-specific interactions: A comparison with conventional analytical techniques. A critical review. *Analytica chimica acta* **712**, 9-29 (2012).

80 Galush, W. J., Nye, J. A. & Groves, J. T. Quantitative fluorescence microscopy using supported lipid bilayer standards. *Biophysical journal* **95**, 2512-2519 (2008).

81 Wu, H.-J. *et al.* Membrane-protein binding measured with solution-phase plasmonic nanocube sensors. *nature methods* **9**, 1189-1191 (2012).

82 Worstell, N. C., Singla, A. & Wu, H.-J. Evaluation of hetero-multivalent lectin binding using a turbidity-based emulsion agglutination assay. *Colloids and Surfaces B: Biointerfaces* **175**, 84-90, doi:https://doi.org/10.1016/j.colsurfb.2018.11.069 (2019).

83 Varki, A. *et al.* (2009).

84 Lauer, S., Goldstein, B., Nolan, R. L. & Nolan, J. P. Analysis of cholera toxin−ganglioside interactions by flow cytometry. *Biochemistry* **41**, 1742-1751, doi:10.1021/bi0112816 (2002).

85 Fishman, P. H. & Atikkan, E. E. Mechanism of action of cholera toxin: effect of receptor density and multivalent binding on activation of adenylate cyclase. *The Journal of membrane biology* **54**, 51-60 (1980).

86 Fasting, C. *et al.* Multivalency as a chemical organization and action principle. *Angewandte Chemie* **51**, 10472-10498, doi:10.1002/anie.201201114 (2012).

87 Shen, L. *et al.* Membrane Environment Can Enhance the Interaction of Glycan Binding Protein to Cell Surface Glycan Receptors. *ACS Chemical Biology* **9**, 1877-1884, doi:10.1021/cb5004114 (2014).

88 Gallegos, K. M. *et al.* Shiga toxin binding to glycolipids and glycans. *Plos One* **7**, e30368, doi:10.1371/journal.pone.0030368 (2012).

89 Ortega-Muñoz, M. *et al.* Click Multivalent Heterogeneous Neoglycoconjugates – Modular Synthesis and Evaluation of Their Binding Affinities. *European Journal of Organic Chemistry* **2009**, 2454-2473, doi:10.1002/ejoc.200801169 (2009).

90 Kuziemko, G. M., Stroh, M. & Stevens, R. C. Cholera toxin binding affinity and specificity for gangliosides determined by surface plasmon resonance. *Biochemistry* **35**, 6375-6384, doi:10.1021/bi952314i (1996).

91 Shi, J. J. *et al.* GM1 clustering inhibits cholera toxin binding in supported phospholipid membranes. *Journal of the American Chemical Society* **129**, 5954-5961, doi:10.1021/ja069375w (2007).

92 Leach, K., Sexton, P. M. & Christopoulos, A. in *Current Protocols in Pharmacology* (John Wiley & Sons, Inc., 2001).

93 Lin, H., Kitova, E. N. & Klassen, J. S. Measuring positive cooperativity using the direct ESI-MS assay. Cholera toxin B subunit homopentamer binding to GM1 pentasaccharide. *J Am Soc Mass Spectrom* **25**, 104-110, doi:10.1007/s13361-013-0751-5 (2014).

94 Schafer, D. E. & Thakur, A. K. Quantitative description of the binding of GM1 oligosaccharide by cholera enterotoxin. *Cell Biophysics* **4**, 25-40, doi:10.1007/bf02788553 (1982).

95 Adam, G. & Delbruck, M. in *Structural chemistry and molecular biology* (eds A. Rich & N. Davidson) 198–215 (W. H. Freeman and Co., 1968).

96 Axelrod, D. & Wang, M. Reduction-of-dimensionality kinetics at reaction-limited cell surface receptors. *Biophysical journal* **66**, 588 (1994).

97 McCloskey, M. A. & Poo, M. Rates of membrane-associated reactions: reduction of dimensionality revisited. *The Journal of cell biology* **102**, 88-96 (1986).

98 Berg, H. C. & Purcell, E. M. Physics of chemoreception. *Biophys J* **20**, 193-219, doi:10.1016/S0006-3495(77)85544-6 (1977).

99 Hardt, S. L. Rates of diffusion controlled reactions in one, two and three dimensions. *Biophysical Chemistry* **10**, 239-243, doi:http://dx.doi.org/10.1016/0301-4622(79)85012-7 (1979).

100 Keizer, J. Diffusion effects on rapid bimolecular chemical reactions. *Chemical reviews* **87**, 167-180, doi:10.1021/cr00077a009 (1987).

101 Szabo, A., Schulten, K. & Schulten, Z. First passage time approach to diffusion controlled reactions. *The Journal of Chemical Physics* **72**, 4350-4357, doi:10.1063/1.439715 (1980).

102 Sengers, B. G. *et al.* Modeling bispecific monoclonal antibody interaction with two cell membrane targets indicates the importance of surface diffusion. *MAbs* **8**, 905-915, doi:10.1080/19420862.2016.1178437 (2016).

103 Jobling, M. G., Yang, Z., Kam, W. R., Lencer, W. I. & Holmes, R. K. A single native ganglioside GM1-binding site is sufficient for cholera toxin to bind to cells and complete the intoxication pathway. *mBio* **3**, e00401-00412, doi:10.1128/mBio.00401-12 (2012).

104 Hsieh, C.-L., Spindler, S., Ehrig, J. & Sandoghdar, V. Tracking single particles on supported lipid membranes: multimobility diffusion and nanoscopic confinement. *The Journal of Physical Chemistry B* **118**, 1545-1554, doi:10.1021/jp412203t (2014).

105 Day, C. A. & Kenworthy, A. K. Mechanisms underlying the confined diffusion of cholera toxin B-subunit in intact cell membranes. *PLoS ONE* **7**, e34923, doi:10.1371/journal.pone.0034923 (2012).

106 Lindblom, G. & Orädd, G. Lipid lateral diffusion and membrane heterogeneity. *Biochimica et Biophysica Acta (BBA) - Biomembranes* **1788**, 234-244, doi:http://dx.doi.org/10.1016/j.bbamem.2008.08.016 (2009).

107 Burns, A. R., Frankel, D. J. & Buranda, T. Local mobility in lipid domains of supported bilayers characterized by atomic force microscopy and fluorescence correlation spectroscopy. *Biophys J* **89**, 1081-1093, doi:10.1529/biophysj.105.060327 (2005).

108 Sachl, R. *et al.* On multivalent receptor activity of GM1 in cholesterol containing membranes. *Biochimica et biophysica acta* **1853**, 850-857, doi:10.1016/j.bbamcr.2014.07.016 (2015).

109 Wang, F., Curry, D. E. & Liu, J. Driving adsorbed gold nanoparticle assembly by merging lipid gel/fluid interfaces. *Langmuir : the ACS journal of surfaces and colloids* **31**, 13271-13274, doi:10.1021/acs.langmuir.5b03606 (2015).

110 Forstner, M. B., Yee, C. K., Parikh, A. N. & Groves, J. T. Lipid lateral mobility and membrane phase structure modulation by protein binding. *Journal of the American Chemical Society* **128**, 15221-15227, doi:10.1021/ja064093h (2006).

111 Scomparin, C., Lecuyer, S., Ferreira, M., Charitat, T. & Tinland, B. Diffusion in supported lipid bilayers: influence of substrate and preparation technique on the internal

dynamics. *The European physical journal. E, Soft matter* **28**, 211-220, doi:10.1140/epje/i2008-10407-3 (2009).

112 Goins, B. M., M,; Barisas, B.; Freire, E. Lateral diffusion of ganglioside GM1 in phospholipid bilayer membranes. *Biophys J* **49**, 849-856, doi:10.1016/S0006-3495(86)83714-6 (1986).

113 Alouf, J. E. & Popoff, M. R. *The comprehensive sourcebook of bacterial protein toxins (Third Edition)*. (Academic Press, 2006).

114 Goluszko, P. & Nowicki, B. Membrane cholesterol: a crucial molecule affecting interactions of microbial pathogens with mammalian cells. *Infection and immunity* **73**, 7791-7796, doi:10.1128/IAI.73.12.7791-7796.2005 (2005).

115 Bricarello, D. A., Mills, E. J., Petrlova, J., Voss, J. C. & Parikh, A. N. Ganglioside embedded in reconstituted lipoprotein binds cholera toxin with elevated affinity. *Journal of lipid research* **51**, 2731-2738, doi:10.1194/jlr.M007401 (2010).

116 Merritt, E. A. *et al.* Crystal structure of cholera toxin B-pentamer bound to receptor GM1 pentasaccharide. *Protein Science* **3**, 166-175, doi:10.1002/pro.5560030202 (1994).

117 Frances M. Platt, G. R., Raymond A. Dwek, and Terry D. Butters. Extensive glycosphingolipid depletion in the liver and lymphoid organs of mice treated with N-Butyldeoxynojirimycin. *The Journal of Biological Chemistry* **272**, 19365-19372 (1997).

118 Stryjewski, M. E. & Sexton, D. J. in *Severe Infections Caused by Pseudomonas Aeruginosa* (eds Alan R. Hauser & Jordi Rello) 1-15 (Springer US, 2003).

119 Gellatly, S. L. & Hancock, R. E. Pseudomonas aeruginosa: new insights into pathogenesis and host defenses. *Pathogens and disease* **67**, 159-173, doi:10.1111/2049-632X.12033 (2013).

120 Chi, E., Mehl, T., Nunn, D. & Lory, S. Interaction of Pseudomonas aeruginosa with A549 pneumocyte cells. *Infection and immunity* **59**, 822-828 (1991).

121 Fleiszig, S. M., Zaidi, T. S., Fletcher, E. L., Preston, M. J. & Pier, G. B. Pseudomonas aeruginosa invades corneal epithelial cells during experimental infection. *Infection and immunity* **62**, 3485-3493 (1994).

122 Fleiszig, S. M. J. *et al.* Relationship between cytotoxicity and corneal epithelial cell invasion by clinical isolates of Pseudomonas aeruginosa. *Infection and immunity* **64**, 2288-2294 (1996).

123 Mewe, M. *et al.* Pseudomonas aeruginosa lectins I and II and their interaction with human airway cilia. *The Journal of laryngology and otology* **119**, 595-599, doi:10.1258/0022215054516313 (2005).

124 Chemani, C. *et al.* Role of LecA and LecB lectins in Pseudomonas aeruginosa-induced lung injury and effect of carbohydrate ligands. *Infection and immunity* **77**, 2065-2075, doi:10.1128/IAI.01204-08 (2009).

125 Fong, J. N. & Yildiz, F. H. Biofilm Matrix Proteins. *Microbiology spectrum* **3**, doi:10.1128/microbiolspec.MB-0004-2014 (2015).

126 Diggle, S. P. *et al.* The galactophilic lectin, LecA, contributes to biofilm development in Pseudomonas aeruginosa. *Environmental microbiology* **8**, 1095-1104, doi:10.1111/j.1462-2920.2006.001001.x (2006).

127 Saiman, L. & Prince, A. Pseudomonas aeruginosa pili bind to asialoGM1 which is increased on the surface of cystic fibrosis epithelial cells. *The Journal of clinical investigation* **92**, 1875-1880, doi:10.1172/JCI116779 (1993).

128 Zheng, S. *et al.* The Pseudomonas aeruginosa lectin LecA triggers host cell signalling by glycosphingolipid-dependent phosphorylation of the adaptor protein CrkII. *Biochimica et biophysica acta* **1864**, 1236-1245, doi:10.1016/j.bbamcr.2017.04.005 (2017).

129 Funken, H. *et al.* Specific association of lectin LecB with the surface of Pseudomonas aeruginosa: role of outer membrane protein OprF. *PLoS One* **7**, e46857, doi:10.1371/journal.pone.0046857 (2012).

130 Cott, C. *et al.* Pseudomonas aeruginosa lectin LecB inhibits tissue repair processes by triggering beta-catenin degradation. *Biochim Biophys Acta* **1863**, 1106-1118, doi:10.1016/j.bbamcr.2016.02.004 (2016).

131 Kühn, K. *et al.* The interplay of autophagy and β-Catenin signaling regulates differentiation in acute myeloid leukemia. *Cell death discovery* **1**, 15031, doi:10.1038/cddiscovery.2015.31 (2015).

132 Schneider, D. *et al.* Lectins from opportunistic bacteria interact with acquired variable-region glycans of surface immunoglobulin in follicular lymphoma. *Blood* **125**, 3287-3296, doi:10.1182/blood-2014-11-609404 (2015).

133 Eierhoff, T. *et al.* A lipid zipper triggers bacterial invasion. *Proceedings of the National Academy of Sciences of the United States of America* **111**, 12895-12900, doi:10.1073/pnas.1402637111 (2014).

134 Imberty, A., Wimmerova, M., Mitchell, E. P. & Gilboa-Garber, N. Structures of the lectins from Pseudomonas aeruginosa: insights into the molecular basis for host glycan recognition. *Microbes and Infection* **6**, 221-228, doi:10.1016/j.micinf.2003.10.016 (2004).

135 Grishin, A. V., Krivozubov, M. S., Karyagina, A. S. & Gintsburg, A. L. Pseudomonas Aeruginosa Lectins As Targets for Novel Antibacterials. *Acta naturae* **7**, 29-41 (2015).

136 Cioci, G. *et al.* Structural basis of calcium and galactose recognition by the lectin PA-IL of Pseudomonas aeruginosa. *FEBS Lett* **555**, 297-301, doi:10.1016/S0014-5793(03)01249-3 (2003).

137 Gilboa-Garber, N., Mizrahi, L. & Garber, N. Purification of the galactose-binding hemagglutinin of Pseudomonas aeruginosa by affinity column chromatography using sepharose. *FEBS Lett* **28**, 93-95, doi:10.1016/0014-5793(72)80685-9 (1972).

138 Lanne, B., Cîopraga, J., Bergström, J., Motas, C. & Karlsson, K.-A. Binding of the galactose-specificPseudomonas aeruginosa lectin, PA-I, to glycosphingolipids and other glycoconjugates. *Glycoconjugate Journal* **11**, 292-298, doi:10.1007/bf00731201 (1994).

139 Blanchard, B. *et al.* Structural basis of the preferential binding for globo-series glycosphingolipids displayed by Pseudomonas aeruginosa lectin I. *J Mol Biol* **383**, 837-853, doi:10.1016/j.jmb.2008.08.028 (2008).

140 Chen, C. P., Song, S. C., Gilboa-Garber, N., Chang, K. S. & Wu, A. M. Studies on the binding site of the galactose-specific agglutinin PA-IL from Pseudomonas aeruginosa. *Glycobiology* **8**, 7-16, doi:10.1093/glycob/8.1.7 (1998).

141 Villringer, S. *et al.* Lectin-mediated protocell crosslinking to mimic cell-cell junctions and adhesion. *Sci Rep* **8**, 1932, doi:10.1038/s41598-018-20230-6 (2018).

142 Mahal, L. K. (Glycan array data in Consortium for Functional Glycomics, 2011).

143 Momoeda, K. *et al.* Developmental changes of neutral glycosphingolipids as receptors for pulmonary surfactant protein SP-A in the alveolar epithelium of murine lung. *J Biochem-Tokyo* **119**, 1189-1195, doi:10.1093/oxfordjournals.jbchem.a021367 (1996).

144 Tao, A., Sinsermsuksakul, P. & Yang, P. Polyhedral Silver Nanocrystals with Distinct Scattering Signatures. *Angewandte Chemie International Edition* **45**, 4597-4601, doi:10.1002/anie.200601277 (2006).

145 Nayhouse, M., Kwon, J. S. I., Christofides, P. D. & Orkoulas, G. Crystal shape modeling and control in protein crystal growth. *Chem Eng Sci* **87**, 216-223, doi:10.1016/j.ces.2012.10.020 (2013).

146 Fallahi-Sichani, M. & Linderman, J. J. Lipid raft-mediated regulation of G-protein coupled receptor signaling by ligands which influence receptor dimerization: a computational study. *PLoS One* **4**, e6604, doi:10.1371/journal.pone.0006604 (2009).

147 Nayhouse, M. *et al.* Modeling and control of ibuprofen crystal growth and size distribution. *Chem Eng Sci* **134**, 414-422, doi:10.1016/j.ces.2015.05.033 (2015).

148 Reynolds, M., Marradi, M., Imberty, A., Penades, S. & Perez, S. Multivalent gold glycoclusters: high affinity molecular recognition by bacterial lectin PA-IL. *Chemistry* **18**, 4264-4273, doi:10.1002/chem.201102034 (2012).

149 Chabre, Y. M. *et al.* Combining glycomimetic and multivalent strategies toward designing potent bacterial lectin inhibitors. *Chemistry* **17**, 6545-6562, doi:10.1002/chem.201003402 (2011).

150 Comolli, J. C., Waite, L. L., Mostov, K. E. & Engel, J. N. Pili binding to asialo-GM1 on epithelial cells can mediate cytotoxicity or bacterial internalization by Pseudomonas aeruginosa. *Infection and immunity* **67**, 3207-3214 (1999).

151 Loira-Pastoriza, C., Todoroff, J. & Vanbever, R. Delivery strategies for sustained drug release in the lungs. *Advanced drug delivery reviews* **75**, 81-91, doi:10.1016/j.addr.2014.05.017 (2014).

152 Cipolla, D., Gonda, I. & Chan, H. K. Liposomal formulations for inhalation. *Therapeutic delivery* **4**, 1047-1072, doi:10.4155/tde.13.71 (2013).

153 Meers, P. *et al.* Biofilm penetration, triggered release and in vivo activity of inhaled liposomal amikacin in chronic Pseudomonas aeruginosa lung infections. *The Journal of antimicrobial chemotherapy* **61**, 859-868, doi:10.1093/jac/dkn059 (2008).

154 Jimenez Blanco, J. L., Ortiz Mellet, C. & Garcia Fernandez, J. M. Multivalency in heterogeneous glycoenvironments: hetero-glycoclusters, -glycopolymers and -glycoassemblies. *Chem Soc Rev* **42**, 4518-4531, doi:10.1039/c2cs35219b (2013).

155 Simons, K. & Toomre, D. Lipid rafts and signal transduction. *Nature reviews. Molecular cell biology* **1**, 31-39, doi:10.1038/35036052 (2000).

156 van Meer, G., Stelzer, E. H., Wijnaendts-van-Resandt, R. W. & Simons, K. Sorting of sphingolipids in epithelial (Madin-Darby canine kidney) cells. *J Cell Biol* **105**, 1623-1635, doi:10.1083/jcb.105.4.1623 (1987).

157 van Meer, G. & Simons, K. The function of tight junctions in maintaining differences in lipid composition between the apical and the basolateral cell surface domains of MDCK cells. *The EMBO journal* **5**, 1455-1464 (1986).

158 Danielsen, E. M. & Hansen, G. H. Lipid raft organization and function in the small intestinal brush border. *Journal of physiology and biochemistry* **64**, 377-382, doi:10.1007/BF03174093 (2008).

159 Danielsen, E. M. & Hansen, G. H. Lipid raft organization and function in brush borders of epithelial cells. *Molecular membrane biology* **23**, 71-79, doi:10.1080/09687860500445604 (2006).

160 Parkin, E. T., Turner, A. J. & Hooper, N. M. Differential effects of glycosphingolipids on the detergent-insolubility of the glycosylphosphatidylinositol-anchored membrane dipeptidase. *The Biochemical journal* **358**, 209-216, doi:10.1042/bj3580209 (2001).

161 Mahfoud, R., Manis, A., Binnington, B., Ackerley, C. & Lingwood, C. A. A major fraction of glycosphingolipids in model and cellular cholesterol-containing membranes is undetectable by their binding proteins. *J Biol Chem* **285**, 36049-36059, doi:10.1074/jbc.M110.110189 (2010).

162 Sonnino, S. *et al.* Role of very long fatty acid-containing glycosphingolipids in membrane organization and cell signaling: the model of lactosylceramide in neutrophils. *Glycoconj J* **26**, 615-621, doi:10.1007/s10719-008-9215-8 (2009).

163 Sheikhpour, M., Barani, L. & Kasaeian, A. Biomimetics in drug delivery systems: A critical review. *Journal of controlled release : official journal of the Controlled Release Society* **253**, 97-109, doi:10.1016/j.jconrel.2017.03.026 (2017).

164 Allen, T. M. & Cullis, P. R. Liposomal drug delivery systems: from concept to clinical applications. *Advanced drug delivery reviews* **65**, 36-48, doi:10.1016/j.addr.2012.09.037 (2013).

165 Duncan, G. A. & Bevan, M. A. Computational design of nanoparticle drug delivery systems for selective targeting. *Nanoscale* **7**, 15332-15340, doi:10.1039/c5nr03691g (2015).

166 Lis, H. & Sharon, N. Lectins: Carbohydrate-Specific Proteins That Mediate Cellular Recognition†. *Chemical reviews* **98**, 637-674, doi:10.1021/cr940413g (1998).

167 Chabre, Y. M. & Roy, R. in *Advances in Carbohydrate Chemistry and Biochemistry* Vol. 63 (ed Derek Horton) 165-393 (Academic Press, 2010).

168 Mammen, M., Choi, S. K. & Whitesides, G. M. Polyvalent interactions in biological systems: Implications for design and use of multivalent ligands and inhibitors. *Angew Chem Int Edit* **37**, 2755-2794, doi:10.1002/(SICI)1521-3773(19981102)37:20<2754::AID-ANIE2754>3.0.CO;2-3 (1998).

169 Wolfenden, M. L. & Cloninger, M. J. Carbohydrate-functionalized dendrimers to investigate the predictable tunability of multivalent interactions. *Bioconjug Chem* **17**, 958-966, doi:10.1021/bc060107x (2006).

170 Ponader, D., Wojcik, F., Beceren-Braun, F., Dernedde, J. & Hartmann, L. Sequence-defined glycopolymer segments presenting mannose: synthesis and lectin binding affinity. *Biomacromolecules* **13**, 1845-1852, doi:10.1021/bm300331z (2012).

171 Sigal, G. B., Mammen, M., Dahmann, G. & Whitesides, G. M. Polyacrylamides Bearing Pendant α-Sialoside Groups Strongly Inhibit Agglutination of Erythrocytes by Influenza Virus: The Strong Inhibition Reflects Enhanced Binding through Cooperative Polyvalent Interactions. *Journal of the American Chemical Society* **118**, 3789-3800, doi:10.1021/ja953729u (1996).

172 Lee, D., Singla, A., Wu, H. J. & Kwon, J. S. I. An Integrated Numerical and Experimental Framework for Modeling of CTB and GD1b Ganglioside Binding Kinetics. *Aiche J* **64**, 3882-3893, doi:10.1002/aic.16209 (2018).

173 Lee, D., Mohr, A., Kwon, J. S. I. & Wu, H. J. Kinetic Monte Carlo modeling of multivalent binding of CTB proteins with GM1 receptors. *Comput Chem Eng* **118**, 283-295, doi:10.1016/j.compchemeng.2018.08.011 (2018).

174 Kemp, B. E. *et al.* Autologous red cell agglutination assay for HIV-1 antibodies: simplified test with whole blood. *Science* **241**, 1352-1354 (1988).

175 Huet, M., Cubizolles, M. & Buhot, A. Real time observation and automated measurement of red blood cells agglutination inside a passive microfluidic biochip containing embedded reagents. *Biosens Bioelectron* **93**, 110-117, doi:10.1016/j.bios.2016.09.068 (2017).

176 Pan, D. *et al.* The Effect of Polymeric Nanoparticles on Biocompatibility of Carrier Red Blood Cells. *PLoS One* **11**, e0152074, doi:10.1371/journal.pone.0152074 (2016).

177 Sharon, N. & Lis, H. Lectins: cell-agglutinating and sugar-specific proteins. *Science* **177**, 949-959 (1972).

178 Shekarchi, I. C., Fuccillo, D. A., Sever, J. L. & Madden, D. M. Avidin-biotin latex agglutination assay for detection of antibodies to viral antigens. *J Clin Microbiol* **26**, 954-956 (1988).

179 Vico, R. V., Voskuhl, J. & Ravoo, B. J. Multivalent interaction of cyclodextrin vesicles, carbohydrate guests, and lectins: a kinetic investigation. *Langmuir : the ACS journal of surfaces and colloids* **27**, 1391-1397, doi:10.1021/la1038975 (2011).

180 Walder, R. B., Honciuc, A. & Schwartz, D. K. Phospholipid diffusion at the oil-water interface. *J Phys Chem B* **114**, 11484-11488, doi:10.1021/jp1053869 (2010).

181 Pautot, S., Frisken, B. J., Cheng, J. X., Xie, X. S. & Weitz, D. A. Spontaneous formation of lipid structures at oil/water lipid interfaces. *Langmuir : the ACS journal of surfaces and colloids* **19**, 10281-10287, doi:10.1021/la034532f (2003).

182 Lothian, G. F. & Chappel, F. P. The Transmission of Light through Suspensions. *J Appl Chem* **1**, 475-482, doi:DOI 10.1002/jctb.5010011102 (1951).

183 Ray, A. K., Johnson, J. K. & Sullivan, R. J. Refractive-Index of the Dispersed Phase in Oil-in-Water Emulsions - Its Dependence on Droplet Size and Aging. *J Food Sci* **48**, 513-516, doi:DOI 10.1111/j.1365-2621.1983.tb10778.x (1983).

184 Linke, C. & Drusch, S. Turbidity in oil-in-water-emulsions — Key factors and visual perception. *Food Research International* **89**, 202-210 (2016).

185 Salvia-Trujillo, L., Soliva-Fortuny, R., Rojas-Grau, M. A., McClements, D. J. & Martin-Belloso, O. Edible Nanoemulsions as Carriers of Active Ingredients: A Review. *Annu Rev Food Sci Technol* **8**, 439-466, doi:10.1146/annurev-food-030216-025908 (2017).

186 Shah, P., Bhalodia, D. & Shelat, P. Nanoemulsion: a pharmaceutical review. *Systematic Reviews in Pharmacy* **1**, 24 (2010).

187 Gupta, A., Eral, H. B., Hatton, T. A. & Doyle, P. S. Nanoemulsions: formation, properties and applications. *Soft Matter* **12**, 2826-2841, doi:10.1039/c5sm02958a (2016).

188 Sivakumar, M., Tang, S. Y. & Tan, K. W. Cavitation technology - a greener processing technique for the generation of pharmaceutical nanoemulsions. *Ultrason Sonochem* **21**, 2069-2083, doi:10.1016/j.ultsonch.2014.03.025 (2014).

189 Kulmyrzaev, A., Chanamai, R. & McClements, D. J. Influence of pH and CaCl2 on the stability of dilute whey protein stabilized emulsions. *Food Research International* **33**, 15-20, doi:Doi 10.1016/S0963-9969(00)00018-1 (2000).

190 O'Neill, M. L. *et al.* Emulsion Stabilization and Flocculation in CO2. 1. Turbidimetry and Tensiometry. *Macromolecules* **30**, 5050-5059, doi:10.1021/ma9616930 (1997).

191 Assenhaimer, C., Domingos, A. S., Glasse, B., Fritsching, U. & Guardani, R. Long-Term Monitoring of Metalworking Fluid Emulsion Aging Using a Spectroscopic Sensor. *Can J Chem Eng* **95**, 2341-2349, doi:10.1002/cjce.22931 (2017).

192 Glasse, B., Assenhaimer, C., Guardani, R. & Fritsching, U. Analysis of the Stability of Metal Working Fluid Emulsions by Turbidity Spectra. *Chem Eng Technol* **36**, 1202-1208, doi:10.1002/ceat.201200590 (2013).

193 Deluhery, J. & Rajagopalan, N. A turbidimetric method for the rapid evaluation of MWF emulsion stability. *Colloid Surface A* **256**, 145-149, doi:10.1016/j.colsurfa.2004.12.001 (2005).

194 Rahn-Chique, K., Puertas, A. M., Romero-Cano, M. S., Rojas, C. & Urbina-Villalba, G. Nanoemulsion stability: experimental evaluation of the flocculation rate from turbidity measurements. *Adv Colloid Interface Sci* **178**, 1-20, doi:10.1016/j.cis.2012.05.001 (2012).

195 Oster, G. Light Scattering from Polymerizing and Coagulating Systems. *J Coll Sci Imp U Tok* **2**, 291-299, doi:Doi 10.1016/0095-8522(47)90031-7 (1947).

196 Reddy, S. R. & Fogler, H. S. Emulsion Stability - Determination from Turbidity. *J Colloid Interf Sci* **79**, 101-104, doi:Doi 10.1016/0021-9797(81)90052-7 (1981).

197 Timasheff, S. N. Turbidity as a Criterion of Coagulation. *J Colloid Interf Sci* **21**, 489-+, doi:Doi 10.1016/0095-8522(66)90047-X (1966).

198 Heller, W. in *Electromagnetic Scattering* Vol. 5 (ed Milton Kerker) 101-119 (The Macmillan Company, 1963).

199 van de Hulst, H. C. *Light scattering by small particles*. (John Wiley & Sons, Inc., 1957).

200 Smoluchowski, M. Versuch einer mathematichen theorie der koagulationskinetic kolloider losungen. *Z. Physik Chem* **92**, 129-168 (1917).

201 Flory, P. J. Molecular size distribution in linear condensation polymers 1. *Journal of American Chemical Society* **58**, 1877-1885 (1936).

202 Hardt, S. L. Rates of diffusion controlled reactions in one, two and three dimensions. *Biophys Chem* **10**, 239-243, doi:http://dx.doi.org/10.1016/0301-4622(79)85012-7 (1979).

203 Kerker, M. *The scattering of light and other electromagnetic radiation*. (Academic Press, Inc, 1969).

204 Duan, J. M. & Gregory, J. Coagulation by hydrolysing metal salts. *Adv Colloid Interfac* **100**, 475-502, doi:Pii S0001-8686(02)00067-2

Doi 10.1016/S0001-8686(02)00067-2 (2003).

205 Gregory, J. Monitoring particle aggregation processes. *Adv Colloid Interface Sci* **147-148**, 109-123, doi:10.1016/j.cis.2008.09.003 (2009).

206 Parker, T. G. & Dalgleish, D. G. The use of light scattering and turbidity measurements to study the kinetics of extensively aggregating proteins: αs-Casein. *Biopolymers: Original Research on Biomolecules* **16**, 2533-2547 (1977).

207 Dieguez, L. *et al. Effect of the Refractive Index of Buffer Solutions in Evanescent Optical Biosensors*. Vol. 7 (2009).

208 Venkataraman, M., Sasisekharan, R. & Raman, R. in *Glycoinformatics* (eds Thomas Lütteke & Martin Frank) 181-190 (Springer New York, 2015).

209 Deluhery, J. & Rajagopalan, N. A turbidimetric method for the rapid evaluation of MWF emulsion stability. *Colloids and Surfaces A: Physicochemical and Engineering Aspects* **256**, 145-149, doi:https://doi.org/10.1016/j.colsurfa.2004.12.001 (2005).

210 Tacconelli, E. *et al.* Discovery, research, and development of new antibiotics: the WHO priority list of antibiotic-resistant bacteria and tuberculosis. *The Lancet Infectious Diseases* **18**, 318-327, doi:10.1016/s1473-3099(17)30753-3 (2018).

211 Fajardo, A. *et al.* The Neglected Intrinsic Resistome of Bacterial Pathogens. *PLOS ONE* **3**, e1619, doi:10.1371/journal.pone.0001619 (2008).

212 Breidenstein, E. B. M., de la Fuente-Núñez, C. & Hancock, R. E. W. Pseudomonas aeruginosa: all roads lead to resistance. *Trends in Microbiology* **19**, 419-426, doi:https://doi.org/10.1016/j.tim.2011.04.005 (2011).

213 Nicas, T. I. & Hancock, R. E. Pseudomonas aeruginosa outer membrane permeability: isolation of a porin protein F-deficient mutant. *Journal of Bacteriology* **153**, 281 (1983).

214 Schurek, K. N. *et al.* Novel Genetic Determinants of Low-Level Aminoglycoside Resistance in <em>Pseudomonas aeruginosa</em&gt. *Antimicrobial Agents and Chemotherapy* **52**, 4213, doi:10.1128/AAC.00507-08 (2008).

215 Dötsch, A. *et al.* Genomewide Identification of Genetic Determinants of Antimicrobial Drug Resistance in <em>Pseudomonas aeruginosa</em&gt. *Antimicrobial Agents and Chemotherapy* **53**, 2522, doi:10.1128/AAC.00035-09 (2009).

216 Stewart, P. S. Mechanisms of antibiotic resistance in bacterial biofilms. *International Journal of Medical Microbiology* **292**, 107-113, doi:https://doi.org/10.1078/1438-4221-00196 (2002).

217 Drulis-Kawa, Z. & Dorotkiewicz-Jach, A. Liposomes as delivery systems for antibiotics. *International Journal of Pharmaceutics* **387**, 187-198, doi:https://doi.org/10.1016/j.ijpharm.2009.11.033 (2010).

218 Ellbogen, M. H., Olsen, K. M., Gentry-Nielsen, M. J. & Preheim, L. C. Efficacy of liposome-encapsulated ciprofloxacin compared with ciprofloxacin and ceftriaxone in a rat model of pneumococcal pneumonia. *Journal of Antimicrobial Chemotherapy* **51**, 83-91, doi:10.1093/jac/dkg024 (2003).

219 Schiffelers, R. M., Storm, G. & Bakker-Woudenberg, I. A. J. M. Host Factors Influencing the Preferential Localization of Sterically Stabilized Liposomes in Klebsiella Pneumoniae-Infected Rat Lung Tissue. *Pharmaceutical Research* **18**, 780-787, doi:10.1023/A:1011080211226 (2001).

220 Schiffelers, R. M., Storm, G. & Bakker-Woudenberg, I. A. J. M. Therapeutic efficacy of liposomal gentamicin in clinically relevant rat models. *International Journal of Pharmaceutics* **214**, 103-105, doi:https://doi.org/10.1016/S0378-5173(00)00643-8 (2001).

221 Schiffelers, R. M. *et al.* In Vivo Synergistic Interaction of Liposome-Coencapsulated Gentamicin and Ceftazidime. *Journal of Pharmacology and Experimental Therapeutics* **298**, 369 (2001).

222 Allen, T. M. Liposomal Drug Formulations. *Drugs* **56**, 747-756, doi:10.2165/00003495-199856050-00001 (1998).

223 Pushparaj Selvadoss, P., Nellore, J., Balaraman Ravindrran, M. & Sekar, U. Novel pyochelin-based PEGylated liposomes for enhanced delivery of antibiotics against resistant clinical isolates of Pseudomonas aeruginosa. *Artificial Cells, Nanomedicine, and Biotechnology* **46**, 2043-2053, doi:10.1080/21691401.2017.1408119 (2018).

224 Forier, K. *et al.* Probing the size limit for nanomedicine penetration into Burkholderia multivorans and Pseudomonas aeruginosa biofilms. *J Control Release* **195**, 21-28, doi:10.1016/j.jconrel.2014.07.061 (2014).

225 Forier, K. *et al.* Lipid and polymer nanoparticles for drug delivery to bacterial biofilms. *J Control Release* **190**, 607-623, doi:10.1016/j.jconrel.2014.03.055 (2014).

226 Dong, D. *et al.* Distribution and Inhibition of Liposomes on Staphylococcus aureus and Pseudomonas aeruginosa Biofilm. *PLOS ONE* **10**, e0131806, doi:10.1371/journal.pone.0131806 (2015).

227 Geng, S. *et al.* Two cholesterol derivative-based PEGylated liposomes as drug delivery system, study on pharmacokinetics and drug delivery to retina. *Nanotechnology* **25**, 275103, doi:10.1088/0957-4484/25/27/275103 (2014).

228 Sercombe, L. *et al.* Advances and Challenges of Liposome Assisted Drug Delivery. *Frontiers in Pharmacology* **6**, doi:10.3389/fphar.2015.00286 (2015).

229 Wu, H.-C. & Chang, D.-K. Peptide-Mediated Liposomal Drug Delivery System Targeting Tumor Blood Vessels in Anticancer Therapy. *Journal of Oncology* **2010**, 723798, doi:10.1155/2010/723798 (2010).

230 Hood, R. R. *et al.* Microfluidic-Enabled Liposomes Elucidate Size-Dependent Transdermal Transport. *PLoS ONE* **9**, e92978, doi:10.1371/journal.pone.0092978 (2014).

231 Wright, B. D. *et al.* Synthesis, characterization, and antimicrobial activity of silver carbene complexes derived from 4, 5, 6, 7-tetrachlorobenzimidazole against antibiotic resistant bacteria. *Dalton Transactions* **41**, 6500-6506 (2012).

232 Immordino, M. L., Dosio, F. & Cattel, L. Stealth liposomes: review of the basic science, rationale, and clinical applications, existing and potential. *Int J Nanomedicine* **1**, 297-315, doi:10.2217/17435889.1.3.297 (2006).

233 Allen, T. M. & Chonn, A. Large unilamellar liposomes with low uptake into the reticuloendothelial system. *FEBS letters* **223**, 42-46 (1987).

234 Thuenauer, R. *et al.* The <em>Pseudomonas aeruginosa</em> lectin LecB causes integrin internalization to facilitate crawling of bacteria underneath host cells. *bioRxiv*, 2019.2012.2012.872739, doi:10.1101/2019.12.12.872739 (2019).

235 Johansson, E. M. V. *et al.* Inhibition and Dispersion of Pseudomonas aeruginosa Biofilms by Glycopeptide Dendrimers Targeting the Fucose-Specific Lectin LecB. *Chemistry & Biology* **15**, 1249-1257, doi:https://doi.org/10.1016/j.chembiol.2008.10.009 (2008).

236 Kolomiets, E. *et al.* Glycopeptide Dendrimers with High Affinity for the Fucose-Binding Lectin LecB from Pseudomonas aeruginosa. *ChemMedChem* **4**, 562-569, doi:10.1002/cmdc.200800380 (2009).

237 Kadam, R. U. *et al.* A Glycopeptide Dendrimer Inhibitor of the Galactose-Specific Lectin LecA and of Pseudomonas aeruginosa Biofilms. *Angewandte Chemie International Edition* **50**, 10631-10635, doi:10.1002/anie.201104342 (2011).

238 Diggle, S. P. *et al.* The galactophilic lectin, LecA, contributes to biofilm development in Pseudomonas aeruginosa. *Environmental microbiology* **8**, 1095-1104, doi:10.1111/j.1462-2920.2006.001001.x (2006).

239 Lesman-Movshovich, E., Lerrer, B. & Gilboa-Garber, N. Blocking of Pseudomonas aeruginosa lectins by human milk glycans. *Canadian Journal of Microbiology* **49**, 230-235, doi:10.1139/w03-027 (2003).

240 Ortega-Gonzalez, M. *et al.* Fructooligosacharides reduce Pseudomonas aeruginosa PAO1 pathogenicity through distinct mechanisms. *PLoS One* **9**, e85772, doi:10.1371/journal.pone.0085772 (2014).

241 Hauber, H.-P. *et al.* Inhalation with fucose and galactose for treatment of Pseudomonas aeruginosa in cystic fibrosis patients. *Int J Med Sci* **5**, 371-376, doi:10.7150/ijms.5.371 (2008).

242 Sun, X., Yang, Z., Mu, X. & Zhang, T. Effects of different fixatives on staining patterns of four lectins in cultured microvascular endothelial cells. *Journal of Histotechnology* **38**, 22-27 (2015).

243 Liao, W.-Y. & Fugmann, S. D. Lectins identify distinct populations of coelomocytes in Strongylocentrotus purpuratus. *PloS one* **12** (2017).

244 Ikehara, Y. *et al.* A carbohydrate recognition–based drug delivery and controlled release system using intraperitoneal macrophages as a cellular vehicle. *Cancer Research* **66**, 8740-8748 (2006).

245 Ikehara, Y. *et al.* Effective induction of anti-tumor immune responses with oligomannose-coated liposome targeting to intraperitoneal phagocytic cells. *Cancer letters* **260**, 137-145 (2008).

246 Hashida, N. *et al.* High-efficacy site-directed drug delivery system using sialyl-Lewis X conjugated liposome. *Experimental eye research* **86**, 138-149 (2008).

247 Hudak, J. E. & Bertozzi, C. R. Glycotherapy: new advances inspire a reemergence of glycans in medicine. *Chemistry and biology* **21**, 16-37 (2014).

248 Bhat, R. *et al.* Lectin-gated and glycan functionalized mesoporous silica nanocontainers for targeting cancer cells overexpressing Lewis X antigen. *Nanoscale* **10**, 239-249 (2018).

249 Hanes, J., Chan, K. W. Y., McMahon, M. T., Yang, M. & Yu, T. Lipid-based drug carriers for rapid penetration through mucus linings. United States patent (2018).

250 Torchilin, V. P. Recent advances with liposomes as pharmaceutical carriers. *Nature reviews Drug discovery* **4**, 145 (2005).

251 Daraee, H., Etemadi, A., Kouhi, M., Alimirzalu, S. & Akbarzadeh, A. Application of liposomes in medicine and drug delivery. *Artificial cells, nanomedicine,and biotechnology* **44**, 381-391 (2016).

252 Alavi, M., Karimi, N. & Safaei, M. Application of Various Types of Liposomes in Drug Delivery Systems. *Adv Pharm Bull* **7**, 3-9, doi:10.15171/apb.2017.002 (2017).

253 Meers, P. *et al.* Biofilm penetration, triggered release and in vivo activity of inhaled liposomal amikacin in chronic Pseudomonas aeruginosa lung infections. *Journal of Antimicrobial Chemotherapy* **61**, 859-868 (2008).

254 Niemann, M. *et al.* Gene mutations versus clinically relevant phenotypes: lyso-Gb3 defines Fabry disease. *Circulation: Cardiovascular Genetics* **7**, 8-16 (2014).

255 Day, C. J. *et al.* Lectin activity of Pseudomonas aeruginosa vaccine candidates PSE17-1, PSE41-5 and PSE54. *Biochem Biophys Res Commun* **513**, 287-290, doi:10.1016/j.bbrc.2019.03.092 (2019).

256 Bianconi, I. *et al.* Genome-based approach delivers vaccine candidates against Pseudomonas aeruginosa. *Frontiers in immunology* **9**, 3021 (2019).